Electronic Thesis and Dissertation Repository

8-14-2017 12:00 AM

Poly(ethyl glyoxylate) Solid-Core Particles for Drug Delivery

Michael Thomas Gambles, *The University of Western Ontario*

Supervisor: Elizabeth Rachel Gillies, *The University of Western Ontario*
A thesis submitted in partial fulfillment of the requirements for the Master of Science degree in Chemistry
© Michael Thomas Gambles 2017

Abstract

The ability to trigger the degradation of polymeric nanoparticles (NPs) by a specific stimulus can provide a method of improved drug targeting and selective release capabilities *in vivo*. The challenge for most polymeric drug delivery systems remains the necessity for many stimuli events to trigger the release of cargo. Polymeric nanotechnology containing "self-immolative polymers" looks to alleviate the reliance on high concentrations of stimuli by undergoing complete end-to-end depolymerization via a single stimulus-mediated reaction of an end-cap. Herein, NPs were developed using poly(ethyl glyoxylate) (PEtG) blended with poly(D,L-lactic acid) (PLA) to encapsulate a hydrophobic cargo to be released upon stimulus-triggered cleavage of the PEtG end-cap. The PEtG-PLA NPs were formed using an oil-in-water emulsion-evaporation technique. Particles responsive to stimuli including UV-light and reducing conditions were prepared and studied. Cleavage of the end-caps of these polymers was accomplished by introducing the relevant stimuli, resulting in a rapid degradation of the particles and subsequent release of cargo. Nile red as a fluorescent probe and the drug celecoxib were encapsulated within the particles and were shown to be released upon introduction of small amounts of the appropriate stimulus. Initial cell culture studies were performed to investigate the behavior of the systems *in vitro*. This system provides the ability to tune the responsiveness of the NPs by simply changing the PEtG end-cap, making them a great prospect for stimuli-responsive drug delivery vehicles.

Keywords

Drug Delivery, Polymer Drug Delivery System, Polymeric Nanoparticles, Triggerable Release, Self-Immolative Polymer, Stimuli-Responsive, Emulsion-Evaporation

Co-Authorship Statement

The work described in this thesis contains contributions from the author as well as coworkers from Western and supervisor Dr. Elizabeth Gillies. The exact contributions to each project are described below.

Chapter 1 was written by the author and edited by supervisor Dr. Gillies. The literature reviews illustrated throughout the work were collected and written by the author and edited by supervisor Dr. Gillies.

The work described in Chapter 3 was a project proposed by Dr. Gillies and conducted by collaboration between the author and other members of the Gillies group. The work corresponding to the letrozole encapsulation within poly(ethyl glyoxylate) nanoparticles was developed by former student Amira Moustafa. Cell viability studies were performed with the help of the Aneta Borecki, lab technician of the Gillies group. All other experimental work corresponding to synthesis, optimization, characterization, and release experiments was conducted by the author. A draft of the manuscript was written by the author and was edited by Dr. Gillies.

Acknowledgements

Foremost, I would like to show my appreciation for my supervisor, Dr. Beth Gillies, for being a great mentor and teacher for me over the past two years.

Dr. Richard Gardiner and Karen Nygard deserve a great deal of credit for bestowing on me their knowledge of the myriad of microscopy techniques used to complete this work.

Aneta Borecki, whose talents are legion, thank you for your help with the sometimes-tedious cell studies and for everything else you taught me.

Dr. Amir Rabiee Kenaree and Dr. Jarret MacDonald, thank you for editing this work. It could not have been completed without your input and expertise.

To all my labmates, past and present, we made it through without any major loss of life, which is a success in itself! Thank you for your guidance and for putting up with my antics. You are all great scientists and it was a pleasure working with each of you.

To my siblings: Andrea, Austin, Caitlyne, Cole, Eric, Jaden, Josh, and Samantha; we are always in it together and this accomplishment is for all of us. I love you all.

Mom, it has been a wild ride. Thank you for always supporting me through the unpredictable escapade that is my life. I could not have made it without you. Thank you for being MY mom. I love you.

Dad, I'm sorry I wasn't there when you needed me. I will support the family in your absence. I miss you, big guy. I wish you were here. I hope it's nothing but fairways and greens in Heaven. Love you, pops. I love you too, Nat. I'll be home soon.

Cami and Ric, thank you for taking me in as one of your own. We make for a weird assortment of family members, but somehow, it works out. Love you both.

Table of Contents

List of Tables

List of Figures

List of Schemes

List of Abbreviations

BnCF	benzyl chloroformate
BnCO	benzyl carbonate
Boc	*tert*-butyloxycarbonyl
CPT	camptothecin
Đ	dispersity
DDS	drug delivery system
Disulfide-PEtG	2-(pyridine-2-yl-disulfanyl)ethyl carbonate-capped poly(ethyl glyoxylate)
DLS	dynamic light scattering
DMEM	Dulbecco's modified Eagle medium
DOX	doxorubicin
DTT	dithiothreitol
DSC	differential scanning calorimetry
EPA	etheylphenylacetate
EPR	enhanced permeability and retention effect
FBS	fetal bovine serum
Fmoc	fluorenylmethyloxycarbonyl
GSH	glutathione stimulating hormone
LG	leaving group
M_n	average molecular weight
MTT	3-(4,5-dimtheylthiazol-2-yl)-2,5-diphenyltetrazolium bromide
MWCO	molecular-weight cut-off
NP	nanoparticles
NVOC-Cl	6-nitroveratryl chloroformate

NVOC-PEtG	nitroveratryl carbonate-capped poly(ethyl glyoxylate)
O/W	oil-in-water
PBC	poly(benzyl carbamate)
PCL	polycaprolactone
PDI	polydispersity index
PDMA	poly(dimethyl acrylamide)
PEO	poly(ethylene oxide)
PEtG	poly(ethyl glyoxylate)
PG	protecting group
PGA	poly(glycolic acid)
PLA	poly(D,L-lactic acid)
PLA-PEtG-nonirr.	non-irradiated nitroveratryl carbonate-capped poly(ethyl glyoxylate)
PPHA	polyphthalaldehyde
PVA	poly(vinyl alcohol)
RES	reticuloendothelial system
SEC	size-exclusion chromatography
SEM	scanning electron microscopy
SIP	self-immolative polymer
SIPsomes	self-immolative polymersomes
T_c	ceiling temperature
T_g	glass transition temperature
T_o	onset degradation temperature
TEA	triethylamine
TEM	transmission electron microscopy
TGA	thermogravimetric analysis

UV   ultraviolet

wt%   weight percent

Z-Avg.   mean particle diameter

1   Introduction

Polymers are a versatile class of materials which can be produced on industrial scales and their properties can be easily tuned for a wide array of applications. The synthesis and manufacturing of polymeric materials increased as the realization of their versatility in a broad range of products became apparent. These ubiquitous materials emerged in the early 1900's and found applications in many industries including rubber, plastic, petrochemical, packaging, agriculture, and pharmaceuticals (Figure 1).
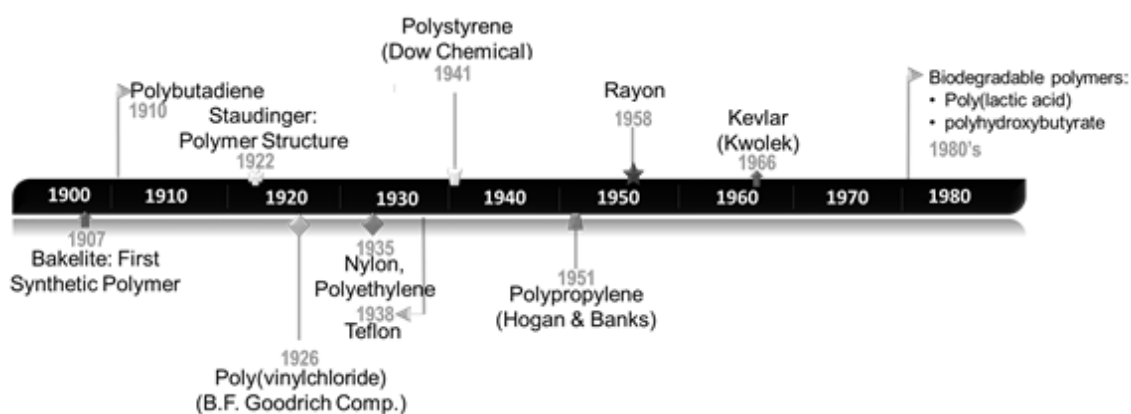
Figure 1. Historical breakthroughs in the field of polymeric materials.

With the discovery of polystyrene and polypropylene, the world began producing hundreds of tons of plastic every year.[1, 2] Synthetic rubbers were already in production by the 50's with production of just under one million tons per year. By 2016, over 300 million tons of plastic and 26 million tons of rubber were produced worldwide.[3]

Synthetic polymers have led to a plethora of versatile materials and inventions that have shaped today's society. The inherent properties of polymers make them adaptable materials. As one small change is made to a monomer, this change can be propagated through the polymer chain resulting in an overall polymer with starkly different physical and chemical properties. Because of their sensitivity to minute changes in their monomer structures, polymers have highly tunable physical and chemical properties that can be readily manipulated either chemically by altering the monomer structure, or by blending with plasticizers and other polymers. The versatility of polymers allows scientists to

create polymeric systems and materials with a wide array of applications from everyday commercial products to highly advanced drug delivery systems (DDS).[4]

There exist many benefits to polymers; however, there remains the problem of how to dispose of these materials once used. The majority of waste generated from plastics and petrochemicals is non-compostable and nondegradable and accounts for over 10% of total municipal waste.[5] Incineration of these materials can release pollutants into the atmosphere and recycling methods have proved to be costly and relatively inefficient. The high stability, low solubility, potential toxicity and sheer volume make these polymers difficult and expensive to dispose of efficiently.[6] To address these critical issues, degradable polymers that can exhibit the desirable properties of traditional nondegradable polymers have emerged.[2]

1.1　Degradable Polymers

As attention has shifted towards decreasing waste buildup and toxic degradation products of synthetic polymers, the focus has turned to the development of non-toxic, degradable polymers without sacrificing too many of the desirable characteristics of traditional plastics such as structural strength or durability.[7] Synthetic polymers can be divided into two major categories based on the chemical composition of their backbone: polymers with heteroatom-containing backbones and polymers with only carbon-containing backbones.[8] Polymers with only carbon-containing backbones consist of carbon-carbon bonds throughout the backbone of the macromolecule while polymers with heteroatom-containing backbones offer the advantage of having atoms other than carbon in the main chain backbone. Heteroatoms commonly used in these polymers include phosphorous (polyphosphoesters, *e.g.,* **1.1**), nitrogen (polycaprolactam, *e.g.,* **1.2**), and oxygen (poly(ethylene glycol), *e.g.,* **1.3**) (Figure 2).
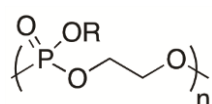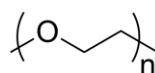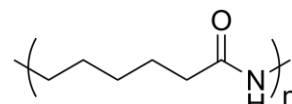
| **1.1** | **1.2** | **1.3** |

Figure 2. Examples of polymers with heteroatom-containing backbones.

While carbon-carbon bonded polymers yield very stable and relatively inert backbones, heteroatoms introduce polarity into the polymer backbone which can be exploited for chemical cleavage reactions.[9] Traditional rubbers and plastics are composed of carbon-chain polymers *i.e.* polybutadiene (**1.4**), polystyrene (**1.5**), polypropylene (**1.6**), and poly(vinyl chloride) (PVC, **1.7**) as shown in Figure 3.

| **1.4** | **1.5** | **1.6** | **1.7** |
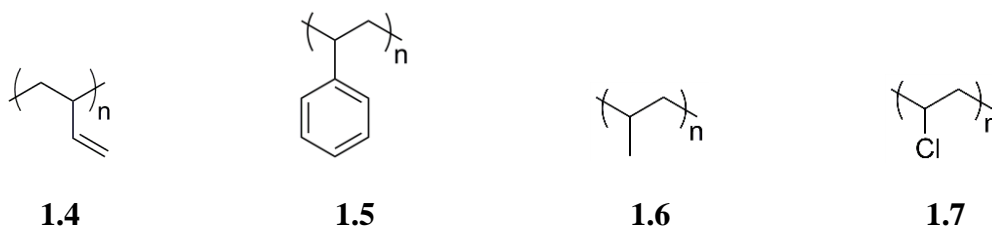
Figure 3. Examples of polymers with only carbon in their backbone.

The polymers in Figure 3 are very durable and inert materials. The introduction of heteroatoms, however, introduces potential areas to exploit for cleavage of the backbone leading to erosion and degradation of the material. For example, inserting oxygen atoms throughout the polymer backbone leads to a polyether. While the ether functional group is quite stable and exhibits low chemical reactivity, their polar bonds can be cleaved by the introduction of strong acids.[10]

1.1.1   Polyesters

Over the past three decades, research has yielded a vast library of degradable materials with wide-scope applications into many fields including pharmaceutics, agriculture, tissue engineering and commodities.[11, 12] Current degradable polymers include polyesters, polyacetals, polyamides, polyanhydrides, polyphosphazenes, polysulphones, polysiloxanes, polyurethanes and polydisulfides. In each of these cases, a heteroatom exists in the polymer backbone which leaves the polymer susceptible to cleavage reactions. Of all the different functional groups of degradable polymers, polyesters have been the most studied because they can be tailored to exhibit desirable properties including biocompatibility and biodegradability.[8] These properties will be discussed in more detail below.

In the early 1950's reports of the first synthetic degradable polyesters, such as polydioxanone (**1.8**), poly-3-hydroxyalkanoate (**1.9**), polyvalerolactone (**1.10**), and polycaprolactone (PCL, **1.11**) were reported for applications in the plastic industry (Figure 4).[4] The hydrolysable ester groups throughout these polymer backbones increase the polymer's susceptibility to degradation, significantly increasing their degradation rates. The problem continues to be that these materials are not as cost effective for large scale production as the more commonly used polymers such as high-density polyethylene, low density polyethylene and polypropylene.

1.8   **1.9**   **1.10**   **1.11**
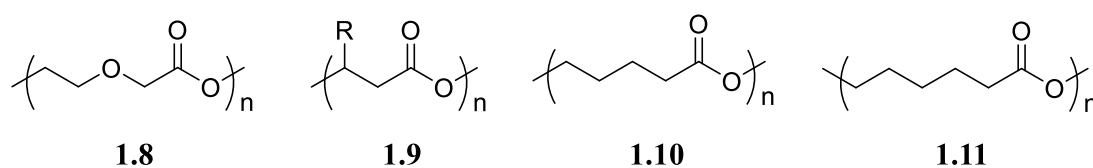
Figure 4. Common degradable polyesters.

An important feature of degradable polymers to consider is their biocompatibility. There exists a subset of degradable polymers that are not only degradable, but also display biodegradability - a feature defined as polymers that can be cleaved and degraded using biological machinery. Biodegradable polymers have backbone linkages that can be cleaved either by hydrolysis and/or enzyme-mediated within an organism.[13] The majority of biodegradable polymers currently in use are polyesters, including PCLs, poly(glycolic acid) (PGA, **1.12**), poly(D,L-lactic acid) (PLA, **1.13**) and poly(L-lactic acid). Variations of these homopolymers along with a variety of blends and copolymers (**1.14**) of these polyesters have been synthesized and proven to afford biodegradability. Figure 5 shows the most common polyesters used in medical applications. Applications of these polymers have been reported in medical devices, tissue engineering scaffolds, and drug delivery vehicles.[14-16]

1.12   **1.13**   **1.14**
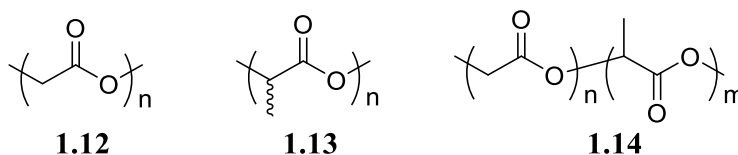
Figure 5. The most common biodegradable polyesters for medical applications.

While many of these materials have proved to be of great benefit, there still exist some limitations inherent to the degradation process of common degradable polymers. Degradable polymers rely on many chain scission cleavage events to slowly break down the long polymer chains into shorter fragments. Over time, this process leads to a complete degradation of the polymer. The degradation time of the polymer can be tuned by manipulating the properties of the polymer either chemically or by mixing one polymer with another to form a blend. However, the degradation of these polymers still includes some inherent randomness or uncontrollable processes.[17] Polyesters degrade by many hydrolysis events of the ester linkages throughout the backbone. The overall rate may be tuned to some degree, but the user has no control over where and when hydrolysis occurs throughout the backbone. The process of degradation is simply random in nature leaving little control as to specific ester bond cleavages. While polyesters and other biodegradable polymers have made a big impact in healthcare and pharmaceutics, there remain some limitations to these polymeric systems that could potentially be improved upon.

In recent years, the evolution of degradable polymers has lead research towards polymers that are not just degradable, but degradable upon introduction of a specific stimulus. The question of how to gain control over the degradation process was addressed with the emergence of self-immolative polymers (SIPs).[18]

1.2   The Development of Self-Immolative Polymers

1.2.1   Stimuli-Responsive Polymers

To overcome the lack of control in degradation of common degradable polymeric materials, attention has moved to the development of stimuli-responsive polymers. Stimuli-responsive polymers exhibit triggerable degradability upon exposure to a specific stimulus. These polymers are synthesized with functional groups that have an inherent sensitivity to certain conditions such as reduction/oxidation chemistry or acid/base chemistry. These polymers show responsiveness when exposed to a specific stimulus that will ultimately lead to their degradation. Specific polymers developed for this purpose

include polyacetals, polydisulfides (**1.15**), poly(ortho esters) (**1.16**), polyketals (**1.17**) and others. (Figure 6).[19]
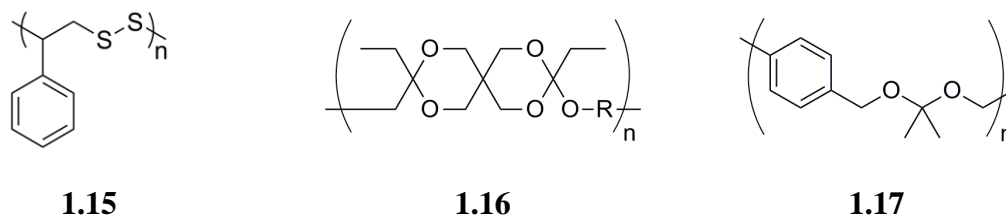
Figure 6. Common stimuli-responsive polymers.

Stimuli-responsive polymers can give rise to materials that exhibit sensitivity to pH (**1.17**), reduction (**1.15**) and temperature (**1.16**). Other stimuli-responsive polymers exist that show responsive behavior to a variety of other factors including humidity, wavelength or intensity of light, and magnetic fields. The physical response from these polymers can be a variety of changes such as altering solubility, color, transparency, conductivity or shape.[20, 21] However, not all of these classes of stimuli-responsive polymers are useful in applications where degradable polymers are required.

The introduction of stimuli-responsive polymers gives the user a more "degrade-on-demand" property to these polymers, but similar to the limitation of polyesters, stimuli-responsive polymers require many stimulus events to completely degrade the backbone. Therefore, these polymers can only be used in situations where stimulus is plentiful. It wasn't until the emergence of "self-immolative" molecules that scientists could begin to control specific stimulus-bond cleavage interactions.

1.2.2　Self-Immolative Small Molecules

A self-immolative system contains a stable bond between protecting and leaving groups (LGs) which becomes labile upon activation leading to a "triggerable" release of the LG.[22] In 1981, Katzenellenbogen and coworkers introduced the first self-immolative spacer into a prodrug delivery system.[23] The spacer was based on *p*-aminobenzyl alcohol, which could undergo a 1,6 elimination reaction to release a LG. This reaction was protected with a triggerable protecting group (PG) on the amine and the drug was

attached through a carbonate bond to the alcohol. With proper stimulus, the aromatic amine can be exposed to undergo the elimination step, releasing the drug (Scheme 1).
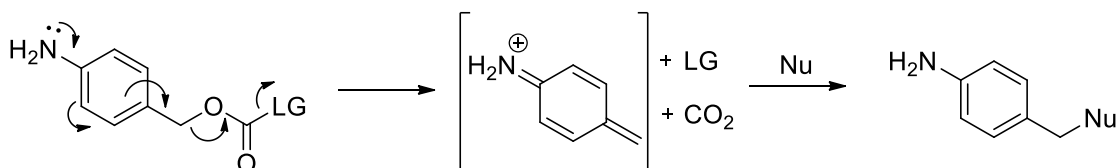
Scheme 1. 1,6-elimination mechanism of *p*-aminobenzyl ester (Nu = nucleophile).

The purpose of introducing a spacer between the concealed drug and the PG was to increase the distance between the bulky drug and the PG. Having the bulky drug close to the PG was shown to reduce the enzymatic cleavage rate of some prodrugs. Katzenellenbogen showed by introducing a self-immolative linker between the two molecules lead to increased enzymatic cleavage due to reduced steric hindrance. Many variations of this 1,6-elimination linker have been developed by using aromatic amine, hydroxyl or thiol moieties, each undergoing a 1,6-elimination reaction.[24]

While the use of prodrugs has led to promising applications in therapeutics, the inherent limiting factor to these types of systems is the continual need of stimulus to release drug. For each equivalent of drug released, there needs to be an equal equivalent of stimulus events. This limits the scope of potential PG that could be used for triggered removal of prodrugs. In certain situations, where specific stimuli concentrations are low, it would be beneficial to have a system in which one triggering event could lead to many equivalents of drug to be released. The combined work of these early reports of self-immolative molecules laid the groundwork for more promising macromolecular structures.

1.2.3 Self-Immolative Macromolecules

The invention of self-immolative linkers led to an expansive idea of combining several of these linkers successively to create macromolecular structures.[25] Self-immolative oligomers and dendrimers were introduced in the early 2000's. These macromolecular structures were developed in an attempt to amplify responsiveness of self-immolative linkers to stimuli. Self-immolative oligomers consist of several linkers covalently bonded together, typically as dimers or trimers. Self-immolative dendrimers are composed of

repeated branches that are organized in concentric layers called "generations" around a central core or focal point.[26] Both have been investigated for applications in drug delivery.

In 2001, Scheeren and coworkers published the first self-immolative oligomer consisting of derivatives of naphthyl and biphenyl moieties that underwent a cascade elimination mechanism similar to that of the earlier aminobenzyl alcohols (Scheme 2a).[27] These linkers, along with *p*-aminobenzyl alcohol linker, can be successively bonded together by carbamate bonds into oligomers. The terminal amine can be deprotected, resulting in successive 1,10-elimination decarboxylation reactions to release a LG (Scheme 2b).
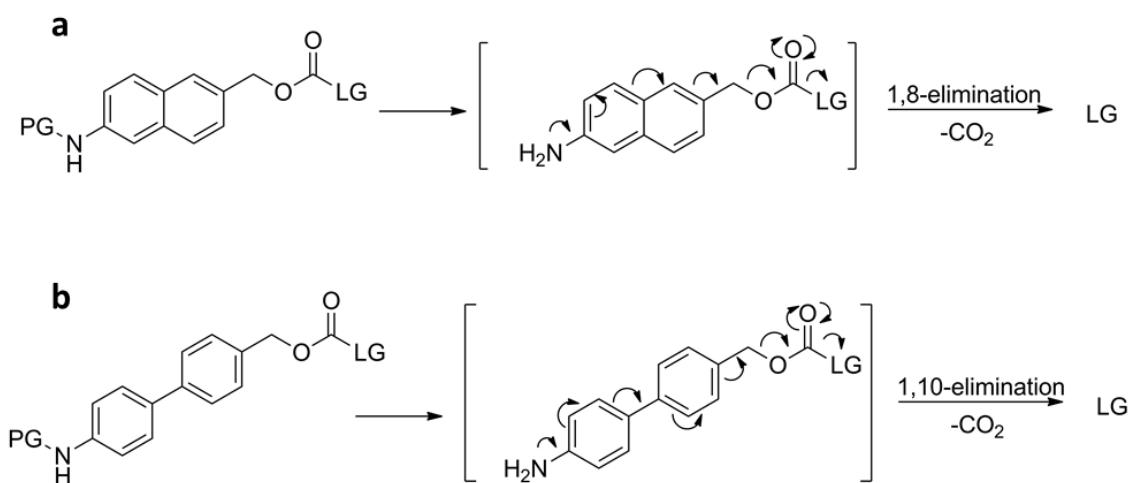
Scheme 2. **(a)** 1,8-elimination mechanism of a naphthyl-based linker and **(b)** 1,10-elimination mechanism of a biphenyl-based linker.

Unfortunately, it was shown that the naphthyl and biphenyl systems failed to undergo the hypothesized elimination cascades. It was hypothesized the energetic cost in dearomatizing the systems in the 1,8- and 1,10-eliminations were too high to achieve a rapid reaction. The aminobenzyl alcohol oligomer, however, could successfully undergo consecutive elimination decarboxylation mechanisms to release a payload. The ratio to stimulus events to molecules of cargo released in these systems is still 1:1, but it laid the ground work for future linear and dendritic systems for signal amplification.

In 2008, Kratz developed the first self-immolative oligomer system that showed increased drug release rates by amplification of stimulus.[28] Kratz's oligomer was based

on a similar 1,6-elimination mechanism as above, but the model drug was also conjugated to the aromatic moieties such that they could be released via 1,4-elimination reactions. The stimulus could be amplified in this system due to multiple molecules of model drug being released for one deprotection reaction (Scheme 3). Three equivalents of a carbamate-linked cargo moiety could be released upon a single stimulus event.
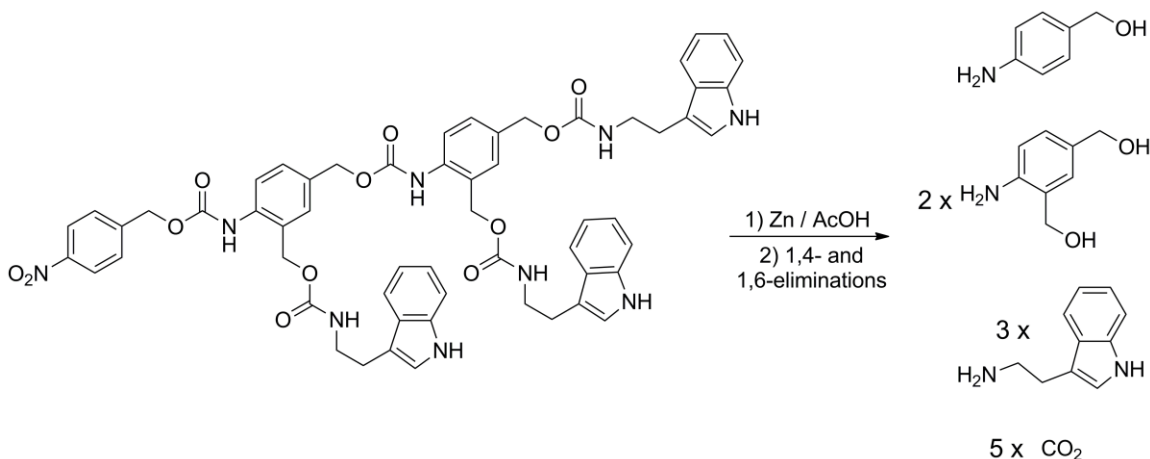
Scheme 3. A self-immolative oligomer capable of 1,6-eliminations through its backbone and 1,4-eliminations of pendant groups.

As the development of self-immolative oligomers continued, another class of self-immolative macromolecular structures were being investigated. In 2003, the first self-immolative dendrimeric system was reported by McGrath and coworkers.[26] A dendrimer consists of repeated branches organized into layers all stemming from a common focal point. McGrath's group used a 2,4-bis(hydroxymethyl)phenol monomer with each generation linked in succession (Scheme 4). Through cleavage of an allyloxybenzyl ether group at the focal point, the cascade elimination that followed released four nitrophenol molecules.
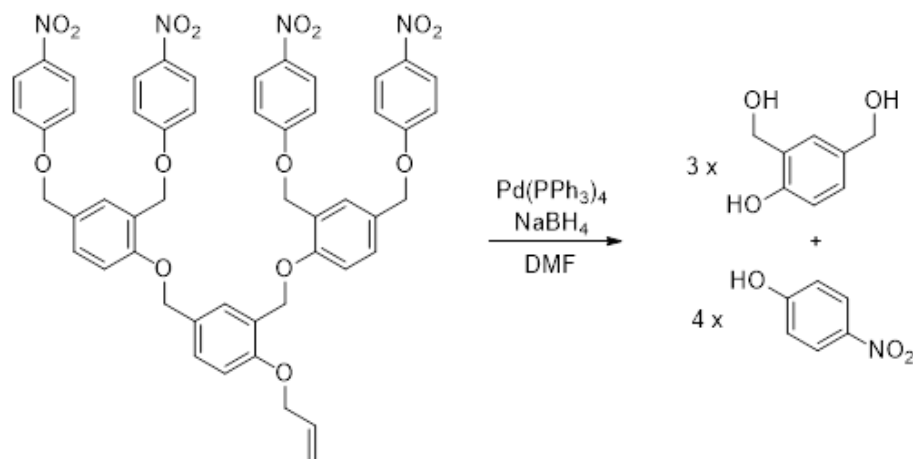
Scheme 4. Example of 2,4-bis(hydroxymethyl)phenol-based dendrimer.

Once again, the self-immolative nature of this system relied on an elimination cascade that propagates through several conjoined fragments to eliminate a cargo molecule. The major advantage to dendrimeric systems is their amplification of the stimulus. With McGrath's early dendrimer, one stimulus event at the focal point allyl ether led to the release of four equivalents of cargo molecule, *p*-nitrophenol. However, the difficulty surrounding dendrimers is their cumbersome synthesis procedures. In addition, the number of generations eventually reaches a maximum due to steric hindrance, leading to a limit in how much cargo can be conjugated and released.

Dendrimeric structures continue to be investigated as drug delivery vehicles with promising properties.[25, 26, 29] With the development of self-immolative oligomers and dendrimers in place, the next logical step was to investigate SIPs as potential stimuli-responsive materials.

1.2.4 Self-Immolative Polymers

SIPs are able to amplify a polymer's sensitivity to a stimulus by only requiring a single stimulus event to initiate a spontaneous chain depolymerization reaction.[30] These polymers can be stabilized by protecting their ends with a stimuli-responsive small molecule. This is called "end-capping". Once a SIP has been properly end-capped, it can then be handled under ambient conditions without significant degradation (Figure 7).

However, cleavage of the end-cap results in end-to-end depolymerization by a cascade of reactions.
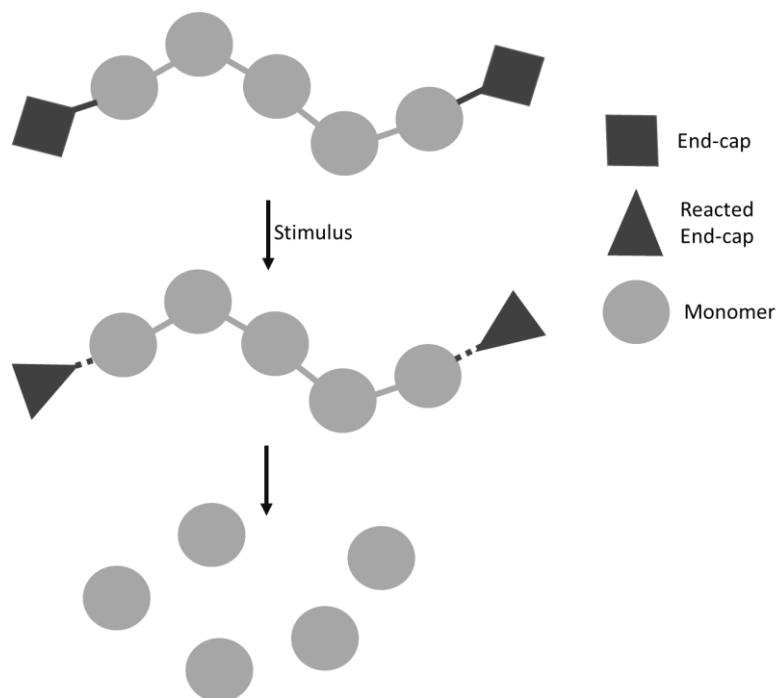
Figure 7. End-capped stabilized SIP subjected to end-cap cleavage followed by depolymerization.

Small molecules used to end-cap polymers that show specific stimuli-responsive behavior are termed stimuli-responsive end-caps. End-caps have shown sensitivity to a range of stimuli including chemical, ultraviolet (UV) light, pH, temperature and redox potential.[30, 31] In each case, the stimulus triggers a specific chemical reaction at the end-cap leading to detachment from the polymer. The polymer, no longer protected, undergoes a rapid end-to-end depolymerization.

To date there are two subclasses of SIPs that are distinguished by the mechanism that governs their depolymerization. The first class of SIPs spontaneously degrade into products that are different from the monomers used to synthesize the polymer.[32, 33] Depolymerization is favored and happens spontaneously due to the stability of the degradation products. The second class of SIPs is governed by the polymer's low ceiling temperature (T_c). Upon cleavage of these stimuli-responsive end-caps, entropy drives

depolymerization of the polymer back to monomer units.[34] This phenomenon can be better understood by examining thermodynamics of polymerizations.

From the Gibbs free energy equation, the free energy of a polymerization reaction is the sum of both the enthalpic and entropic contributions (eq. 1).

$$\Delta G = \Delta H - T\Delta S \qquad \text{eq. 1}$$

$$\Delta G = \Delta H - T\Delta S = 0 \qquad \text{eq. 2}$$

$$T = \Delta H/\Delta S = T_c \qquad \text{eq. 3}$$

For a given monomer with a set concentration, the enthalpy and entropy are fixed and specific to that monomer. Therefore, the only variable that can be manipulated is the temperature. An appropriate temperature must be found to make ΔG negative giving a spontaneous reaction of monomers into polymer. Furthermore, there must exist a temperature where $\Delta G = 0$ (eq. 2) and the system is in equilibrium. In other words, the rate of polymerization is equivalent to the rate of depolymerization. At $\Delta G = 0$, temperature can be calculated by the ratio of ΔH and ΔS (eq. 3). This is called the polymer's T_c. At temperatures above a polymer's T_c, the rate of depolymerization is faster than the rate of polymerization. Conversely, at temperatures below the T_c of a polymer, the rate of polymerization is faster than the rate of depolymerization. This principle can also be represented graphically (Figure 8).[35]
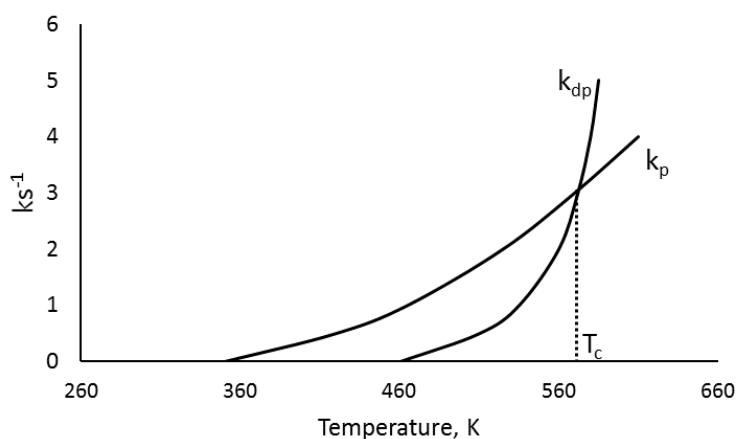
Figure 8. Rates of depolymerization and polymerization as a function of temperature. They intersect at the T_c.

The second class of SIPs takes advantage of polymers with lower than ambient T_c. The monomers are first polymerized below their T_c, allowing for the growth of long chains. Then, before the material is allowed to warm, the ends of the polymer chains are capped with a stimuli-responsive small molecule to trap the polymer chains and stabilize the system. The material can then be warmed to temperatures higher than the T_c and can be manipulated for different applications. When this material is subjected to its responsive stimulus at ambient temperatures, the stabilizing end-cap substituents are removed and the material spontaneously degrades.[36] The major advantage to SIPs is their ability to amplify the response to a stimulus. One cleavage event at a polymer end-cap leads to complete end-to-end depolymerization of the entire polymer chain. In 2008, Shabat reported the first SIP, which belongs to the first class of SIPs. The Shabat polmyer consisted of a polycarbamate backbone that upon removal of the bis(trimethylsilyl)acetamide-responsive end-cap, underwent a domino-like 1,6-elimination-decarboxylation cascade, resulting in complete degradation of the macromolecule into carbon dioxide and azaquinone methide (Scheme 5).[18] Altering the sensitivity of the end-caps to a variety of stimuli yielded a material that could be triggered to degrade in response to different triggers. The versatility of these materials has provided efficacy in a multitude of areas including drug delivery, bio-sensors, agriculture, and consumer products.[37-40]
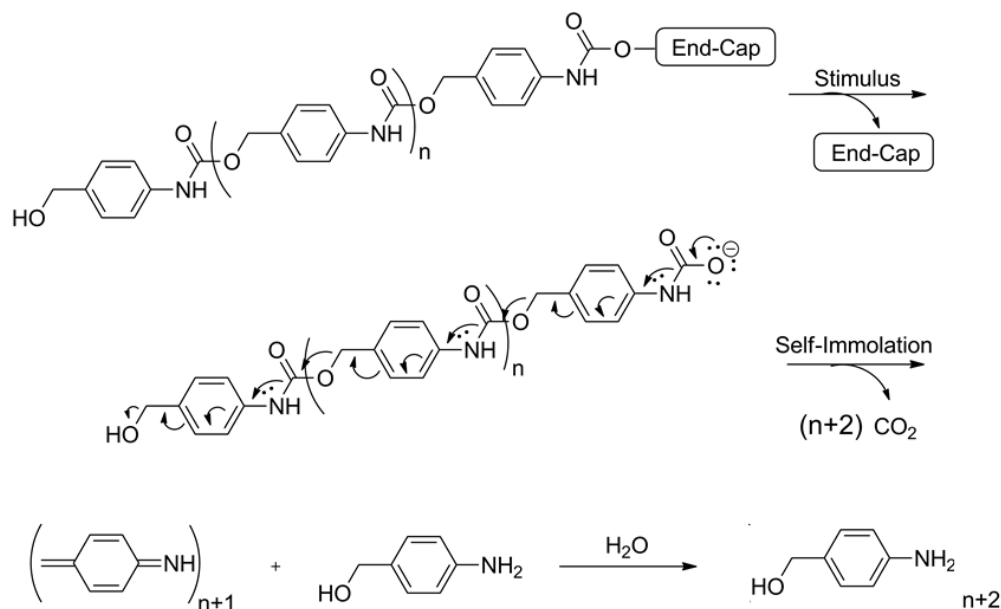
Scheme 5. Degradation mechanism of a polycarbamate-based SIP.

In 2009, Dewit and Gillies reported another carbamate-based SIP that degraded through alternating intramolecular cyclization and 1,6-elimination reactions (Scheme 6).[41] The backbone consisted of alternating *N,N'*-dimethylethylenediamine and 4-hydroxybenzyl alcohol units linked through carbamate bonds. A *tert*-butylcarbamate (Boc) group was used to protect the terminal amine as a model end-cap. The polycarbamate was stable in aqueous solution, but upon removal of the Boc group from the amine, an intramolecular cyclization revealed the phenol to undergo a 1,6-elimination followed by a decarboxylation to yield a consecutive free amine. The cascade continued from end-to-end until the polymer completely degraded into *N,N'*-dimethylimidazolidinone, CO_2, and 4-hydroxybenzyl alcohol products. The intramolecular cyclization step was the slower, rate determining step in the degradation mechanism. In follow-up work, the insertion of different cyclization reactions was used to tune the rate of depolymerization.[42]
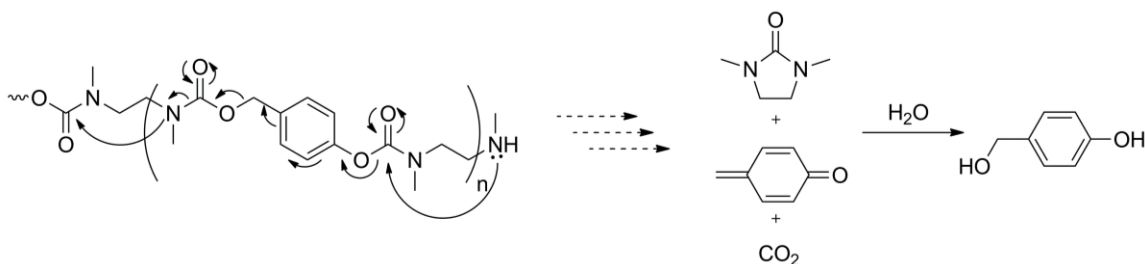
Scheme 6. Cyclization depolymerization mechanism of a SIP.

Phillips furthered the versatility of the SIP backbones by developing a polyacetal SIP based on phthalaldehyde (Scheme 7).[43] This backbone belongs to the second class of SIPs, with degradation governed by the low T_c. By using a chloroformate derivative of 6-nitroveratrole, a polyphthalaldehyde-based SIP that exhibited responsivity to UV light was produced. His group later showed this polymer was capable of forming microparticles that could be triggered to release a cargo upon introduction of UV light.[44,45] Due to the low T_c of polyphthalaldehyde (PPHA), polymerization of the dialdehyde was carried out at -78 °C. The end-cap reaction of terminal hemiacetal was conducted before the material was allowed to warm to room temperature. They also proved control over molecular weights by correlating the M_n to the concentration of the initiator. At ambient temperatures, just 30 minutes of UV radiation reduced the weight percent (wt%) of polymer coatings by 90%.
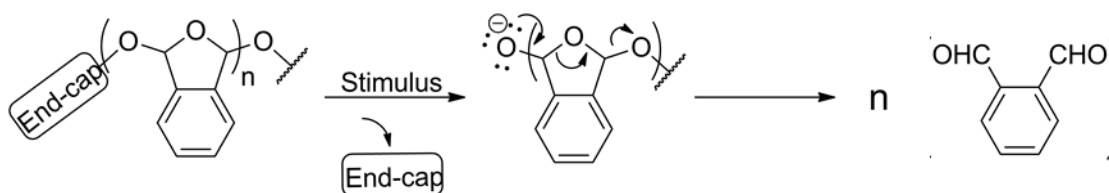
Scheme 7. Degradation mechanism of polyphthalaldehyde.

While the above backbones are promising and in further development, the degradation products of these SIPs are known to show toxicity *in vitro*. This has made the use of SIPs as potential drug delivery materials difficult. However, over the past several years, Gillies has developed another polyacetal SIP, poly(ethyl glyoxylate) (PEtG), that holds the potential to be non-toxic.[46] Similar to PPHA, PEtG is a polyacetal SIP with a low T_c of around -5 °C. The polymerization is carried out at -40 °C to -20 °C in the presence of a

catalytic amount of triethylamine (TEA) (Scheme 8a). Our current hypothesis is that TEA acts as a proton shuttle during the polymerization. The polymerization is believed to initiate from trace amounts of hydrate present in the monomer solution. At room temperature, non-end-capped PEtG chains spontaneously depolymerize back to ethyl glyoxylate monomer units (Scheme 8b).
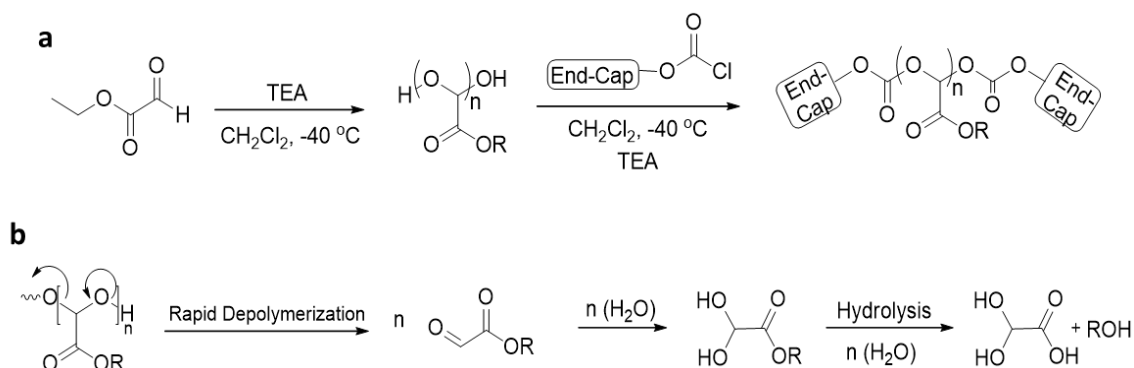
Scheme 8. **(a)** Synthesis of PEtG and **(b)** Depolymerization mechanism for PEtG and subsequent hydration/hydrolysis of the corresponding small molecules.

The hemiacetal ends can be capped by the addition of chloroformate derivatives of stimuli-responsive small molecules, creating carbonate linkages between the polymer and end-cap. The most promising feature of PEtG is that *in vitro* these monomers ultimately degrade into glyoxylic acid hydrate and ethanol, both of which should be relatively nontoxic and can be processed by the human body.[47] It is hypothesized that drug delivery vehicles manufactured from PEtG could provide an SIP-based DDS in the form of polymeric self-assemblies.

For PEtG to be a viable drug delivery material, the polymer needs to be stable in biological conditions of 37 °C. To achieve this, the hydroxyl end groups of the polymer are stabilized by reacting them with stabilizing small molecules. These molecules protect the reactive ends of the polymer and hinder end-to-end depolymerization, resulting in a polyacetal that is quite stable at physiological pH and temperature. A range of end-caps have been reported for this purpose. The few that are important to this thesis are benzyl chloroformate (BnCF), which is non-responsive and serves as a control (**1.18**); 6-nitroveratryl chloroformate (NVOC-Cl), which is sensitive to UV light (**1.19**); and 2-(pyridine-2-yl-disulfanyl)ethyl chloroformate (PDS-Cl), which is sensitive to reducing

conditions (**1.20**) (Figure 9).[48] These molecules react with hemiacetal alcohols at the termini of the polymer to yield BnCO-, NVOC-, and disulfide-capped PEtG polymers. It has been shown in previous work by Gillies and coworkers that these end-caps stabilize the PEtG polymers and allow them to withstand temperatures over 120 °C without degradation in the dry state.
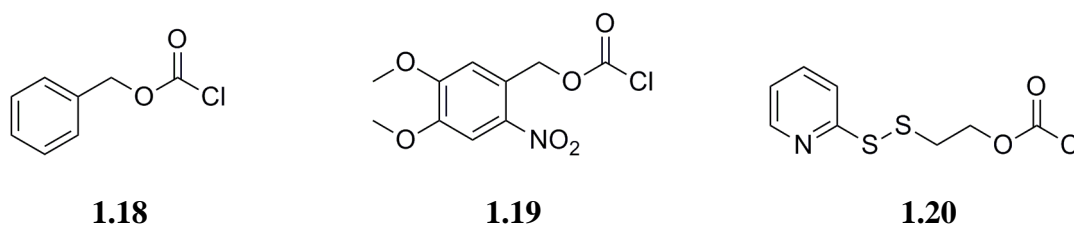
Figure 9. Chloroformate-based molecules for end-capping PEtG.

From the past decade of research into SIPs as potential candidates for stimuli-responsive DDSs, it is hypothesized that PEtG could be a promising material in this field due to its amplified response to stimuli and its potentially non-toxic degradation products.

1.3 Polymeric Drug Delivery Systems

One important potential application of SIPs is in polymeric DDSs. Polymer assemblies including micelles, worm-like micelles, vesicles, and solid-core particles have been extensively researched and developed for biomedical and drug delivery purposes. PLA, PGA, PCL, PEO and their copolymer assemblies have been extensively applied towards drug delivery research with varying degrees of success.[49-52] From decades of polymeric self-assembly research, several important features for an efficient polymeric DDS have been determined. First, the polymer must exhibit an acceptable host response and its degradation products must be considered non-toxic.[53] Second, there is a specific range of sizes for a DDS to ensure it does not get cleared from the body before it can deliver its payload.[54] Third, the DDS must be capable of carrying significant loads of cargo and also releasing their cargo in the short time frame they remain in circulation.[55] DDSs that do not meet at least these criteria, show inefficient treatment results *in vivo*.[56]

1.3.1   Self-Assembled Nanostructures

Lipid-based vesicles were among the first nanotechnology DDSs.[16] These structures consist of a self-assembled sphere of phospholipids that surround a water droplet. It is well understood that when phospholipids are placed in an aqueous environment, they spontaneously arrange themselves in order to minimize unfavorable hydrophobic-hydrophilic interactions. This creates a bilayer where the hydrophobic tails of the phospholipids are close to one another and oriented away from the aqueous surroundings. This leaves the hydrophilic heads of the phospholipids arranged outward toward the aqueous surrounds. Ultimately, spherical structures are formed with the inside filled with the aqueous media (Figure 10a).
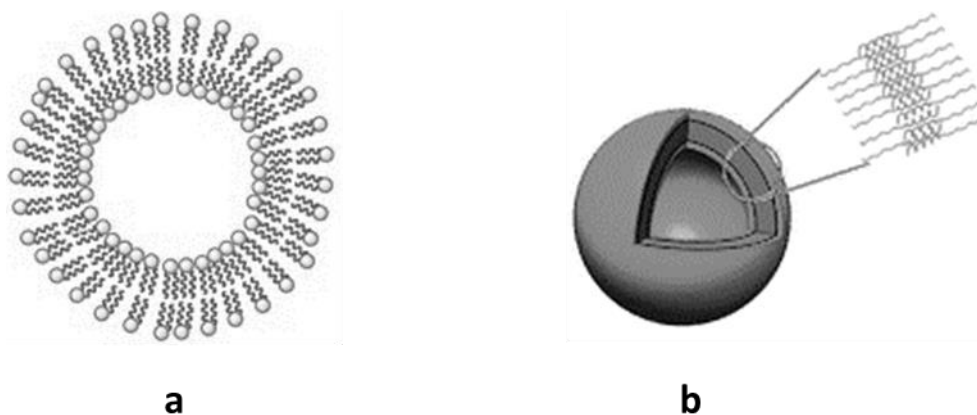
Figure 10. (a) Self-assembled phospholipid liposome and **(b)** Self-assembled polymersome.

Similar structures can be made using other biologically-based materials that possess amphiphilic properties including polypeptides (Figure 10b) and polysaccharides.[57] These technologies have seen much clinical success due to their biocompatibility and low toxicity *in vivo*.

Similar to amphiphilic phospholipids and polypeptides, polymers also exhibit self-assembling behavior in solution. Polymers with amphiphilic properties orient themselves to minimize unfavorable interactions with the surrounding solvent. Amphiphilic polymers are typically made by sequential polymerization of hydrophobic block and hydrophilic blocks or by the conjugation of these blocks post-polymerization. Depending on the ratio of the blocks, different self-assembled structures can be made.[58] With a higher fraction of

hydrophilic block, micelle structures are typically formed (Figure 11a). With a higher fraction of hydrophobic block, vesicle structures are often formed (Figure 11c). Marginal differences in the hydrophobic:hydrophilic ratio lead to intermediate structures like the worm-like micelle (Figure 11b). For hydrophobic homopolymers, solid-core particles form and can be suspended in aqueous solution by the addition of a surfactant to coat the surface of the particles (Figure 11d).
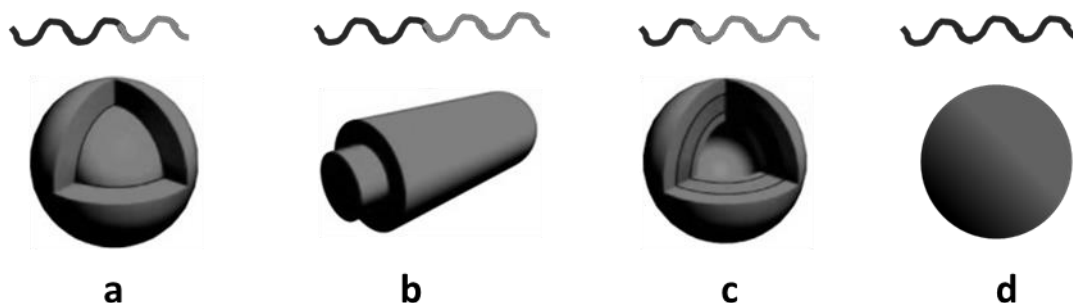
Figure 11. Examples of self-assembled architectures based on polymers containing different ratios of hydrophobic and hydrophilic blocks.

Biodegradable polymers can serve as alternatives to lipids. One benefit of using polymers is their degradability can be tuned to control when and/or how fast a drug is released. The common polyesters, PLA, PGA and their copolymers have been the most widely studied for drug delivery.[8, 13, 50] Degradation rates can be tuned in the range of weeks to years using different compositions of these polymers. A major drawback is their relative instability in blood compared to liposomal counterparts. Intravenous injection being one of the most effective ways to treat disease, it is important to understand and develop DDSs capable of withstanding the blood stream.[59]

1.3.2   Clearance of DDSs from the Body

When a therapeutic drug delivery vehicle is administered into a person's blood stream, a number of biological factors diminish or limit the overall efficacy of the DDS.[53] Depending on how the DDS are administered into the body, they must bypass a number of barriers in order to reach their therapeutic target. The body is effective at identifying foreign objects within and has a variety of effective ways it can clear the system of these foreign bodies. An intravenously administered DDS must make its way through a myriad

of immune response cellular pathways and blood filtering organs before ultimately making it to the targeted tissue.[60] The barriers inherent to intravenous injection pose a challenge for virtually all intravenously administered DDS. Specifically, the challenge of how to effectively dose and get the physical drug to the tissue of concern before the host removes them from the body.

One of the most important factors influencing a DDS's ability to remain circulating in the blood stream is its size.[61, 62] Particles smaller than 20 nanometers in diameter will be removed from circulation by the reticuloendothelial system (RES) and kidneys within a few hours of injection. Particles with a diameter greater than 300 nanometers begin to accumulate in the spleen and liver within minutes of injection.[58] Therefore, to maximize blood circulation time of a drug loaded DDS, the average size of the particles should be around 100 nm. This size should be sufficiently large to avoid filtration by the kidneys and slow the opsonization process of macrophages in the RES. It also should be small enough to avoid being filtered by blood filtration organs like the spleen and liver.[63]

Based on these criteria, it is difficult to design a polymeric DDS that can effectively shuttle a cargo to a target tissue before it is cleared from the body. First, the rate of degradation needs to compete with the rate of clearance of the particles from circulation.[64] If the rate of degradation is too slow and a significant amount of drug remains trapped inside the particles as they are cleared from the blood, incomplete administration could occur. Blood circulation times of nanoparticles (NPs) are on the order of hours; thus, degradation times need to be on the same timeframe. Second, current stimuli-responsive DDSs rely on many stimulating events for complete release of cargo. Stimuli-responsive polymers such as those discussed above require a high concentration of stimulus due to the many stimulus-polymer interactions required for degradation. In target tissues lacking a strong concentration of stimulus, these systems may be inefficient at releasing cargo.[65]

The development of SIPs could potentially address these difficulties. Self-immolative polymeric DDSs respond to low concentrations of specific stimuli leading to rapid release of a payload in specific environments.[48] This provides an amplified response to stimulus

that is lacking in current polymer DDSs. The rapid depolymerization rates of SIPs also negates the concern of clearance before the cargo is released.[66]

1.3.3   Efficiently Delivering Cargo

One of the most difficult problems regarding drug development is low solubility of hydrophobic drugs in aqueous environments. It has been estimated that 40% of active compounds identified through combinatorial screenings show poor water solubility[67]. Poor solubility of hydrophobic drugs leads to complications including variable bioavailability, slow onset of action and poor performance. This leads scientists to either alter the design of the drug to increase its water solubility or to simply discard the molecule all together. Polymeric DDSs aim to increase drug bioavailability and effectiveness while also reducing drug toxicity by introducing a method to control release.[68] Polymer DDSs have proven to be an effective method to overcome the difficulty of poorly soluble pharmaceutics. This is accomplished by either encapsulating the drug within a hydrophobic polymer nanostructure or covalently binding the drug to a water-soluble polymer via labile bonds that can be broken *in vivo*.[69]

NP-based DDSs in particular have emerged as effective methods for overcoming the pharmacokinetic limitations of poor solubility and drug toxicity of medicaments. In these DDSs, drugs can exist as a reservoir in the circulatory system with drug continually being delivered to target tissue over time. Elongated circulation time led to the discovery of an important characteristic of tumor cells, the enhanced permeability and retention effect (EPR).[70] The EPR is a phenomena observed when macromolecules, circulating in the blood, demonstrate a heightened accumulation in tumors due to leaky vessels in these tissues. This effect gives a passive targeting capability to NP DDSs for the delivery of chemotherapeutics to tumors via the blood stream.

1.3.4   Emulsion Evaporation Technique for Nanoparticle Synthesis

Several methods exist to produce NPs in the range of $10 - 300$ nm. For hydrophobic homopolymers, the general approach for the preparation of a DDSs is to encapsulate a hydrophobic drug within a hydrophobic solid-core polymer particle that is dispersed in

aqueous solution using surfactants.[71] This approach often utilizes the oil-in-water (o/w) emulsion-evaporation technique for the manufacturing of polymeric NPs (Figure 12).[72]
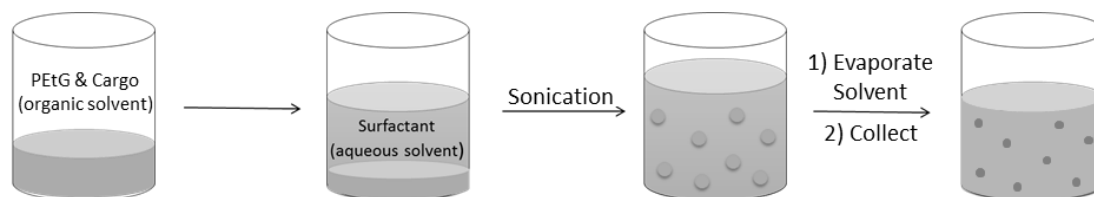
Figure 12. O/W emulsification for the encapsulation of a hydrophobic cargo within solid-core polymeric NPs.

In an o/w emulsion, the hydrophobic polymer is first dissolved in an organic solvent. Separately, an amphiphilic surfactant molecule is dissolved in the aqueous phase. The oil phase is then added to the water phase and a form of mechanical energy such as stirring or ultrasonication is introduced to produce the emulsion. After an emulsion is obtained, the organic solvent is evaporated out of the nanodroplets leaving a suspension of polymer coated with surfactant dispersed in the aqueous media.[73]

The surfactant's purpose is to serve as a stabilizer between the hydrophobic polymer particle with the surrounding aqueous environment. The surfactant allows for the oil phase droplets to suspend in the aqueous environment upon formation. The organic phase contains the polymer along with the hydrophobic cargo. The organic solvent is then slowly removed by evaporation while stirring. After complete removal of the organic phase, the particles remain suspended in the aqueous solution by a coating of surfactant.

1.4 Applications of SIPs in DDSs

In terms of drug delivery, polymeric NPs have been shown to improve drug targeting capabilities, decreasing drug toxicity and increasing efficacy in a variety of different hydrophobic therapies.[74] These benefits are highly sought after for treatments of certain diseases such as cancer with cytotoxic medicaments. Often, a chemotherapeutic is administered systemically with the hope that the majority of chemotherapy will make its way to infected tissue before it affects healthy tissue. It is unavoidable that some healthy tissues will be affected in this method of administration leading to the unwanted side-effects associated with chemotherapy treatments. Stimuli-responsive polymer NPs have

the potential to provide a way to not only target specific areas of the body, but to also provide a "smart" characteristic to the drug. Upon encountering a certain stimulus related to the target site, the "smart" system will release its cargo.[69]

To date, only a handful of SIP systems demonstrating potential for controlled release have been reported. The first reported polymeric self-assembling system featuring a SIP was by Dewit and Gillies in 2009.[41] Their polycarbamate SIP, which was discussed in section 1.2.4, was end-capped with poly(ethylene oxide) (PEO) through an ester linkage providing an amphiphilic block copolymer. This copolymer was found to self-assemble into NPs capable of encapsulating and subsequently releasing a fluorescent dye in aqueous solution. This proof-of-concept application opened the door to other stimuli-responsive SIP delivery systems.

In 2010, Moore developed a microcapsule composed of a self-immolative poly(benzyl carbamate) (PBC) similar to the polycarbamate reported by Shabat (Scheme 9). Pendant protected alcohol moieties were conjugated to the aromatic rings. After polymerization of the monomer, the polymer was end-capped with either a fluorenylmethyloxycarbonyl (Fmoc) or *tert*-butyloxycarbonyl (Boc) group. The pendant alcohols were then deprotected and converted to isocyanates. From here, microcapsules were synthesized via an interfacial polymerization reaction between the isocyanates and 1,4-butanediol.[75] To a solution containing a surfactant was added the PBC. The PBC was dissolved in etheylphenylacetate (EPA), which made up the core of the microcapsules. An emulsion was formed between the two solvents and the resulting emulsion was heated at 70 °C for 1.5 h. Microcapsules in the 5 – 40 µm size range were produced using this method (Figure 13).
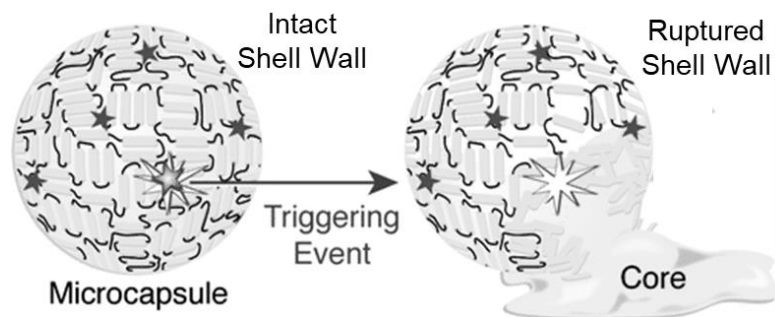
Figure 13. PBC-based core-shell microcapsules. (Reprinted with permission from Moore *et. al.*, 2010. Copyright 2017 American Chemical Society.)
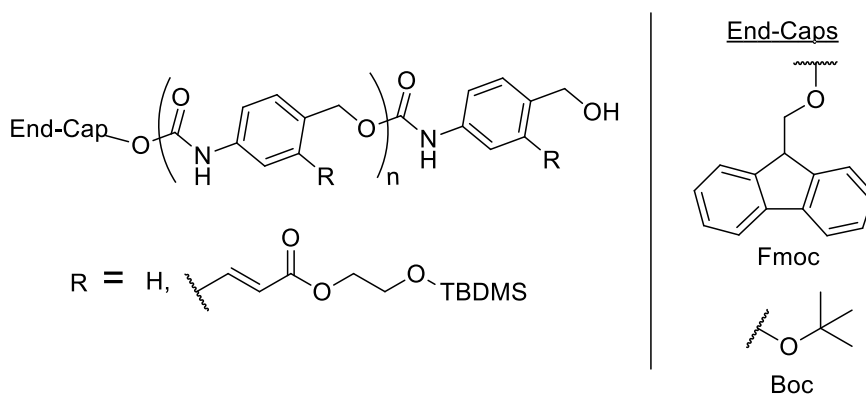
Scheme 9. A PBC with pendant tert-butyldimethylsilyl-protected alcohols.

Upon Boc or Fmoc removal by the addition of HCl or piperidine respectively, the capsules were degraded. To measure the degradation, the amount of EPA released was monitored by gas chromatography. Under these conditions, it was found that close to 100% of the contents were released within 48 h whereas controls showed less than 10% release.

The Phillip group developed and used PPHA to manufacture microcapsules capable of carrying a hydrophilic cargo dissolved in an aqueous environment.[45] An improvement to the Moore's method was the use of flow-focusing microfluidics which gives control over

the thickness of the microcapsule shell. A microfluidics device used a pump to push a water-soluble cargo dissolved in an aqueous, surfactant-containing solution through an organic, polymer-containing solvent well. With control of the flow rate, droplets of aqueous phase are coated with polymer-containing organic phase. These particles then passed through the organic phase into a separate aqueous phase. The microcapsules can then be collected and remaining organic solvent evaporated from the shell. PPHA microcapsules were made with responsiveness to fluoride by capping the PPHA terminus with a silyl ether moiety with similar cargo release rates observed.

More recently, Liu reported amphiphilic block copolymers that incorporated a hydrophobic, polycarbamate SIP block conjugated to a hydrophilic poly(dimethyl acrylamide) (PDMA) block (Scheme 10, Figure 14).[76] Using self-assembly techniques, self-immolative polymersomes (SIPsomes) around 250 nm in diameter were manufactured with the capability of encapsulating both hydrophilic and hydrophobic cargos. Hydrophilic cargos were dissolved in the aqueous core while hydrophobic cargos were encapsulated in the hydrophobic polymer shell. Several stimuli-responsive end-caps were used to manufacture SIPsomes capable of triggerable degradation to visible light, UV light, and reduction (Scheme 10).
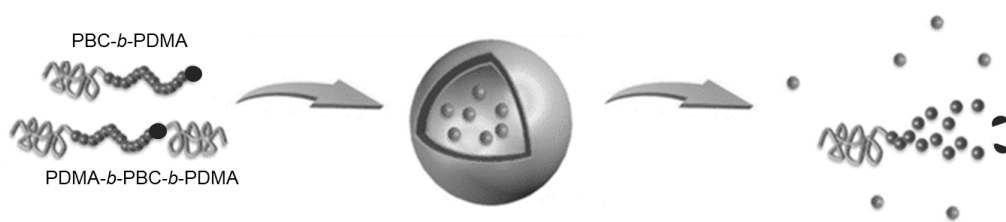
Figure 14. PBC-PDMA multi-block copolymer SIPsomes and their triggerable cargo release. (Adapted with permission from Liu *et. al.*, 2014. Copyright 2017 American Chemical Society.)
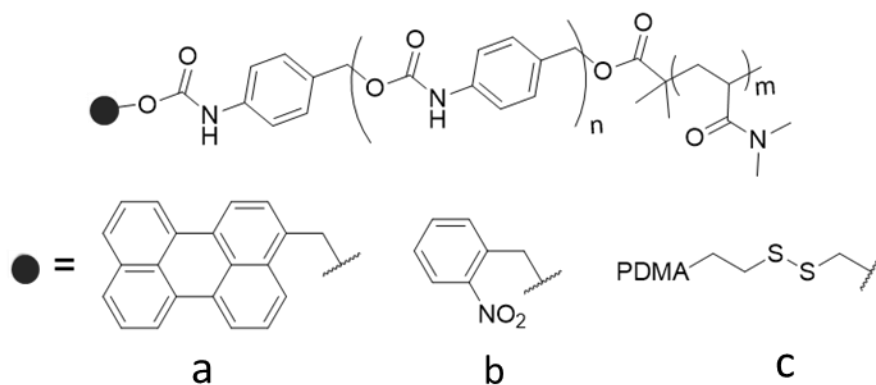
Scheme 10. (a) visible light, **(b)** UV light, and **(c)** reduction-sensitive PBCs.

To take advantage of the dual loading potential of this system for combinational therapy, a co-encapsulation of hydrophobic camptothecin (CPT) and hydrophilic doxorubicin (DOX) was done. For end-capped polymers responsive to reduction, controls showed only ~4% DOX and ~19% CPT released over 20 h. Upon the addition of 31 mmol glutathione (GSH), a biological reducing agent, ~86% DOX and ~82% CPT were released over the same timeframe.

Gillies and coworkers recently showed the promising application of PEtG as a drug delivery vehicle.[48] The promising advantage of PEtG is that the degradation products (*i.e.,* ethanol and glyoxylic acid) have the potential to exhibit low toxicity. PEtG was end-capped with modified linker end-caps capable of conjugating to PEO to form amphiphilic block copolymers. These modified end-caps were still capable of undergoing their respective stimuli-responsive reactions, resulting in triggered degradation of the SIP blocks. These block copolymers were self-assembled to form micellular NPs capable of encapsulating hydrophobic cargos (Figure 15).

Figure 15. Stimuli-responsive NPs based on a triblock SIP. (Reprinted with permission from Gillies *et. al.*, 2017. Copyright 2017 American Chemical Society.)

These particles showed triggerable degradation in response to thiol reducing agents, UV light, H_2O_2 and combinations of these depending on the linker end-caps used. Nile red, DOX, and curcumin were all lo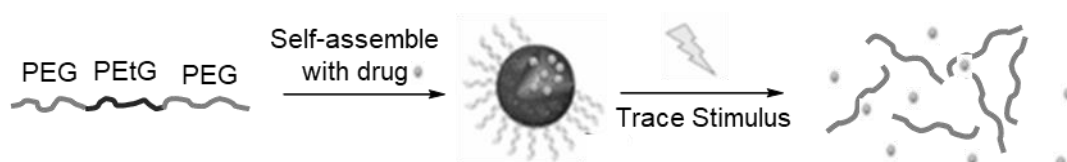aded into the particle cores. Their release in response to stimulus was measured. The disulfide-capped PEtG showed appreciable payload release in concentrations of stimulus, such as dithiothreitol (DTT), as low as 0.1 mM over 48 h and close to complete release at higher concentrations of the stimulus (10 mM) over the same timeframe. Similar studies were conducted using various responsive end-caps concluding triggerable release of cargo with different stimulants simply by altering the PEtG end-cap.

1.5   Thesis Objectives

The objective of this work was to prepare and study surfactant-coated PEtG solid-core particles for drug delivery. In contrast to the NP systems described above, this does not require the preparation of block copolymers. The first goal was to optimize conditions for generating PEtG NPs. In particular, we targeted a reproducible method providing a mean particle diameter (Z-avg.) of ~100 nm for the reasons described above. The size and morphology was characterized by dynamic light scattering (DLS) and transmission electron microscopy (TEM).

Additionally, PEtG was blended with varying ratios of PLA. As discussed above, PLA is a well-known and established biocompatible and biodegradable polymer. It was hypothesized that the addition of this polymer to create PLA-PEtG blends would increase the hydrophobicity and rigidity of the NP cores allowing for tunable rates of release to this DDSs based on wt% PLA. Each PLA-PEtG blend was characterized by thermogravimetric analysis (TGA) and differential scanning calorimetry (DSC) in order to determine the phase separation behavior of these polymers.

After determination of the synthetic route and characterization of these particles, the focus shifted toward testing the stimuli-responses behavior of these solid-core PLA-PEtG particles. A fluorescent small molecule was used as a molecular probe to test for triggerable release of a hydrophobic cargo. Furthermore, a model drug was encapsulated and the release kinetics studied. Investigation into the optimal loading efficiency and

percent weight cargo was determined for drug-loaded PLA-PEtG NPs. Triggerable release was tested using a UV-responsive end-cap. This end-cap serves as an ideal model system as it can be cleanly and rapidly removed by irradiation with UV light. However, in most applications, it would not be possible to apply UV light *in vivo*. Therefore, to further investigate the possibility of triggering release using biologically accessible triggers, an end-cap responsive to reducing agents was also investigated as a potential triggerable end-cap.

Finally, the triggerable release of drug-loaded PLA-PEtG NPs was tested *in vivo* in MDA-MB-231 cells. 3-(4,5-dimtheylthiazol-2-yl)-2,5-diphenyltetrazolium bromide (MTT) assays will be conducted to test for viability of this cell line treated with drug-loaded PLA-PEtG particles.

2 Experimental

2.1 General Procedures and Materials

6-Nitroveratryl carbonate end-capped poly(ethyl glyoxylate) (NVOC-PEtG) (M_n = 70,000 g/mol, $Đ$ = 2.4), benzyl carbonate end-capped poly(ethyl glyoxylate) (BnCO-PEtG) (M_n = 56,000 g/mol, $Đ$ = 1.6), 2-(pyridine-2-yl-disulfanyl)ethyl carbonate end-capped poly(ethyl glyoxylate) (disulfide-PEtG) (M_n = 24,000 g/mol, $Đ$ = 1.4) were prepared as previously reported.[46] All other chemicals were obtained from commercial suppliers and used without further purification. TGA was performed on a Q50 from TA Instruments with the following conditions: heat rate of 10 °C/min ranging from 35−500 °C under nitrogen atmosphere. Size-exclusion chromatography (SEC) was performed in THF at 1 mL/min using a viscotek GPC Max VE2001 solvent module equipped with a Viscotek VE3580 RI detector operating at 30 °C, two Agilent Polypore (300x7.5mm) columns, and a Polypore guard column (50x7.5mm). A calibration curve was obtained using polystyrene standards. Fluorescence spectra were obtained using a QM-4 SE spectrometer from Photon Technology International equipped with double excitation and emission monochromators. UV-visible spectra were obtained on a Varian UV/Vis Cary 300 spectrophotometer. Centrifugation was performed using a Clinical 200 VWR centrifuge at 6000 rpm. Ultrapure water was obtained from a Barnstead EASYpure II system. Sonication was conducted using a Branson 450 digital sonifier. Spectra/Por regenerated cellulose membranes were used for dialysis. 0.22 µm Acrodisc Syringe Filter Non-Pyrogenic 13 mm were used to filter all particle suspensions.

2.2 Preparation of Poly(ethyl glyoxylate)-poly(D,L-lactic acid) Blends

Poly(ethyl glyoxylate)-poly(D,L-lactic acid) (PLA-PEtG) blends were made by combining 9.0, 7.0 and 5.0 mg PEtG with 1.0, 3.0 and 5.0 mg, respectively, of PLA to obtain blends that were 10, 30 and 50 wt% PLA. These polymer samples were then dissolved in dichloromethane (1 mL) and stirred for 30 min to allow for complete mixing of the polymers.[77] The solvent was removed *in vacuo* for analyses.

2.3 Method for Preparing Nanometer-sized Particles

PEtG (10.0 mg) was dissolved in dichloromethane (1 mL). A separate solution of sodium cholate (50 mg) was prepared in distilled water (10 mL) for a final concentration of 12 mM. The organic phase was added to the aqueous phase by glass pipette into a 20 mL glass vial. The sonication amplitude was set to 10% on a Branson 450 digital sonifier. The biphasic mixture was then sonicated for three 30 s intervals with 10 s breaks in between for a total of 90 s of sonication over 120 s.[78] To the resulting emulsion mixture, a magnetic stir bar was added and the solution was vigorously stirred overnight (16 h) to evaporate the organic phase. After evaporation of the organic phase, the particle suspension was dialyzed (3,500 g/mol molecular-weight cut-off (MWCO) dialysis membrane, 8 h) against distilled water to remove any excess sodium cholate. The particle suspension was then passed through a 0.22 μm syringe filter.

To create PLA-PEtG blended NPs, select weight percentages of PLA were incorporated into the PEtG organic phase. Specifically, 10 wt%, 30 wt% and 50 wt% PLA-PEtG blends were prepared as described above. The dichloromethane solutions of these blends were added to the aqueous phase, then the biphasic mixture was sonicated, dried and dialyzed and the resulting particles were dialyzed by the methods described above.

2.4 Dynamic Light Scattering

DLS was performed using a Zetasizer Nano ZS instrument from Malvern Instruments at 25 °C at a concentration of 0.1 mg/mL of polymer assemblies. The Z-average diameter and polydispersity index for each series of particles was measured in triplicate.

2.5 Preparing Particles for Imaging

TEM imaging was done using a Phillips CM10 microscope operating at an acceleration voltage of 80 kV with a 40 μm aperture. 20 μL of particle suspension (1.0 mg/mL) was placed on a copper grid. The resulting sample was air-dried for 24 h before imaging.

2.6 NP Degradation Studied by DLS

NPs were prepared as above, with the exception that the suspensions were dialyzed against 100 mM, pH 7.4 phosphate buffer (1 L, 24 h, water changed once at ~12 h). The polymer concentration was 0.1 mg/mL. The count rate was measured by DLS while fixing the attenuator at 7. For NVOC-PEtG and BnCO-PEtG, irradiation with UV light was performed in an ACE Glass photochemistry cabinet containing a mercury light source (450 W bulb, 2.8 mW/cm^2 of UVA radiation) for 30 minutes. For disulfide-PEtG and the BnCO-PEtG control, DTT (7.7 mmol) was added. Control experiments without stimulus were also included in each case after applying the stimulus, the samples were incubated at 37 °C in the dark and the DLS count rate was measured at selected time points. Each experiment was performed and studied in triplicate.

2.7 Loading and Release of Nile Red

Nile red-loaded NPs were prepared by the addition of Nile red (0.1 mg, 0.03 mmol) to the organic phase containing defined weight percentages of PEtG and PLA. The organic phase was allowed to stir for several hours to facilitate complete mixture of the blends and Nile red. The polymer-Nile red solution was added to the surfactant-containing aqueous phase and subjected to sonication, as described above. After sonication and evaporation, the particle suspensions were dialyzed against water using a 3,500 g/mol MWCO dialysis membrane for 24 h to remove excess surfactant and any trace unencapsulated Nile red.

To test for triggerable release of Nile red from the particles, NPs were again prepared as above with 0.1 mg Nile red added to the organic phase. The particle suspensions were dialyzed against 100 mM, pH 7.4 phosphate buffer. After 24 h of dialysis, the solutions were diluted 10-fold in pH 7.4 phosphate buffer to yield a Nile red concentration (3 µM) within the detectable range of the fluorimeter. Using an excitation wavelength of 540 nm, the initial emission intensity of Nile red was measured at 602 nm to obtain fluorescence at T_0 (starting time). At this point, the appropriate stimulus (UV light for NVOC-PEtG and DTT for disulfide-PEtG) was added, or not added in the case of controls, and the solutions were placed in a 37 °C oven. Fluorescence measurements were taken at

incremental time points over a 24 h period. By comparing the fluorescence at each time point with its initial fluorescence, the percent initial fluorescence was calculated. These measurements were taken in triplicate and conducted for each of the three polymer blends.

2.8 Preparation of Letrozole-Loaded NPs

NPs were prepared as above with the addition of letrozole (30 wt%, 3 mg, 0.86 mmol) dissolved in the organic phase with the polymer mixtures before sonication. After sonication, the suspensions were again dialyzed in a 3,500 g/mol MWCO membrane for 24 h to remove any unencapsulated letrozole. After dialysis, the solutions were passed through a 0.22 μm syringe filter and a portion was lyophilized to calculate the loading efficiency and drug wt%. The lyophilized pellet was weighed and then dissolved in 1 mL of acetonitrile. The absorbance of the resulting solution was measured by UV-visible spectroscopy at 240 nm. The concentration was calculated based on a letrozole calibration curve (ε = 30,600 L/mol·cm, acetonitrile) and the loading efficiency and drug content of the NPs was calculated as followed:

$$Loading\ Efficiency = \frac{Drug\ Encapsulated}{Drug\ Loaded} \times 100$$

$$Drug\ wt\% = \frac{Encapsulated\ Drug\ Mass}{Total\ Mass} \times 100$$

2.9 Triggerable Release of Letrozole

For drug release studies, NPs were prepared as described above with the exception that after sonication and evaporation, the particle suspensions were dialyzed against 100 mM, pH 7.4 phosphate buffer (1 L, 16 h, dialysate exchanged at ~8 h) using a 3,500 g/mol MWCO membrane to remove any unencapsulated letrozole and excess surfactant. The particles were then filtered through a 0.22 μm syringe filter and diluted 10-fold with 100 mM, pH 7.4 phosphate buffer. An initial absorbance measurement was taken (T_0). Subsequently, the appropriate stimulus was introduced as described above for the DLS experiments. The samples were then each placed in an individual 3,500 g/mol MWCO

dialysis membrane and dialyzed in 7.4 phosphate buffer in a 37 °C oven. To measure the letrozole release rates, 200 µL of each sample were taken at incremental time points and passed through a 0.22 µL syringe filter. From the filtered solution, three 50 µL aliquots were taken and diluted into 1 mL of acetonitrile to fully dissolve the polymer particles and remaining encapsulated drug. The absorbance was measured at 240 nm (ε = 30,600 L/mol·cm). Release rates were obtained by plotting the absorbance at each time point as a percentage of initial absorbance.

2.10 Triggerable Release of Celecoxib

For celecoxib release studies, disulfide-PLA-PEtG and BnCO-PEtG NPs were prepared as described above and dialyzed against 100 mM, pH 7.4 phosphate buffer (1 L, 16 h, dialysate exchanged at ~8 h) using a 3,500 g/mol MWCO membrane to remove any unencapsulated celecoxib and any excess surfactant. They were then filtered through a 0.22 µm syringe filter and diluted 10-fold with 100 mM, pH 7.4 phosphate buffer. An initial absorbance measurement was taken by removing 200 µL of each sample and dissolving it in 1 mL acetonitrile. The absorbance was measured at 253 nm (ε = 16,400 L/mol·cm for celecoxib based on a calibration curve in the same medium) in order to quantify the total amount of drug initially encapsulated in the system. Subsequently, the appropriate stimulus was introduced as described above for the reduction-responsive DLS experiments. The samples were then each placed in an individual 20 mL vial with a small bar magnet, stirred at low rpm and kept in a 37 °C oven for the duration of the study. At distinct time points, each sample was centrifuged for three minutes at 6,000 rpm to separate the precipitated drug from the particles and encapsulated drug that remained suspended in the medium. The suspension was decanted back into the initial vial and placed back into the oven while the pellet was dissolved in 1 mL acetonitrile and the absorbance at 253 nm was taken to quantify the amount of drug that had been released and consequently precipitated. This amount was compared to the initial amount of encapsulated drug in order to determine the percentage of released drug.

2.11 Cell Toxicity Study

Dulbecco's modified Eagle medium (DMEM) with 4.5 g/L D-glucose and 110 mg/L sodium pyruvate was obtained from Gibco. Penstrep, 10% fetal bovine serum (FBS) and trypsin-EDTA (0.25%) were obtained from Gibco. The MDA-MB-231 cells were cultured in DMEM with 10% FBS and 100 units/mL of Penstrep in an atmosphere of 5% CO_2 at 37 °C. The cells were seeded in a 96 well plate (Corning Flat Bottom Plate) at a concentration of 5,000 cells/well. Cells were placed in an incubator for 24 h (37 °C, 5% CO_2). Following the incubation, the medium was aspirated and replaced with various treatments of NPs of 1, 0.5, 0.25, 0.13, 0.06 mg/mL. For UV-sensitive particle studies, the cells were irradiated with 30 minutes of 360 nm light using light emitting diode flashlights. Negative controls include either just media or the test material. The cells were then incubated at 37 °C for 48 h. The medium was then aspirated and replaced with 100 µL of fresh medium containing 0.5 mg/ml (3-(4,5-dimethylthiazol-2-yl)-2,5-diphenyltetrazolium bromide) (MTT) reagent and allowed to react for 4 h in the incubator at 37 °C. After 4 h the plate was removed and the MTT reagent solution was aspirated. 50 µL of dimethyl sulfoxide was added to each well to solubilize the metabolic reagent of MTT. The plate was then placed in a plate reader (Tecan Infinite M1000 Pro, absorbance 540 nm) to obtain cell counts. No biological replicates were performed; six technical replicates were performed per treatment.

3 Results & Discussion

3.1 Stimuli-Responsive Poly(ethyl glyoxylate) Synthesis

PEtG was synthesized as previously reported (Scheme 11).[46] The purity of ethyl glyoxylate monomer was the limiting factor on the molecular weight of PEtG. The monomer was purchased as a 50:50 volume ratio in toluene. After two distillations over phosphorus pentoxide (P_2O_5) as a drying agent, pure monomer was obtained. The monomer was cooled to −20 °C and polymerization initiated by adding a catalytic amount of TEA. The mechanism of polymerization is hypothesized to be initiated from trace amounts of hydrated monomer. After polymerization, the polymer was held at −20 °C and the desired chloroformate-functionalized end-cap was added. In this work, polymers with three different stimuli-responsive end-caps were prepared: NVOC-PEtG, which is responsive to UV light; disulfide-PEtG, which is responsive to reducing agents such as DTT; BnCO-PEtG, which is non-responsive and serves as a control. The molar mass data for the polymers used in this work is shown in Table 1.

Table 1. Average molecular weight (M_n) and polydispersity of end-capped PEtG used.

polymer	M_n (SEC) (g/mol)	$Đ$	T_o (°C)
NVOC-PEtG	70,000	2.4	203
disulfide-PEtG	24,000	1.4	191
BnCO-PEtG	56,000	1.6	162
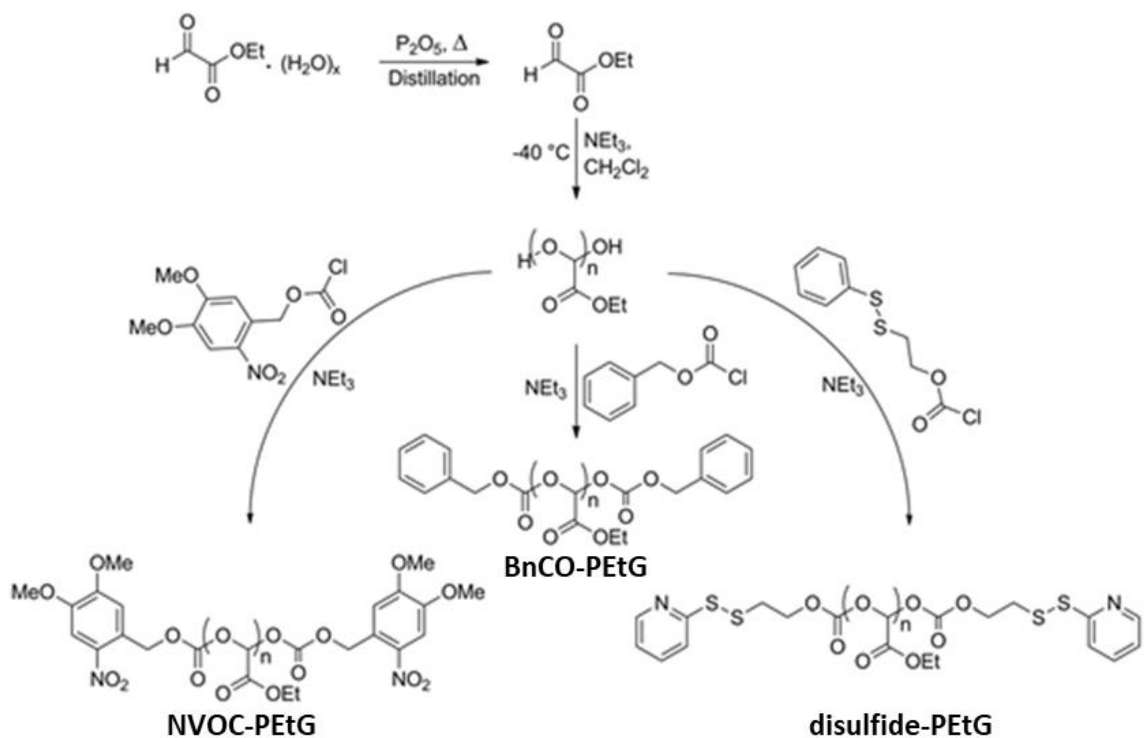
Scheme 11. Synthesis of different classes of PEtGs.

3.2 Emulsion Optimization

3.2.1 Determination of Optimal Surfactant Concentration

One of the most common surfactants used in NP research has been PVA due to its biocompatibility and non-toxicity.[61] However, previous work done by the Gillies group determined that PVA used as the surfactant for PEtG emulsion methods gave particles diameters of 400 nm - too large to be optimal for intravenous drug delivery.[74] Further research on appropriate surfactants concluded that PEtG NPs stabilized with sodium cholate as the surfactant could be manufactured with particle sizes of 120 nm.[79] Cholic acid (3α,7α-trihydroxy-5β-cholan-24-oic acid) is a primary bile acid produced by the liver. The sodium or potassium salts of cholic acid are water dispersible and are naturally used by the body in its digestion of fats and oils. Therefore, sodium cholate can act as a biocompatible surfactant for NPs.[80]

Parameters of the O/W emulsion technique were investigated with efforts focused on preparing particles with diameters in the 100 nm range.[81] The two variables found to contribute the most towards controlling the diameter were surfactant:polymer ratio and sonication time. As the particles get smaller, their surface area increases which increases the overall oil-water interactions. Therefore, to get smaller particles, higher concentrations of surfactant were required. To determine the appropriate surfactant:polymer ratio, the concentration of PEtG was kept constant (1 mg/mL) while varying the surfactant concentration from 0 mg/mL to 100 mg/mL. The biphasic mixture was subjected to two minutes of sonication and the resulting emulsion was dried and then dialyzed in distilled water as described above. The particle diameter was then measured by DLS. As expected, 0 mg surfactant led to precipitation of polymer after evaporation. As the surfactant concentration increased, the diameter of the particles decreased (Figure 16).
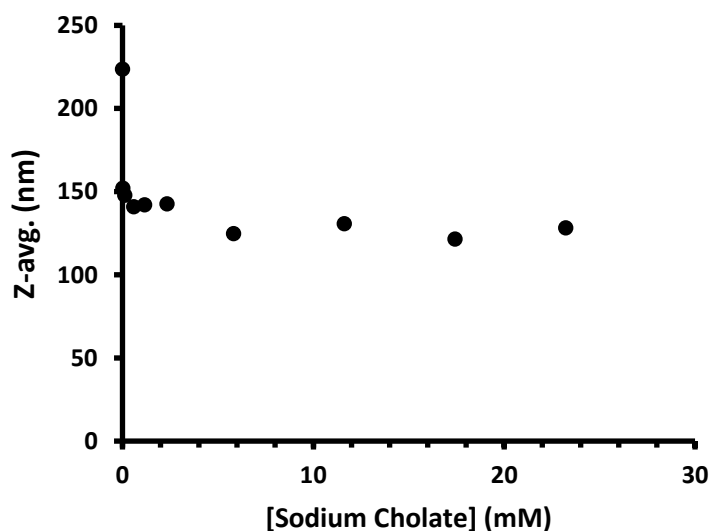
Figure 16. Concentration of sodium cholate vs. Z-avg. while the concentration of PEtG was kept constant at 1 mg/mL.

Although a meaningful change in the Z-avg. was not detected by measuring the diameter of these systems, at low concentrations of surfactant, significant precipitation of polymer was observed. This can be attributed to the necessity of a high concentration of surfactant for small particles due to the high surface area. A sodium cholate concentration of 12 mM

was found to yield the desired particle diameter with no appreciable precipitation of polymer. This gave a surfactant:polymer weight ratio of 5:1.

3.2.2   Determination of Optimal Sonication Time

The second major factor in controlling the particle diameter was the sonication time. To examine the effect of the sonication, the relationship between sonication time to particle diameter was studied. The PEtG concentration was fixed at 1 mg/mL as above, and the sodium cholate concentration was fixed at 5 mg/mL. The two solutions were combined and emulsified using sonication for varying lengths of time. The resulting emulsion was then stirred overnight and purified by dialysis as above. The resulting particles were measured using DLS to determine the Z-avg. It is known that prolonged shearing forces introduced by sonication can cleave polymer backbones over time. With the relatively labile polyacetal backbone of PEtG, it was important to find the minimum amount of sonication time needed to produce NPs close to 100 nm (Figure 17).[82] The data showed significant decrease in particle size up to approximately 90 s. After that, the particle size appeared to not change significantly with increased sonication time. With this data, along with results presented in Figure 16, all particle batches going forward were performed under Table 2 conditions.
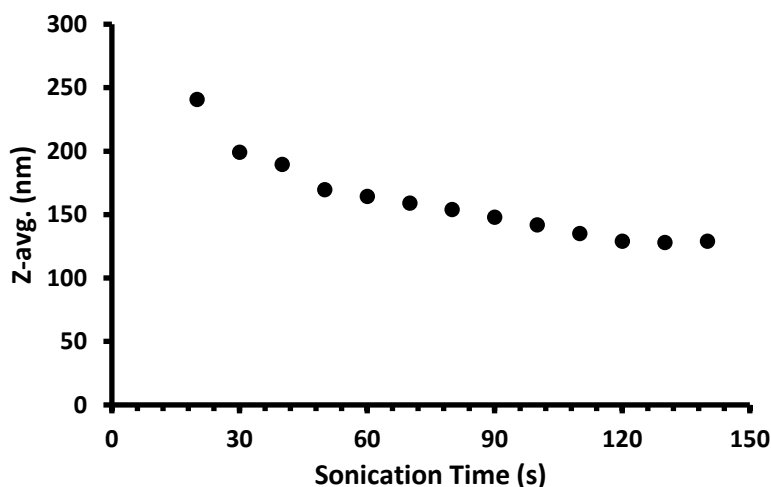
Figure 17. Emulsion sonication time vs. Z-avg. for PEtG NPs while keeping the concentration of PEtG constant at 1 mg/mL and sodium cholate concentration at 5 mg/mL.

Table 2. Emulsification conditions for the production of 100 - 150 nm-sized PEtG-based NPs.

Sodium Cholate (mg)	PEtG (mg)	D.I. H$_2$O (mL)	CH$_2$Cl$_2$ (mL)	Sonication Time
50	10	10	1	3 rounds (30 s) with intervals (10 s)

3.2.3   PLA-PEtG Polymer Blend Characterizations

PEtG was anticipated to provide rapid release upon stimulation. To provide further control and tuning of the release properties, PEtG was blended with varying weight percentages of PLA. It was anticipated that the PEtG phases of NPs would provide a burst release at the target, while the polyester domains would afford continual slow release as these domains would degrade more slowly. The presence of a non-stimuli-responsive polymer would lead to increase in overall degradation time which may lead to tunability of cargo release. Specific weight percentages of PLA were substituted for PEtG. Blends of 0 wt%, 10 wt%, 30 wt%, 50 wt%, and 100 wt% PLA were prepared by dissolving the two polymers in dichloromethane.

Characterization of each polymer blend was conducted using both thermogravimetric analysis (TGA) and differential scanning calorimetry (DSC). TGA data showed two-step thermal degradation in the three blends and the blend ratios were consistent with the incremental weight percentages of PLA present in each sample (Figure 18). Pure PLA matched literature values of degradation temperatures showing PLA stable up to 300 °C.[83] The PEtG sample matched reported values of 180−200 °C for end-capped PEtG.[46] The addition of PLA appears to stabilize PEtG in some way. This can be seen by the increase in onset degradation temperature (T$_o$) of PEtG in each of the three blends. The degradation of PEtG increased about 100 °C by the incorporation of 10 wt% and 30 wt% PLA, and even more so with 50 wt% PLA. This could be due to favorable intermolecular forces between regions of the two polymers.
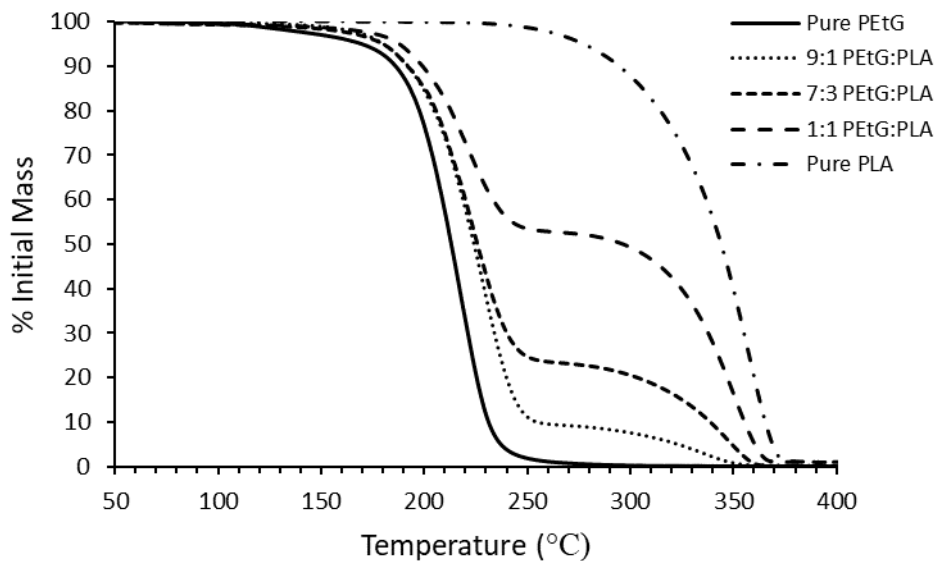
Figure 18. TGA data for the PLA-PEtG blends.

DSC data showed the two polymers were mostly phase separated in the blends (Figure 19). This can be seen from the two distinct glass transition temperature (T_g) values arising from the two different polymers (Table 3). The T_g for PEtG can be clearly seen for each blend and matches the literature value of about −5 °C. There may be some slight miscibility between these two polymers because the reported T_g for PLA is 50 °C, but the Tg values for PLA in the blends range from 41 to 46 °C. In addition, the T_g of PEtG increased from −8 °C for the pure PEtG to −1 °C for the 50% PLA blend.
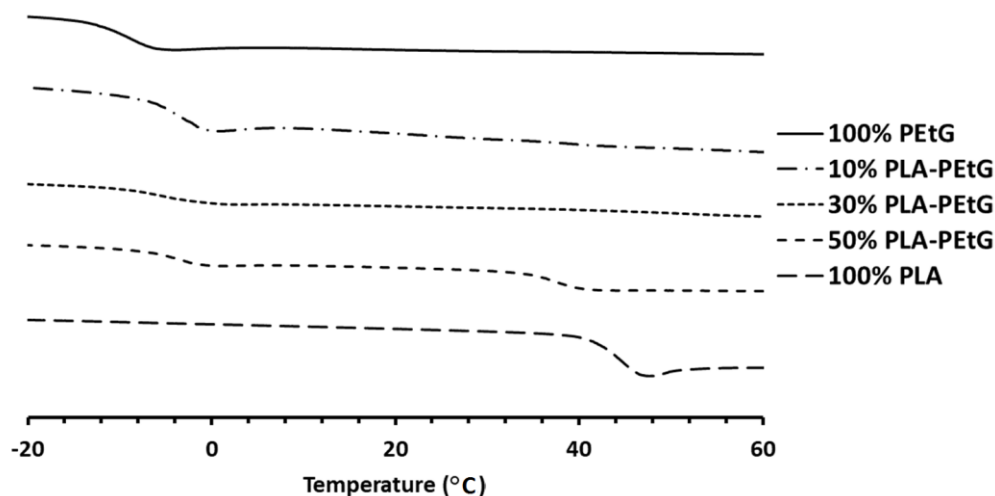
Figure 19. DSC thermograms recorded for pure PEtG, pure PLA and the three blends.

Table 3. T_gs recorded for the PLA-PEtG blends.

Blend	PEtG T_g (°C)	PLA T_g (°C)
100% PEtG	−7.6	-
10% PLA	−5.3	43.6
30% PLA	−3.2	40.8
50% PLA	−1.1	39.8
100% PLA	-	46.0

The immiscibility of these polymers suggests microphase separation of the polymers. When PEtG is degraded, a porous PLA scaffold should be left which will rely on random hydrolysis to degrade completely. The phase separation suggests an initial burst release of cargo followed by a slower release of residual cargo encapsulated within the remaining PLA scaffold. The burst release would then be incrementally less with increasing PLA content, while the fraction undergoing slow release should increase. With a better understanding of the nature of these polymer blends in hand, the synthesis of these particles with their varying blends was investigated and their properties analyzed.

3.3   Characterization of Particles

3.3.1   Characterization of Particles by DLS

The first method of characterization performed was the determination of the Z-avg. The diameter for each blended batch of particles was determined using DLS. Each particle suspension was prepared using conditions described earlier (section 3.2.2). Subsequently, the particle suspensions were diluted to 0.1 mg/mL with distilled water to give appropriate concentrations for DLS. In Figure 20 data are presented for the five blend compositions. The Z-avg. diameters ranged from 128–144 nm and did not change significantly with the incorporation of PLA. The PDI values ranged from 0.03–0.26, which is considered relatively low. A summary of these DLS diameter distributions is shown in Table 4.
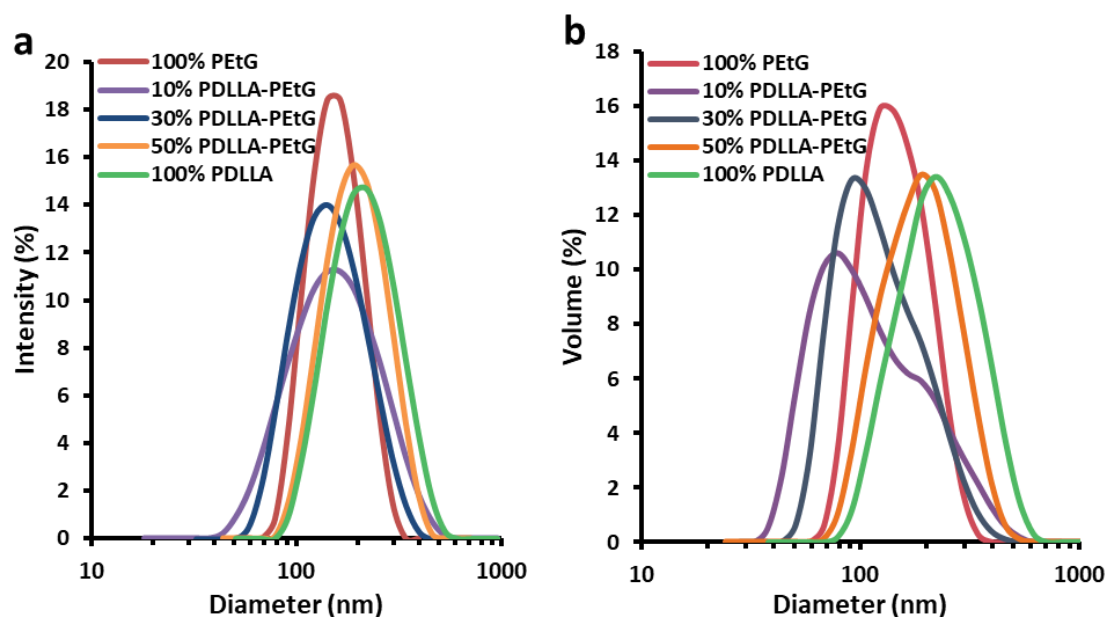
Figure 20. Representative DLS diameter distributions of the PLA-PEtG blends: **(a)** intensity distributions and **(b)** volume distributions.

Table 4. Z-avg. and polydispersity indices for the PLA-PEtG blends.

Blend	Z-avg. (nm)	PDI
0% PLA	144 ± 13	0.19 ± 0.07
10% PLA	137 ± 19	0.26 ± 0.11
30% PLA	128 ± 7	0.11 ± 0.03
50% PLA	133 ± 8	0.12 ± 0.03
100% PLA	132 ± 10	0.13 ± 0.04

3.3.2 Characterization of Particles Using Transmission Electron Microscopy

With understanding of the blend characteristics and particle diameters in hand, it was important to image the particles to confirm the morphologies and the particle diameters. Due to the inability to freeze dry low PLA-content particles because of the low T_g of PEtG, scanning electron microscopy (SEM) proved difficult as the particles tended to fuse together. Therefore, TEM was employed as the imaging technique for the particles. Using this imaging technique, samples prepared from particle suspensions could be made, bypassing the need to freeze dry.

Figure 21 shows images for pure PEtG particles and those prepared from each of the three blends. The particle diameters observed by TEM were in general smaller than those measured by DLS. The observation of smaller diameters in TEM imaging is quite common, as TEM measures the samples in their dehydrated state whereas DLS measures the samples in their hydrated state. In agreement with the DLS results, increasing the PLA content to 30 wt% (Figure 21c) and 50 wt% (Figure 21d) does not seem to destabilize the morphology of the particles even though the two polymers are immiscible. The particles in these samples appear to be spherical and monodisperse.
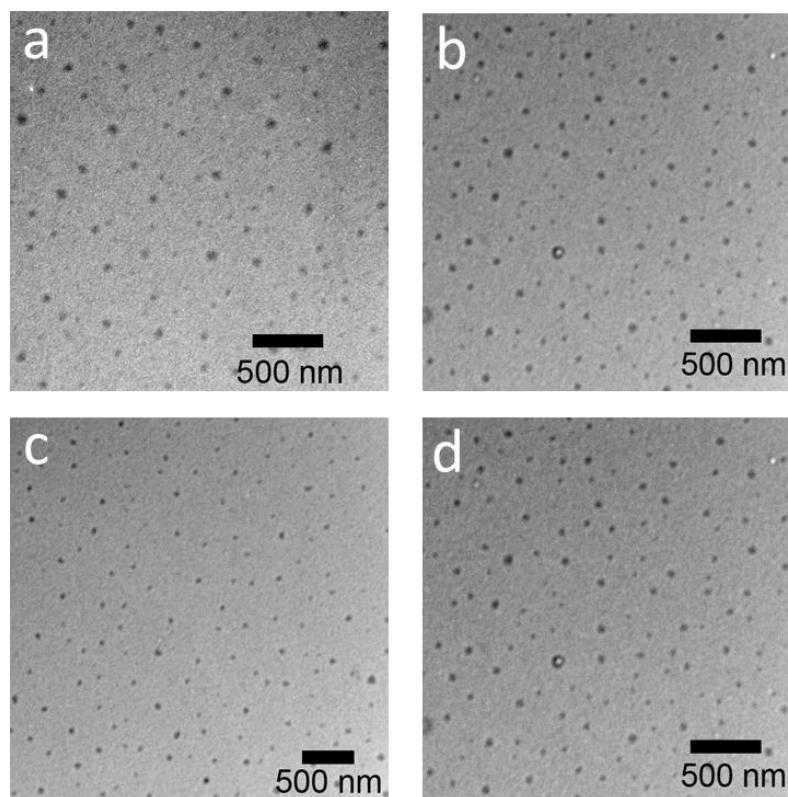
Figure 21. Transmission electron micrographs of NPs prepared from **(a)** 100% PEtG, **(b)** 10 wt% PLA, **(c)** 30 wt% PLA, **(d)** 50 wt% PLA.

3.4 Triggerable Degradation Studies

3.4.1 Degradation Measured by DLS

After it was concluded that PEtG could be successfully blended with PLA and made into relatively monodisperse NPs, investigating the triggerable degradation nature of these particles was the next step. In addition to NVOC-PEtG which was used for the above work, particles were prepared from disulfide-PEtG and BnCO-PEtG by the same method described above. Changing only the end-cap did not lead to any significant changes in the particle diameter or morphology as determined by DLS and TEM (Figures A-3 − A-5 in the appendix).

DLS was employed to test for degradation of particles in response to stimuli. This technique can be used to probe for particle degradation because the count rate is proportional to both the number of particles in suspension as well as their size. A decrease in either the size or number of particles arising from degradation would lead to a

reduction in the count rate. The appropriate concentration for the DLS studies of the particle suspensions was found to be 0.1 mg/mL. Keeping the attenuator fixed, the light scattering count rate was measured initially and then at various time points after introduction of the stimulus. Control experiments involved application of the stimulus to non-responsive BnCO-PEtG particles to account for any non-specific effects on the particles. Each ratio of PEtG:PLA was studied.

Figure 22 shows the response of the NVOC-PEtG and BnCO-PEtG (PEtG-control) particles to 30 minutes of UV irradiation. Two important observations came from this study. First, for each PEtG:PLA ratio of NVOC-PEtG particles there is a rapid decrease in count rate over the first hour following UV irradiation that likely corresponded to degradation of particles. On the other hand, the scattered light intensity from the BnCO-PEtG control particles stayed relatively constant at 100% of their initial count rate over a 24 h period. Secondly, with increasing PLA content in the particles, there was a plateau of the degradation which corresponded approximately to the amount of PLA in the particles. Pure PEtG particles appeared to approach zero counts at the 24 h time point, 10 wt% particles degraded to roughly 10% of their original count rate and then remained constant, 30 wt% plateaued at 30% of the initial count rate and 50 wt% PLA particles plateaued at 50% of the initial count rate. Also, light scattered from the pure PLA particles remained constant at 100% original counts over the 24 h period.
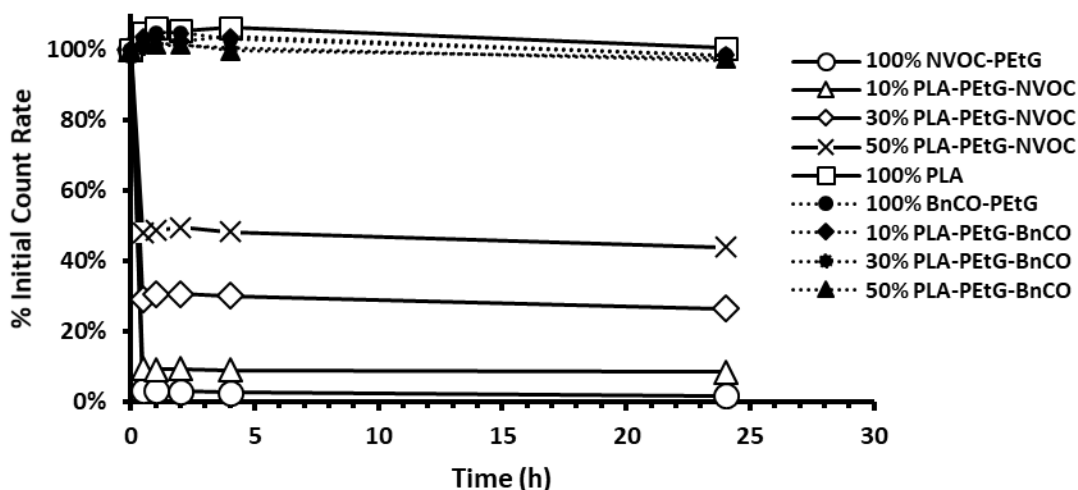
Figure 22. % Initial scattering count rate (DLS) vs. time for NVOC-PEtG and BnCO-PEtG control particles following UV irradiation for 30 min.

To demonstrate the system can show responsiveness to several different stimuli just by changing the end-cap, the study was repeated for disulfide-PEtG, which contains an end-cap susceptible to reduction through its disulfide linkage. The reducing agent used to trigger the end-cap was DTT. Figure 23 shows the DLS count rate over a period of 48 h following the addition of 7.7 mmol DTT to the particles. It was observed that overall, the reduction in count rate occurred more slowly than for the NVOC-PEtG particles in the UV study. There are two factors that may be causing this: 1) the UV reaction could proceed at a faster rate than the reduction reaction; 2) the DTT is limited by only being able to react with surface end-cap groups first allowing fewer reactions to occur simultaneously whereas UV light can penetrate past the surface. Again, the particles containing less PLA underwent larger reductions in the count rate over the experiment, likely corresponding to more complete degradation. The scattered light intensities from the PEtG-control and pure PLA particles all remained near 100% of their original values.
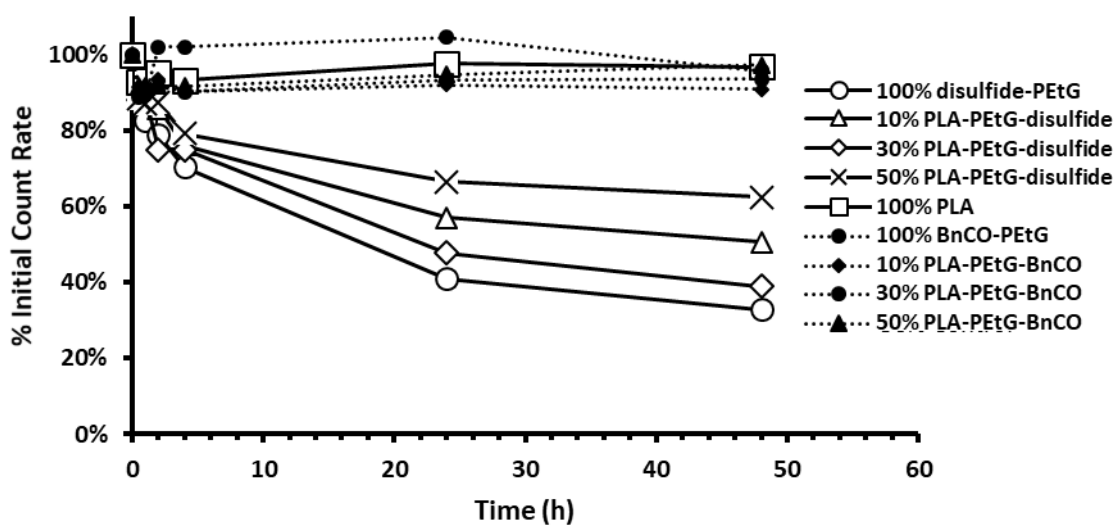
Figure 23. % Initial scattering count rate (DLS) vs. time for disulfide-PEtG and BnCO-PEtG control particles following the addition of 7.7 mmol DTT.

Overall, the data collected for both NVOC-PEtG and disulfide-PEtG show that it is possible to trigger degradation of the particles specifically by matching the stimulus with the end-cap and that it appears possible to trigger different percentages of degradation by tuning the PLA content in the particles.

3.4.2   Triggerable Release of a Fluorescent Probe

As an initial study to test for triggerable release of an encapsulated cargo, a fluorescent cargo molecule was used as a probe. The same conditions were used as for the DLS study where NVOC-PEtG particles were used as the UV-light responsive particles and disulfide-PEtG were used as reduction responsive particles. BnCO-PEtG particles were again used as a non-stimuli responsive control. Nile red dye was selected as an appropriate proof-of-concept cargo. Nile red can be loaded at low concentrations which allows for effective probing of triggerable release of cargo by measuring fluorescence of particle suspensions at incremental time points post-stimulus exposure. In hydrophobic environments, Nile red is highly fluorescent, while, in hydrophilic environments, Nile red undergoes aggregation and its fluorescence is significantly quenched.[84] Therefore, Nile red encapsulated within PEtG NPs will fluoresce and as it is released into the surrounding aqueous environment, the fluorescence will decrease.

Nile red encapsulated NPs were prepared by the same method described above except that 2 wt% of Nile red relative to polymer was incorporated into the dichloromethane phase to load the particles. Batches were made for each of the PLA weight percentages as above, including pure PEtG and pure PLA. Qualitatively, the fluorescence of Nile red in different hydrophobic environments can be seen in Figure 24. The far-right vial (24e) contains the 100% PLA Nile red-loaded particles. This represents the most hydrophobic environment for the Nile red and this is seen by the intensity of the color.[85] Moving to the left are NVOC-PEtG samples with decreasing wt% PLA. With decreasing wt% PLA in the particles, the intensity of the color drops off with each incremental decrease of PLA. This further supports the different environments present in the cores of the different PLA-PEtG blended particles. The PLA adds hydrophobic character to the particles, whereas the PEtG is more hydrophilic which could help facilitate more Nile red encapsulation in the particles with the higher PLA content, leading to a more intense color.

Figure 24. Nile red-loaded PLA-PEtG NP suspensions: **(a)** 100% PEtG, **(b)** 10 wt% PLA, **(c)** 30 wt% PLA, **(d)** 50 wt% PLA, and **(e)** 100% PLA.

The initial fluorescence intensity was measured for each sample along with controls. During the duration of the study, the samples were kept in a 37 °C oven in 100 mM, pH 7.4 phosphate buffer. Each successive time point following application of the stimulus was measured as a percent of initial fluorescence. An example of these data taken for 0% PLA NVOC-PEtG is shown in Figure 25. The graph tracks the fluorescence from T_0, which was taken for NVOC-PEtG particles prepared with 100% PEtG before UV-light exposure up to 60 minutes after exposure. The data can further be processed to plot a percent initial fluorescence over time by taking the maximum value for each time point as

a percentage of the initial fluorescence (Figure 26). Using these data allows for comparison between the different weight percentage PLA-PEtG particles and their Nile red release rates.
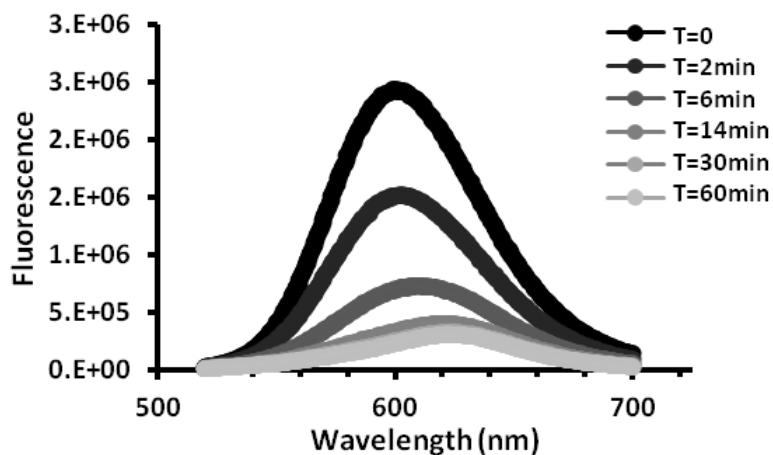
Figure 25. Fluorescence emission spectra of Nile red-loaded 100% NVOC-PEtG NPs over a period of 1 h post-UV exposure.
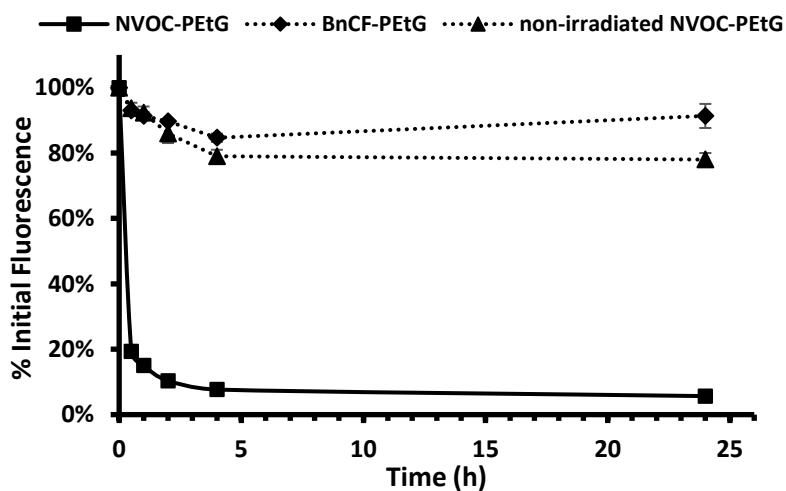
Figure 26. Fluorescence behavior of Nile red-loaded 100% NVOC-PEtG NPs.

The Nile red fluorescence experiments were conducted for both UV light-responsive and reduction-responsive particles using NVOC-PEtG and disulfide-PEtG, along with BnCO-PEtG control NPs for each stimulus. The fluorescence changes over time following application of the stimulus for the different PEtG:PLA ratios are shown in Figure 27 for UV light and Figure 28 for DTT as a stimulus. The findings correspond with previous

experimental results from the DLS degradation studies. Specifically, these data show that the NVOC-PEtG particles exhibited a significant burst release of Nile red within the first hour after being exposed to UV light. This is due to the PEtG fraction of the particles being degraded. Each different PLA wt% then plateaued at a different value, corresponding to the remaining PLA in the particles. In other words, a percentage of the particle's hydrophobic core remained, which was still able to encapsulate Nile red within a hydrophobic environment. Figure 28 shows that the release of Nile red following application of DTT to the disulfide-PEtG NPs was slower than for the light-responsive particles. As for the DLS study, this can likely be attributed to slower end-cap cleavage. As for the NVOC-PEtG particles, increasing the PLA content resulted in a higher retention of Nile red. In each experiment, the controls of BnCO-PEtG particles with applied stimuli showed a $10 - 20\%$ reduction in Nile red fluorescence, which can likely be interpreted as passive diffusion of Nile red from the periphery or edges of the particles.
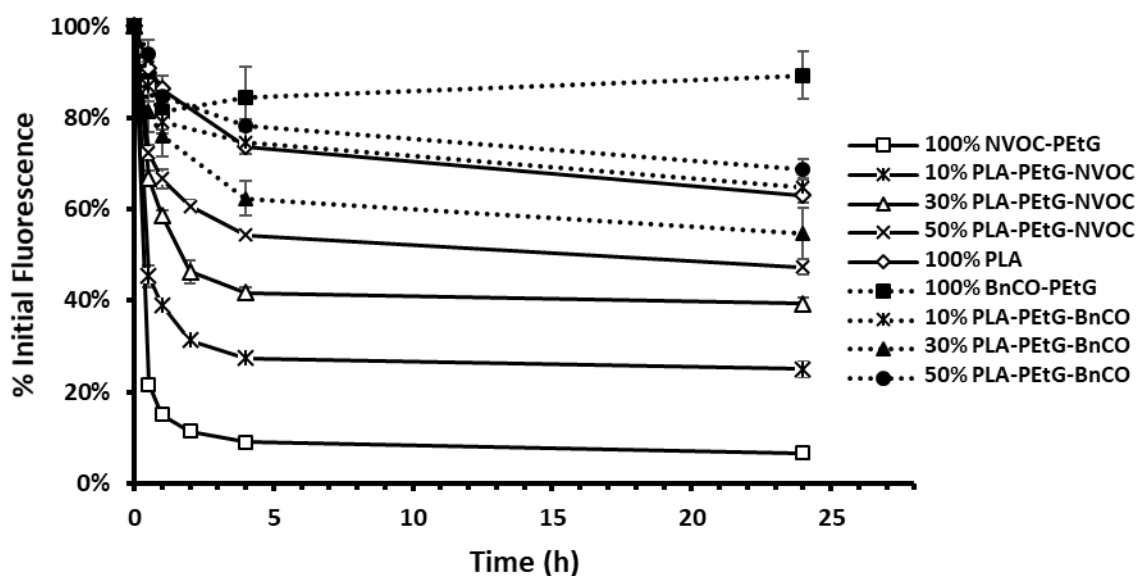
Figure 27. Fluorescence emission behavior observed at different time intervals for NVOC-PEtG and BnCO-PEtG control particles with varying PLA content after the UV light irradiation (30 min).
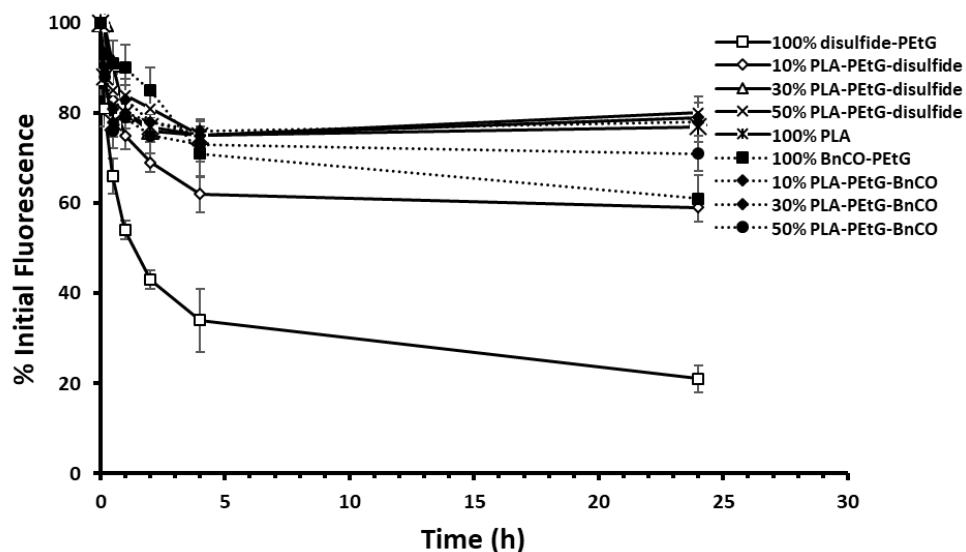
Figure 28. Fluorescence emission behavior observed at different time intervals for disulfide-PEtG and BnCO-PEtG with varying PLA content after the addition of DTT.

In terms of controlling the release of Nile red, UV light as a stimulus did not give significant control over the burst release. After exposure to UV light, each particle suspension resulted in a quick burst release consistent with the corresponding PLA content, followed by a slower rate of release from the PLA regions. There does however appear to be some control over where the slower, plateau region occurs by varying the wt% of PLA content in these particles. Using 7.7 mmol DTT as a stimulus led to a better control in the burst release. The difference can be seen in the 100% PEtG sample that took 24 h to release 80% of the Nile red compared to the UV sample that took less than 1 h to release the same amount. Due to this slower release profile, the plateau regions in the DTT-responsive data are not as apparent.
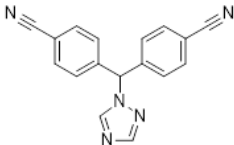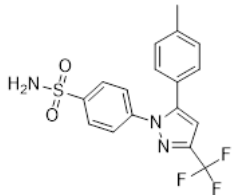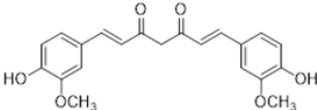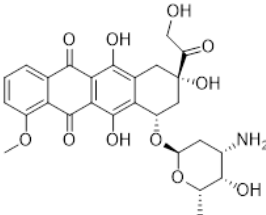
3.5 Hydrophobic Cargo Encapsulation and Release

3.5.1 Characterization of Drug-Loaded PLA-PEtG NPs

The DLS studies, along with the Nile red studies, provided sufficient proof of concept for triggerable degradation of PEtG NPs. The next step was to load the particles with a model drug and test for triggerable release of this drug.[86] A common literature procedure for these studies involves encapsulating a UV active drug molecule within the DDS and placing the particle suspensions in dialysis. Using a drug that absorbs UV or visible light

above ~210 nm, the drug release can be tracked by taking UV-Vis spectroscopy measurements of the dialysate or the suspension within the dialysis membrane over time to obtain a release profile. Several hydrophobic drugs were investigated as potential candidates for encapsulation and drug release. The loading efficiency and drug content calculations were made for each drug and are summarized in Table 5. Surprisingly, the four different drugs tested had starkly different loading efficiencies and drug contents. Curcumin, an herbal supplement, showed the worst encapsulation efficiency at 21% with a drug content of only 3%. The most successful candidate was celecoxib, an anti-inflammatory medication. Celecoxib had a loading efficiency of 77% and a 25% drug content. Letrozole, used to treat breast cancer, and DOX, a common chemotherapy, were also tested with moderate loading efficiencies of 44% and 38% respectively. Based on the loading efficiencies and drug content of these four candidates, letrozole and celecoxib were chosen as the two drugs for further studies.

Table 5. Drug loading properties of 30% PLA-PEtG NPs.

Drug	Structure	Loading Efficiency	Drug Content (wt%)	λ_{max} (nm)
Letrozole		$44 \pm 5\%$	$17 \pm 2\%$	240
Celecoxib		$77 \pm 9\%$	$25 \pm 3\%$	253
Curcumin		$21 \pm 3\%$	$3 \pm 1\%$	524
Doxorubicin		$38 \pm 7\%$	$22 \pm 4\%$	485

PLA-PEtG NPs containing letrozole were characterized using DLS and TEM to examine any differences between loaded and unloaded particles in terms of average diameter and morphology. In Figure 29 and Table 6 data collected for unloaded PLA-PEtG particle diameters from DLS studies were compared with those collected for their respective loaded counterparts. Drug-loaded particles were similar in size to unloaded particles, but significantly larger diameters ($p < 0.05$) were observed for 100% PEtG, 30% PLA-PEtG, 50% PLA-PEtG and 100% PLA particles. The PDIs for the loaded particles were also significantly larger for 30% PLA-PEtG particles. However, loaded particles were well below the 300 nm cutoff for maximum particle diameter and the PDIs were all below 0.3, which is the benchmark for uniformity in size.

Table 6. Size specifications of the letrozole-loaded/unloaded particles based on PLA-PEtG blends. (Standard Error, n = 3)

Blend	Loaded		Unloaded[*]	
	DLS Z-avg. (nm)	PDI	DLS Z-avg. (nm)	PDI
100% PEtG	144 ± 9	0.16 ± 0.06	114 ± 9	0.19 ± 0.07
10% PLA-PEtG	137 ± 21	0.29 ± 0.10	127 ± 19	0.28 ± 0.11
30% PLA-PEtG	128 ± 16	0.22 ± 0.04	118 ± 7	0.11 ± 0.03
50% PLA-PEtG	133 ± 10	0.17 ± 0.03	122 ± 8	0.12 ± 0.03
100% PLA	138 ± 9	0.17 ± 0.04	109 ± 10	0.13 ± 0.04

[*]The data recorded for unloaded particles were repeated for comparison.
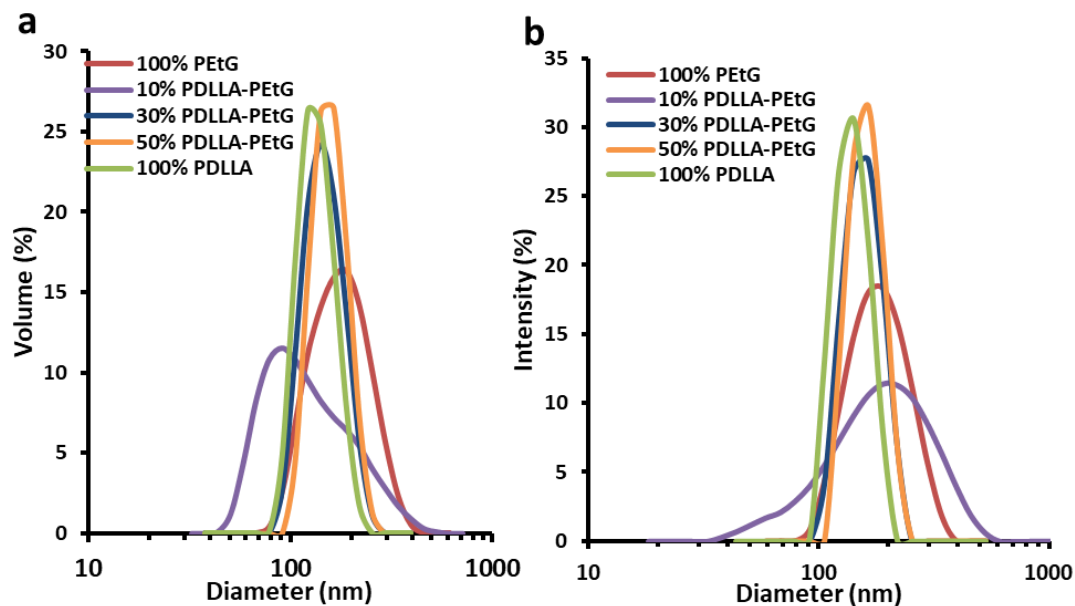
Figure 29. Representative DLS diameter distributions for each letrozole-loaded PLA-PEtG blend. **(a)** volume distributions and **(b)** intensity distributions.

Loaded particles prepared from 100% PEtG and 50% PLA-PEtG were also examined by TEM (Figure 30). The images show mostly spherical particles with diameters of 50–80 nm. As mentioned above, the average particle diameter in the TEM images are smaller than those measured by DLS.
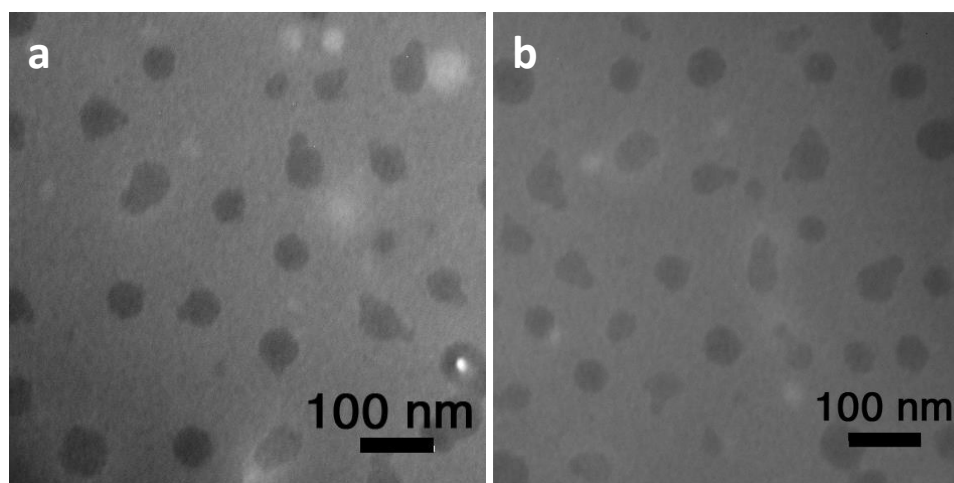
Figure 30. TEM images of letrozole-loaded **(a)** 100% PEtG NPs and **(b)** 50% PLA-PEtG NPs.

3.5.2   Triggerable Release of Letrozole

The novelty of the PEtG system, being the rapid burst release after triggering, posed a challenge of tracking released drug using conventional methods like dialysis. It was observed that the particles degraded so rapidly after application of the stimuli that the drug precipitated, leading to sedimentation within the dialysis membrane (Figure A-6a). On the other hand, the BnCO-PEtG controls showed no precipitation or sedimentation over the same time frame (Figure A-6b). Measurements of the dialysate were therefore not an accurate representation of released drug. To overcome this, 200 µL samples were taken of the contents within the dialysis membrane at incremental time points. These 200 µL samples were passed through 0.22 µm syringe filters. The resulting filtered suspensions were then diluted with acetonitrile to dissolve the particles and remaining encapsulated drug. The absorbance was measured at 240 nm to quantify the amount of drug that had remained encapsulated. The study was conducted for NVOC-PLA-PEtG NPs. BnCO-PEtG particles were used as the non-responsive control and non-irradiated NVOC-PEtG (PLA-PEtG-nonirr.) particle samples were also measured as an additional control. In Figure 31, the release of letrozole from each PLA-PEtG particle system is shown. Figure 32 shows the release profiles for each of the control samples.
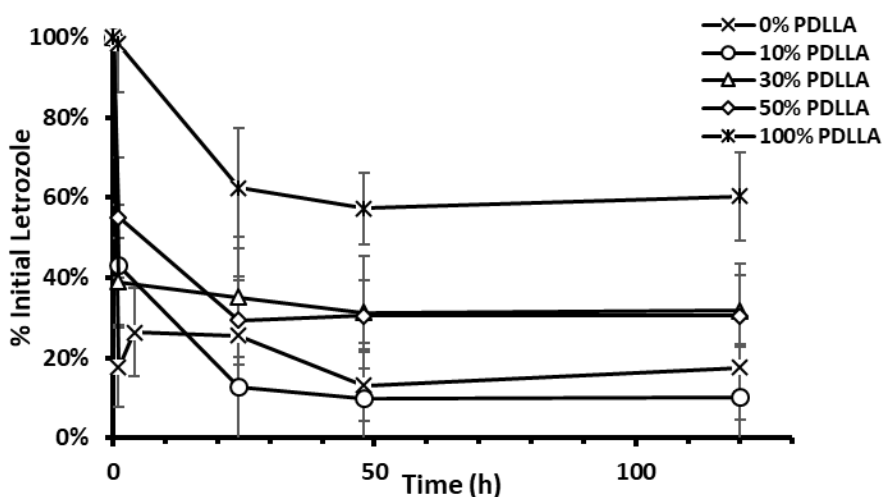
Figure 31. Release profile of letrozole-loaded, UV-irradiated NVOC-PEtG particles.
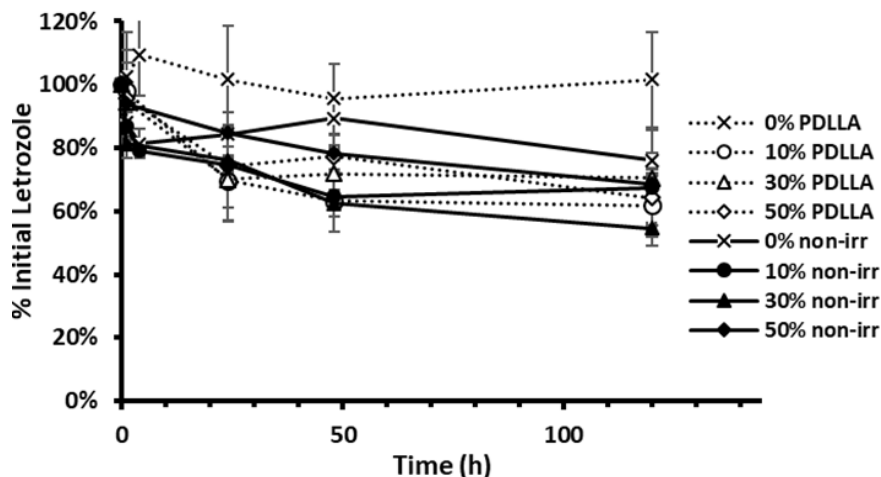
Figure 32. Release profile of letrozole-loaded particle controls: BnCO-PEtG and negative controls.

After irradiation with UV light, a significant burst release was observed with the irradiated NVOC-PEtG particles, which was not seen in the 100% PLA sample or the control samples. This can be attributed to successful and specific triggerable release using UV light as a stimulus in this study. For example, the 100% NVOC-PEtG particles released over 80% of the encapsulated letrozole over the first hour whereas the non-irradiated control retained essentially all of the encapsulated drug for more than 100 h. The second important observation was the noticeable trend of increasing wt% PLA leading to a plateau in drug release at increased remaining drug percentages. This is consistent with previous DLS and Nile red studies. The only major exception to this general trend was several of the 100% NVOC-PEtG measurements which had higher retained drug, which could result from some particle destabilization and aggregation or simply the sample-to-sample variability on the measurements. The third, unfavorable observation was the relatively fast rate of release of letrozole from the control particles. Approximately 20 – 40% of letrozole was released from all control samples except non-irradiated 100% PEtG over the period of five days. The release may arise from letrozole partitioning gradually into the aqueous environment and diffusing out through the dialysis membrane. The solubility of letrozole is 80 µg/mL in water. This value multiplied by 100 mL of dialysate equates to 8 mg that can be dissolved in the dialysate. Only 3 mg of letrozole was used in this study per sample so passive diffusion of the controls into the dialysate is plausible.

3.5.3   Triggerable Release of Celecoxib

To test a different stimuli-responsive end-cap in this system, particles were synthesized using a reduction-sensitive end-cap containing a disulfide bond. The common small triggering molecule used in these systems is DTT. Complications arose when attempting to monitor the release of cargo from disulfide-PEtG particles using letrozole and celecoxib due to DTT having strong absorbance character in the 200−250 nm region. The absorbance of the stimulus gave inconsistent results in release studies by drowning out the signal of the drug molecule, even when accounted for when running a background of the same concentration of stimulus present. To overcome the erroneous data acquired from background stimulus in the sample, a different approach to measuring the release was needed. It was hypothesized that the quick release could be taken advantage of using centrifugation. After release, the precipitated drug could be removed by centrifugation to collect a pellet at incremental time points. The remaining particle suspension could be decanted off and the study continued, leaving released drug as a pellet that could be dissolved then the concentration quantitatively measured to determine the amount of released drug. This would avoid the presence of stimulus absorbance when measuring the UV absorbance.

Celecoxib was chosen to show versatility in potential cargo encapsulation, as well as for its high loading efficiency and drug content. Particles were prepared as with previous studies, including each PLA-PEtG blend, pure PEtG, pure PLA particles. The samples were in 100 mM, pH 7.4 phosphate buffer and kept in a 37 °C oven for the duration. DTT was used as the stimulus with a concentration of 15 mmol introduced to both the disulfide-PEtG and BnCO-PEtG control samples. No DTT was added for separate disulfide-PEtG samples for a negative control. At specific time points, the samples were centrifuged and the pellet was collected. The pellet was distributed into thirds and dissolved in 1 mL acetonitrile. At the first time point, the disulfide-PEtG samples were instead dissolved into 1 mL d_3-acetonitrile for NMR analysis. It was important to distinguish if the pellet contained significant amounts of intact PEtG which could signify presence of intact particles in the pellet. The samples were analyzed using UV-Vis spectroscopy to determine the concentration of celecoxib present in the pellet. The

release profiles for the DTT-treated particles are shown in Figure 33a. and the controls are shown in Figure 33b.
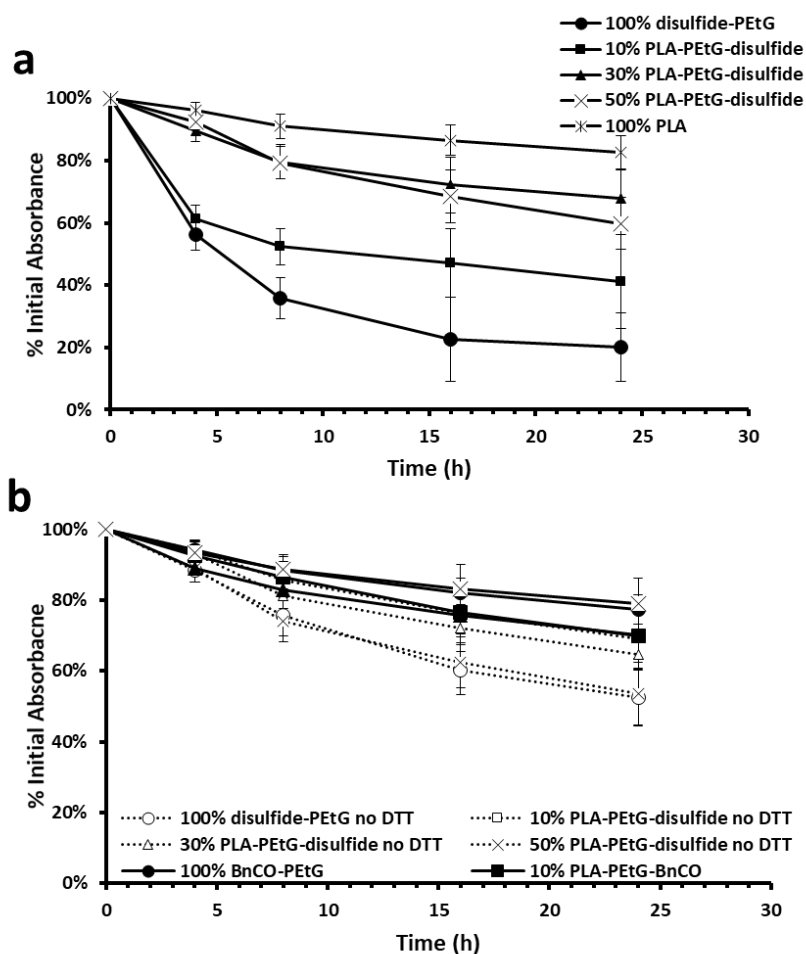
Figure 33. Release profile of celecoxib-loaded PLA-PEtG-disulfide NPs and their controls. **(a)** celecoxib-loaded, 15 mmol DTT added PLA-PEtG-disulfide particles and **(b)** celecoxib-loaded particle controls: BnCO-PEtG and negative control.

The same general trend seen in the DLS and Nile red studies was observed for the release of celecoxib. Pure PEtG particles exhibited the fastest release and with increasing PLA content, the release is slowed. There is no significant burst release seen in this study which is consistent with previous reduction-responsive particle studies. The controls appear to be roughly linear in their release profile with no significant burst release. The gradual, slow release of celecoxib in these samples is consistent across both the control samples and the disulfide-PEtG with no added DTT samples. The release from the controls can be attributed to slow, passive diffusion of the celecoxib out of the particles.

It is important to note that the centrifugation method is not a perfect analysis. For example, during centrifugation, not all of the precipitated drug goes into the pellet. There is visible drug still suspended in the decanted solution that is not being accounted for in the release. The small portion of drug left suspended in the sample may account for the pure PEtG sample not reaching 100% release. The presence of free drug was a noticeable problem with both the 100% PEtG sample and 10% PLA-PEtG sample. It is possible that the release in these two samples is much faster than what is shown. Secondly, there is an unavoidable small volume (~ 100 µL) of sample that remains in the centrifuge tube after decanting. This residual volume, although small, does contain particles encapsulated with celecoxib. It also is possible that some of the "release" depicted in the controls is actually celecoxib that was still encapsulated within intact particles in this residual small volume.

The pellet content was also examined by NMR spectroscopy to determine qualitatively the presence of PEtG. Stimuli-responsive samples should show very little intact PEtG peaks and should compose mostly of celecoxib peaks and/or PLA peaks. If there exists significant PEtG, it is possible that either particles were present in the pellet or in the residual sample left after decanting. NMR spectra were taken for each sample at t = 4 h and t = 24 h post-DTT treatment. The aromatic peaks of celecoxib are used as an indicator of the presence of celecoxib. The backbone proton of PLA appears as a broad singlet at 5.1 ppm and the backbone proton of PEtG appears as another broad singlet at 5.6 ppm. This can be examined for each sample in the celecoxib release study found in appendix Figures A-16–A-27. The 10% PLA-PEtG-disulfide sample is depicted in Figure 34 for discussion. Coinciding with the concentration of celecoxib found by UV-vis spectroscopy, the NMR spectrum of 10% PLA-PEtG-disulfide shows the majority of the pellet to be celecoxib. There is very minimal intact PEtG present as can be concluded from the absence of the proton signal in the backbone of the intact polymer. There is a sharp singlet present at 5.7 ppm which is consistent with the hydrated version of the ethyl glyoxylate monomer. There is also presence of PLA in the pellet which is most likely due to the precipitated of PLA in the aqueous environment as the PEtG degrades, destabilizing the PLA portions of the particles. The 24 h spectrum is consistent with the UV data where a significant portion of celecoxib was not released at this time point. Each disulfide-PEtG sample showed similar NMR spectra results, the most important result

being the absence of intact PEtG. The BnCO-PEtG control samples as well as the disulfide-PEtG with no DTT stimulus controls do show some intact PEtG in their spectra.
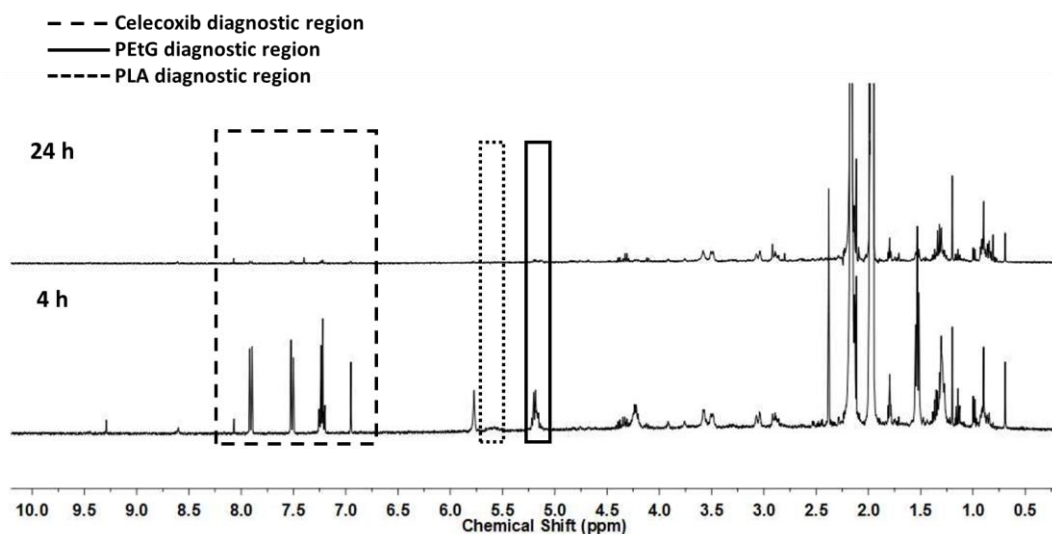
Figure 34. ^{1}H NMR spectra of pellet collected from celecoxib release study of 10% PLA-PEtG-disulfide sample after 4 and 24 h (CD$_3$CN, 400 MHz).

Overall, from the celecoxib release profiles, along with the NMR spectra, it can be concluded that celecoxib could be triggered to release from the PLA-PEtG-disulfide particles to a much higher extent than from control samples. Furthermore, increasing PLA content led to a slower release rate over a 24 h period. These data are consistent with the letrozole-loaded NVOC-PEtG studies, as well as, the DLS and Nile red studies.

3.6 PLA-PEtG NP Cell Viability Studies

It was important to determine how these particles behaved *in vitro* to ascertain effectiveness of PLA-PEtG NPs as potential DDSs. To study their behavior in cells, MTT (3-[4,5-dimethylthiazol-2-yl]-2,5-diphenyltetrazolium bromide) assays were conducted on MDA-MB-231, human breast cancer cells. This assay measures the metabolic activities of cells. In living and metabolically active cells, the MTT reagent is reduced to a compound that can be measured spectrophotometrically. Due to the high loading efficiency and drug content, celecoxib was chosen as the cargo molecule for these

studies. Cells were seeded on 96-well plates for each cell viability study. Free celecoxib, unloaded 100% NVOC-PEtG, unloaded 50% PLA-PEtG-NVOC, non-irradiated celecoxib-loaded 100% NVOC-PEtG and non-irradiated celecoxib-loaded 50% PLA-PEtG-NVOC were each administered to a seeded, 96-well plate and allowed to incubate for 48 h to determine the cell viability for each of these controls. Untreated cells grown in the aforementioned media, as well as a media-only control were tested. Lastly, celecoxib-loaded 100% NVOC-PEtG and celecoxib-loaded 50% PLA-PEtG-NVOC were administered to the cells. The cells were then irradiated with 30 minutes of 360 nm light using light emitting diode flashlights.

It is hypothesized that the particles will enter the cell by the active transportation via endocytosis and exist in vesicles inside the cell where the release of cargo can occur. Unloaded 100% PEtG and 50% PLA-PEtG particles were studied to determine the toxicity of the materials themselves. Neither particles showed signs of cell toxicity even at 1 mg/mL, the highest concentration of particles evaluated (Figure 35). Free celecoxib had a half maximal inhibitory concentration (IC_{50}) of 79 µM which is consistent with the literature value (Figure 36).[87] For the celecoxib-loaded particles and celecoxib-loaded-irradiated particles, the concentration was plotted as the log of celecoxib concentration to compare cell viability of free celecoxib with irradiated and non-irradiated cell plates. The concentration of celecoxib in the loaded particles was calculated based on the loaded wt% of celecoxib within the particles multiplied by the concentration of particles administered. These plots are shown in Figure 36 and Figure 37. From the data, several conclusions can be made. First, the celecoxib-loaded particles were much less toxic than the free drug. Significant cell death was only seen at the highest concentration of particles (~ 600 µM of drug). This suggests that the free drug was not released fully within the cells or was released over a longer time frame, leading to lower toxicity. In addition, the UV irradiated particles showed no significant difference in toxicity relative to the non-irradiated particles. It would be expected that irradiated particles would release their celecoxib contents and induce cell death in this manner, but this was not seen. It could be possible that the celecoxib was precipitating out of solution once released, as seen in the release studies. In addition, it is known known whether the particles were taken up by

cells. This will require further investigation and other stimuli will need to be studied. However, it is still important to conclude that PEtG NPs showed no toxicity to MDA-MB-231 cells and they could decrease the celecoxib toxicity to this cell line.
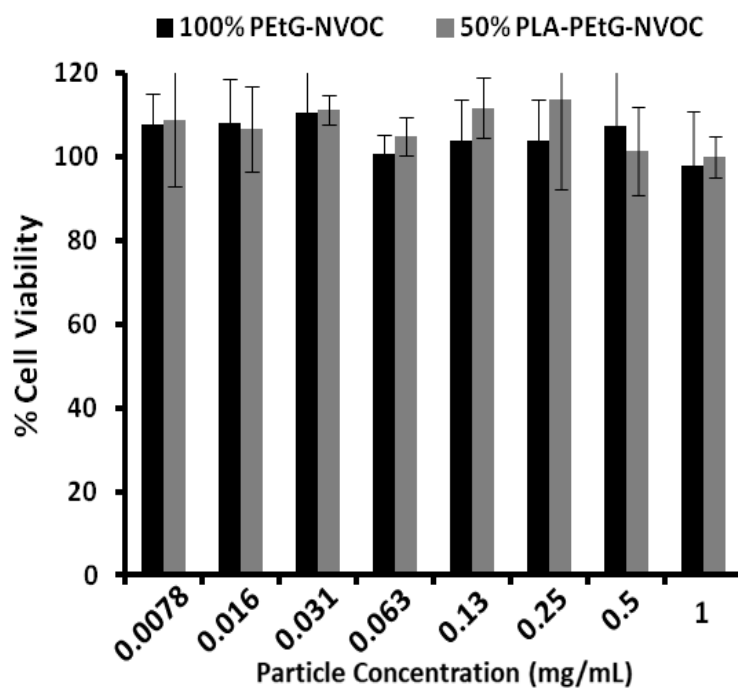
Figure 35. MTT assays of unloaded 100% NVOC-PEtG and unloaded 50% PLA-PEtG-NVOC NPs in MDA-MB-231 cells. Error bars represent the standard deviations on the measurements.
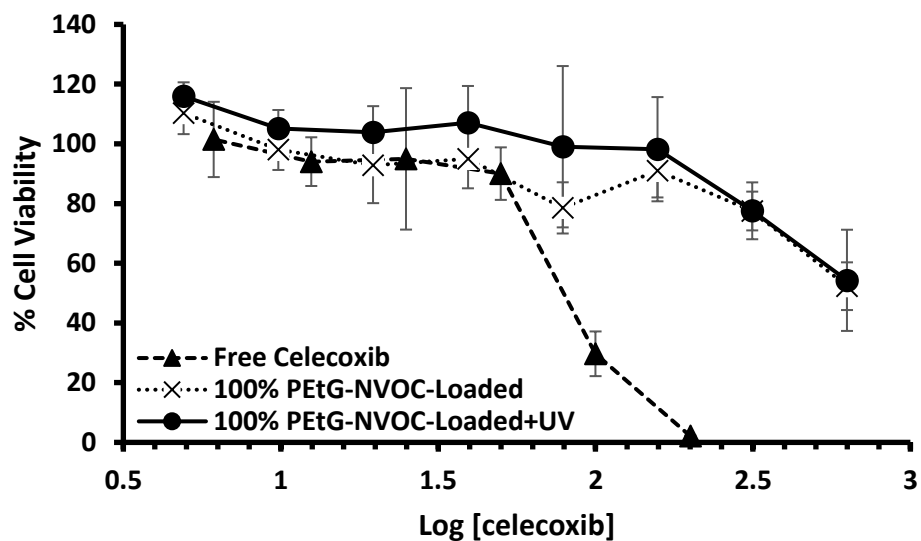
Figure 36. MTT assay cell viability studies of free celecoxib, 100% NVOC-PEtG-loaded and 100% NVOC-PEtG-loaded irradiated with 30 minutes of UVA light in MDA-MB-231 cells. Error bars represent the standard deviations on the measurements.
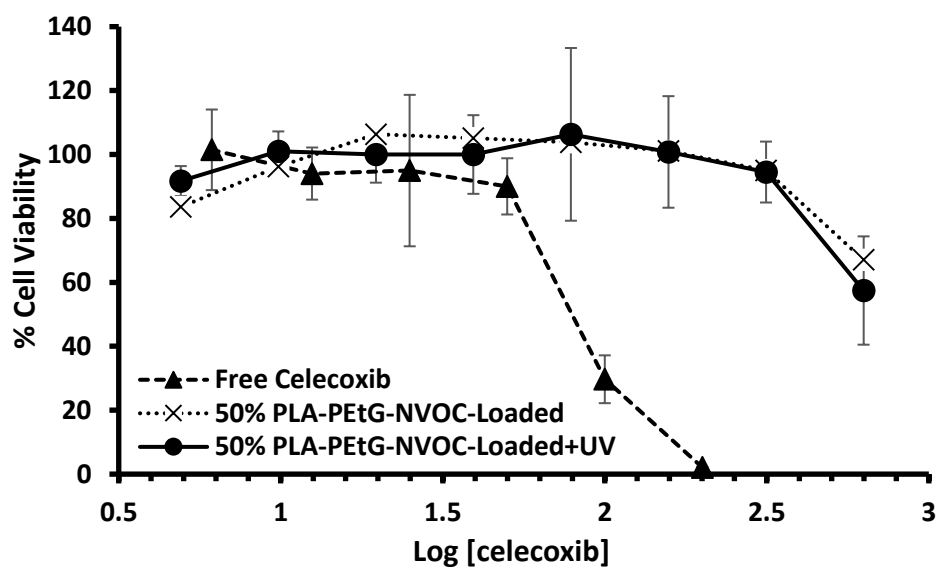
Figure 37. MTT assay cell viability studies of free celecoxib, 50% PLA-PEtG-NVOC-loaded and 50% PLA-PEtG-NVOC-loaded irradiated with 30 minutes of UVA light in MDA-MB-231 cells. Error bars represent the standard deviations on the measurements.

4   Conclusions & Future Work

The results of this work led to several significant findings relevant to the use of PEtG in DDSs. First, it was shown that PEtG can be used as hydrophobic homopolymer to synthesize polymeric NPs using an O/W emulsion technique. 100% PEtG NPs are stable in solution and can be synthesized with ~100 nm diameters, which is in the optimal range for intravenous injection. These particles were demonstrated to be stimuli-responsive when manufactured with a stimuli-responsive end-capped PEtG. These stimuli-responsive particles could be loaded with a hydrophobic cargo and triggered to release that cargo upon introduction of relatively small concentrations of stimulus.

In addition, while pure PEtG NPs rapidly release a large fraction of their cargo in response to stimuli, it was possible to tune the extent of this burst release using blends with PLA. By changing the wt% PLA, it was found that the release rates of cargo molecules can be tuned. Increasing PLA character led to a slower release of cargo. The morphology and diameter of blended particles showed no significant difference to 100% PEtG particles. This was confirmed by DLS and TEM.

Two stimuli-responsive end-capped PEtG NPs were studied in this work, UV light sensitive and reduction sensitive. These two stimuli-responsive particles had interesting differences in their release profiles. NVOC-PEtG particles showed a very rapid, burst release within the first hour post-UV irradiation. This was followed by a plateau region correlating to the amount of PLA present in the particles. This gave a two-part release: a quick burst release of drug at the beginning due to rapid degradation of PEtG followed by a slower release of drug from the remaining PLA domains. Disulfide-PEtG particles showed less initial burst release, but still showed slower release with increasing PLA content. These trends were seen for DLS studies, Nile red studies and hydrophobic drug studies.

Finally, PLA-PEtG NPs showed no toxicity to MDA-MB-231 cells, even at the highest concentration of particles evaluated (1 mg/mL). When these particles were loaded with celecoxib, no toxicity was seen until a concentration of 600 μM. This is well above the IC_{50} of celecoxib which is reported to be around 79 μM in MDA-MB-231 cells.

Unfortunately, it was found that celecoxib-loaded NVOC-PEtG particles administered to this cell line did not show a decrease of cell viability when irradiated with 30 minutes of UV light. It is not known if the nanoparticles were taken up by cells. This would require further studies to investigate this using labeled particles. It is also possible that the released celecoxib could be precipitating out of solution, therefore unavailable to the cells.

To extend this work, several areas could be further investigated. First, research towards alternative surfactants could produce PEtG particles that are less susceptible to aggregation upon drying. This would allow for ease in drying and dispersing the particles back into solution, increasing their shelf-life. Second, it would also be interesting to test a library of stimuli-responsive particles by exchanging the end-cap on PEtG. This would increase the versatility of PEtG NPs and possibly increase their potential applications. This work tested UV and reduction-responsive particles. Particles responsive to pH or temperature might lead to interesting applications. Lastly, further investigation into cellular uptake is essential. Why UV-responsive, celecoxib-loaded particles irradiated with UV light did not lead to a significant drop in cell viability remains unknown.

5 References

1. Albertsson, A.-C.; Huang, S. J., *Degradable polymers, recycling, and plastics waste management*; M. Dekker: New York, 1995.

2. Billingham, N., *Polym. Degrad. Stab.* **1996**, *2*, 269–270.

3. D. A. Schluter; C. J., Hawker; C. H., J. Sakamoto, *Synthesis of Polymers: New Structures and Methods;* 1st ed.; Wiley-VCH Verlag, 2012.

4. Amass, W.; Amass, A.; Tighe, B., *Polym. Int.* **1998**, *47*, 89–144.

5. Huang, S. J., *J. Macromol. Sci., Pure Appl. Chem.* **1995**, *32*, 593–597.

6. Chen, G.-Q.; Patel, M. K., *Chem. Rev.* **2012**, *112*, 2082–2099.

7. Scott, G., *Degradable polymers: principles and applications*. 2nd ed.; Springer: 2002.

8. Nair, L. S.; Laurencin, C. T., *Prog. Polym. Sci.* **2007**, *32*, 762–798.

9. Sionkowska, A., *Prog. Polym. Sci.* **2011**, *36*, 1254–1276.

10. Kawai, F.; Schink, B., *Crit. Rev. Biotechnol.* **1987**, *6*, 273–307.

11. Gunatillake, P. A.; Adhikari, R., *Eur. Cell. Mater.* **2003**, *5*, 1–16.

12. Luckachan, G. E.; Pillai, C., *J. Polym. Environ.* **2011**, *19*, 637–676.

13. Anderson, J. M.; Shive, M. S., *Adv. Drug Deliv. Rev.* **2012**, *64*, 72–82.

14. Bergsma, J. E.; De Bruijn, W.; Rozema, F.; Bos, R.; Boering, G., *Biomaterials* **1995**, *16*, 25–31.

15. Mi, F.-L.; Lin, Y.-M.; Wu, Y.-B.; Shyu, S.-S.; Tsai, Y.-H., *Biomaterials* **2002**, *23*, 3257–3267.

16. Allen, T. M.; Cullis, P. R., *Science* **2004**, *303*, 1818–22.

17. Grijpma, D.; Nijenhuis, A.; Pennings, A., *Polymer* **1990**, *31*, 2201–2206.

18. Sagi, A.; Weinstain, R.; Karton, N.; Shabat, D., *J. Am. Chem. Soc.* **2008**, *130*, 5434–5435.

19. Bawa, P.; Pillay, V.; Choonara, Y. E.; Du Toit, L. C., *Biomed. Mater.* **2009**, *4*, 22001.

20. Galaev, I.; Mattiasson, B., *Smart Polymers for Bioseparation and Bioprocessing*; 1st ed.; CRC Press: London, 2001.

21. Wang, D.; Jin, Y.; Zhu, X.; Yan, D., *Prog. Polym. Sci.* **2017**, *64*, 114–153.

22. Blencowe, C. A.; Russell, A. T.; Greco, F.; Hayes, W.; Thornthwaite, D. W., *Polym. Chem.* **2011**, *2*, 773–790.

23. Carl, P. L.; Chakravarty, P. K.; Katzenellenbogen, J. A., *J. Med. Chem.* **1981**, *24*, 479–480.

24. Neumann, K.; Jain, S.; Gambardella, A.; Walker, S. E.; Valero, E.; Lilienkampf, A.; Bradley, M., *ChemBioChem* **2017**, *18*, 91–95.

25. Wong, A. D.; DeWit, M. A.; Gillies, E. R., *Adv. Drug Deliv. Rev.* **2012**, *64*, 1031–1045.

26. Szalai, M. L.; Kevwitch, R. M.; McGrath, D. V., *J. Am. Chem. Soc.* **2003**, *125*, 15688–15689.

27. de Groot, F. M. H.; Loos, W. J.; Koekkoek, R.; van Berkom, L. W. A.; Busscher, G. F.; Seelen, A. E.; Albrecht, C.; de Bruijn, P.; Scheeren, H. W., *J. Org. Chem.* **2001**, *66*, 8815–8830.

28. Kratz, F.; Muller, I. A.; Ryppa, C.; Warnecke, A., *ChemMedChem* **2008**, *3*, 20–53.

29. Stover, T. C.; Kim, Y. S.; Lowe, T. L.; Kester, M., *Biomaterials* **2008**, *29*, 359–369.

30. Peterson, G. I.; Larsen, M. B.; Boydston, A. J., *Macromolecules* **2012**, *45*, 7317–7328.

31. Kim, J.-K.; Garripelli, V. K.; Jeong, U.-H.; Park, J.-S.; Repka, M. A.; Jo, S., *Int. J. Pharm.* **2010**, *401*, 79–86.

32. Esser-Kahn, A. P.; Sottos, N. R.; White, S. R.; Moore, J. S., *J. Am. Chem. Soc.* **2010**, *132*, 10266–10268.

33. Steichen, S. D.; Caldorera-Moore, M.; Peppas, N. A., *Eur. J. Pharm. Sci.* **2013**, *48*, 416–427.

34. Wang, W.; Alexander, C., *Angew. Chem. Int. Ed.* **2008**, *47*, 7804–7806.

35. Dadmun, M. D.; Hook, W. A.; Noid, D. W.; Melnichenko, Y. B.; Sumpter, B. G., *Computational studies, nanotechnology, and solution thermodynamics of polymer systems*; Springer: New York, 2001.

36.	Fan, B.; Gillies, E. R., Self-immolative Polymers. In *Encyclopedia of Polymer Science and Technology;* Wiley-VCH Verlag: **2015**.

37.	Steiger, A. K.; Pardue, S.; Kevil, C. G.; Pluth, M. D., *J. Am. Chem. Soc.* **2016**, *138*, 7256–7259.

38.	Wong, A. D. Design and Implementation of Multi-Responsive Azobenzene Triggers in Self-Immolative and Degradable Polymers. Ph.D. Dissertation, The University of Western Ontario, London, ON, 2016.

39.	Matikonda, S. S.; Fairhall, J. M.; Tyndall, J. D.; Hook, S.; Gamble, A. B., *Org. Lett.* **2017**, *19*, 528–531.

40.	Iturmendi, A.; Monkowius, U.; Teasdale, I., *ACS Macro Lett.* **2017**, *6*, 150–154.

41.	DeWit, M. A.; Gillies, E. R., *J. Am. Chem. Soc.* **2009**, *131*, 18327–18334.

42.	Chen, E. K. Y.; McBride, R. A.; Gillies, E. R., *Macromolecules* **2012**, *45*, 7364–7374.

43.	DiLauro, A. M.; Robbins, J. S.; Phillips, S. T., *Macromolecules* **2013**, *46*, 2963–2968.

44.	DiLauro, A. M.; Lewis, G. G.; Phillips, S. T., *Angew. Chem. Int. Ed.* **2015**, *54*, 6200–6205.

45.	DiLauro, A. M.; Abbaspourrad, A.; Weitz, D. A.; Phillips, S. T., *Macromolecules* **2013**, *46*, 3309–3313.

46.	Fan, B.; Trant, J. F.; Wong, A. D.; Gillies, E. R., *J. Am. Chem. Soc.* **2014**, *136*, 10116–10123.

47.	Belloncle, B.; Bunel, C.; Menu-Bouaouiche, L.; Lesouhaitier, O.; Burel, F., *J. Polym. Environ.* **2012**, *20*, 726–731.

48.	Fan, B.; Gillies, E. R., *Mol. Pharm.* DOI: 10.1021/acs.molpharmaceut.7b00030.

49.	Lassalle, V.; Ferreira, M. L., *Macromol. Biosci.* **2007**, *7*, 767–783.

50.	Brannon-Peppas, L., *Int. J. Pharm.* **1995**, *116*, 1–9.

51.	Julienne, M.; Alonso, M.; Gomez Amoza, J.; Benoit, J., *Drug Dev. Ind. Pharm.* **1992**, *18*, 1063–1077.

52.	Wischke, C.; Schwendeman, S. P., *Int. J. Pharm.* **2008**, *364*, 298–327.

53.	Alexis, F.; Pridgen, E.; Molnar, L. K.; Farokhzad, O. C., *Mol. Pharm.* **2008**, *5*, 505–515.

54. Gaumet, M.; Vargas, A.; Gurny, R.; Delie, F., *Eur. J. Pharm. Biopharm.* **2008**, *69*, 1–9.

55. Blanco, E.; Shen, H.; Ferrari, M., *Nat. biotechnol.* **2015**, *33*, 941–951.

56. Dadwal, M. *J., Adv. Pharm. Edu. Res.* **2014**, *4*, 20–30.

57. Liu, G.-Y.; Chen, C.-J.; Ji, J., *Soft Matter* **2012**, *8*, 8811–8821.

58. Zhang, Y.; Chan, H. F.; Leong, K. W., *Adv. Drug Deliv. Rev.* **2013**, *65*, 104–120.

59. López-Sagaseta, J.; Malito, E.; Rappuoli, R.; Bottomley, M. J., *Comput. Struct. Biotechnol. J.* **2016**, *14*, 58–68.

60. Owens, D. E.; Peppas, N. A., *Int. J. Pharm.* **2006**, *307*, 93–102.

61. Schipper, M. L.; Iyer, G.; Koh, A. L.; Cheng, Z.; Ebenstein, Y.; Aharoni, A.; Keren, S.; Bentolila, L. A.; Li, J.; Rao, J., *Small* **2009**, *5*, 126–134.

62. Carrstensen, H.; Müller, R. H.; Müller, B., *Clin. Nutr.* **1992**, *11*, 289–297.

63. He, J.; Qi, X.; Miao, Y.; Wu, H.-L.; He, N.; Zhu, J.-J., *Nanomedicine* **2010**, *5*, 1129–1138.

64. Naahidi, S.; Jafari, M.; Edalat, F.; Raymond, K.; Khademhosseini, A.; Chen, P., *J. Control. Release* **2013**, *166*, 182–194.

65. Cheng, W.; Gu, L.; Ren, W.; Liu, Y., *Mater. Sci. Eng. C.* **2014**, *45*, 600–608.

66. Gungor, T. M. Self-Assembly and Stimuli-Responsive Properties of Amphiphilic Self-Immolative Block Co-Polymers. The University of Western Ontario, M.Sc. Dissertation, The University of Western Ontario, London, ON, 2015.

67. Lipinski, C., *Am. Pharm. Rev.* **2002**, *5*, 82–85.

68. Farokhzad, O. C.; Langer, R., *Adv. Drug Deliv. Rev.* **2006**, *58*, 1456–1459.

69. Safari, J.; Zarnegar, Z., *J. Saudi Chem. Soc.* **2014**, *18*, 85–99.

70. Matsumura, Y.; Maeda, H., *Cancer Res.* **1986**, *46*, 6387–6392.

71. Murakami, H.; Kobayashi, M.; Takeuchi, H.; Kawashima, Y., *Int. J. Pharm.* **1999**, *187*, 143–152.

72. Gutiérrez, J.; González, C.; Maestro, A.; Sole, I.; Pey, C.; Nolla, J., *Curr. Opin. Colloid Interface Sci.* **2008**, *13*, 245–251.

73. McCall, R. L.; Sirianni, R. W., *J. Vis. Exp.* **2013**, *82*, e51015.

74. Koo, O. M.; Rubinstein, I.; Onyuksel, H., *Nanomedicine* **2005**, *1*, 193–212.

75. Pathak, T.; Waldmann, H., *Curr. Opin. Chem. Biol.* **1998**, *2*, 112–120.

76. Liu, G.; Wang, X.; Hu, J.; Zhang, G.; Liu, S., *J. Am. Chem. Soc.* **2014**, *136*, 7492–7497.

77. Duvvuri, S.; Janoria, K. G.; Mitra, A. K., *Pharm. res.* **2006**, *23*, 215.

78. Lamprecht, A.; Ubrich, N.; Yamamoto, H.; Schäfer, U.; Takeuchi, H.; Lehr, C.-M.; Maincent, P.; Kawashima, Y., *J. Control. Release* **2001**, *71*, 297–306.

79. Moustafa, A.; Mahmoud, M.; Zilinskas, G. J.; Gillies, E. R., *Can. J. Chem. Eng.* **2015**, *93*, 2098–2106.

80. Sahli, H.; Tapon-Bretaudière, J.; Fischer, A.-M.; Sternberg, C.; Spenlehauer, G.; Verrecchia, T.; Labarre, D., *Biomaterials* **1997**, *18*, 281–288.

81. O'Donnell, P. B.; McGinity, J. W., *Adv. Drug Deliv. Rev.* **1997**, *28*, 25–42.

82. Fan, B.; Trant, J. F.; Yardley, R. E.; Pickering, A. J.; Lagugné-Labarthet, F.; Gillies, E. R., *Macromolecules* **2016**, *49*, 7196–7203.

83. Liu, X.; Zou, Y.; Li, W.; Cao, G.; Chen, W., *Polym. Degrad. Stab.* **2006**, *91*, 3259–3265.

84. Klymchenko, A. S.; Roger, E.; Anton, N.; Anton, H.; Shulov, I.; Vermot, J.; Mely, Y.; Vandamme, T. F., *RSC Adv.* **2012**, *2*, 11876–11886.

85. Greenspan, P.; Fowler, S. D., *J. Lipid Res.* **1985**, *26*, 781–9.

86. D'souza, S. S.; DeLuca, P. P., *Pharm. res.* **2006**, *23*, 460–474.

87. Vital-Reyes, V.; Rodriguez-Burford, C.; Chhieng, D. C.; Oelschlager, D. K.; Reyes-Fuentes, A.; Barnes, M.; Grizzle, W. E., *Arch. Med. Res.* **2006**, *37*, 689–95.

Appendix
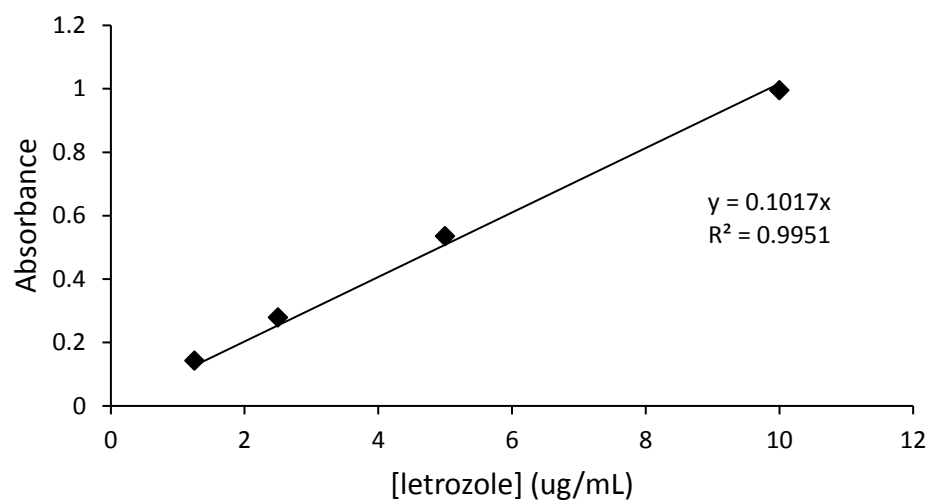
Figure A-1. Letrozole calibration curve in acetonitrile ($\lambda = 240$ nm, $\varepsilon = 30{,}600$ L/cm·cm).
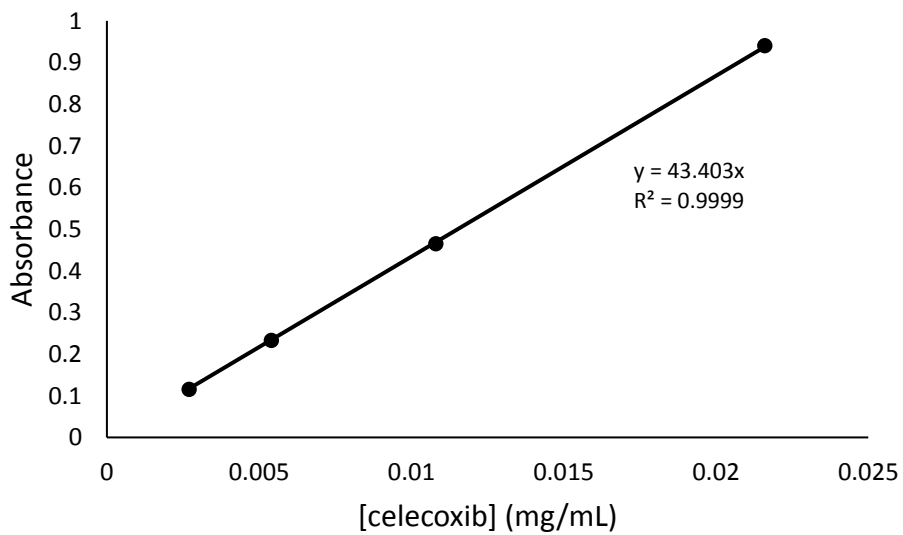
Figure A-2. Celecoxib calibration curve in acetonitrile ($\lambda = 253$ nm, $\varepsilon = 16{,}400$ L/cm·cm).
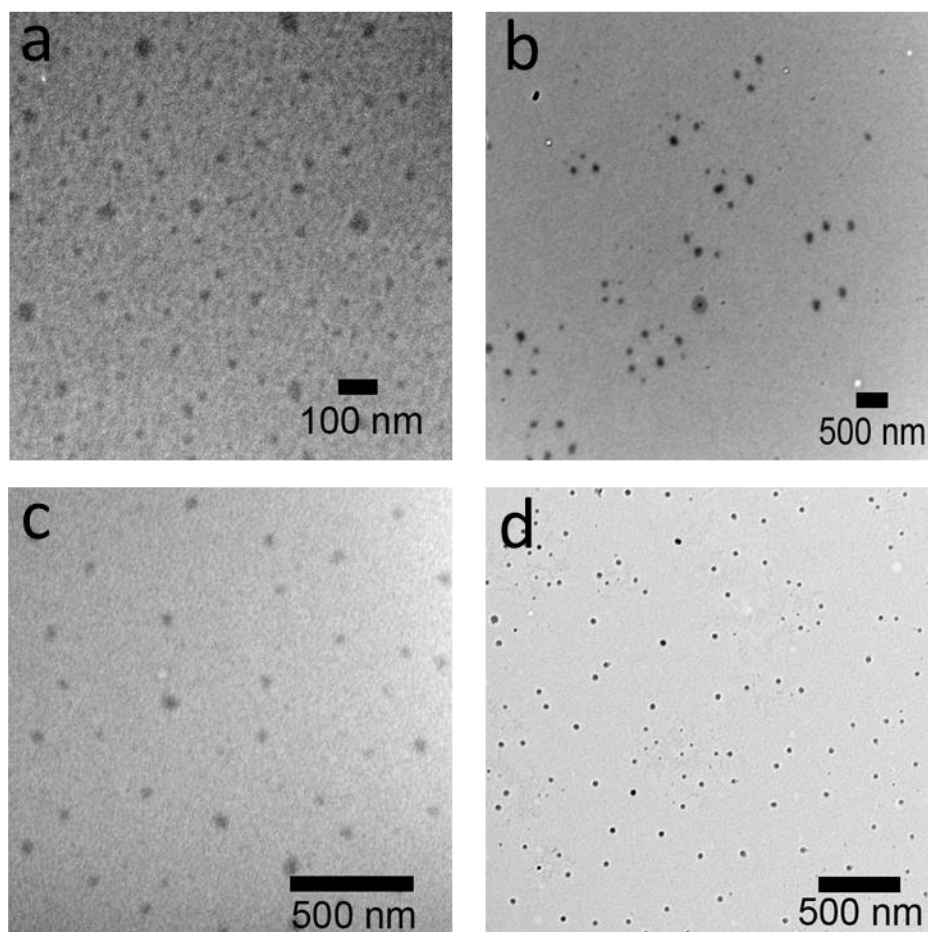
Figure A-3. TEM images of **(a)** pure BnCO-PEtG NPs, **(b)** 10 wt% PLA, **(c)** 30 wt% PLA, and **(d)** 50 wt% PLA.
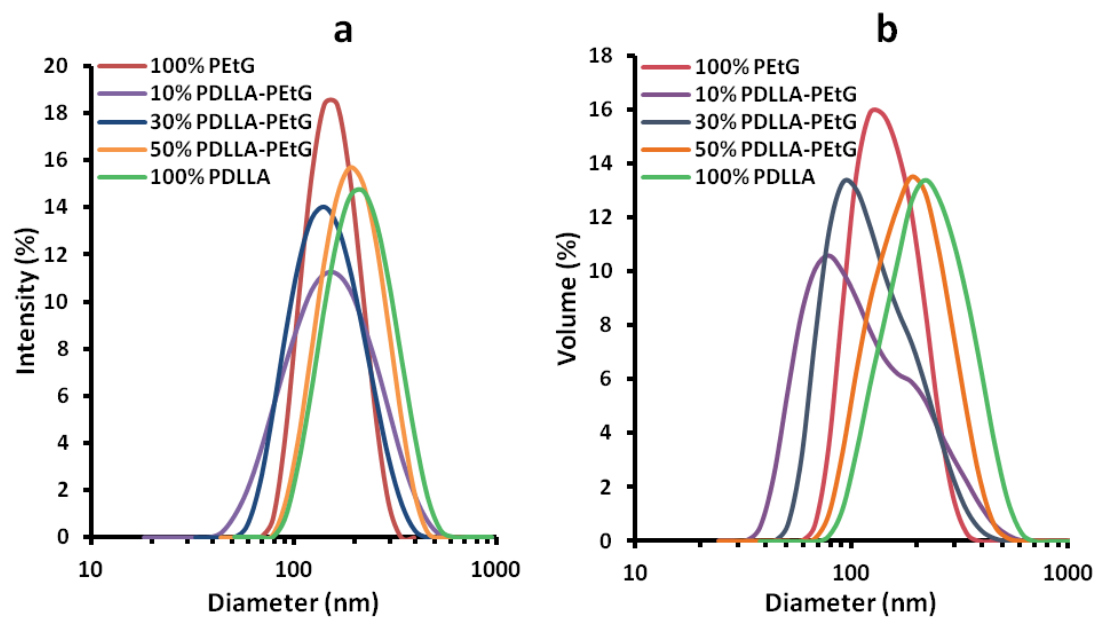
Figure A-4. Determination of particle diameters and disparities by DLS for PLA-PEtG-BnCO blends. (**a**) intensity distribution and (**b**) volume distribution.
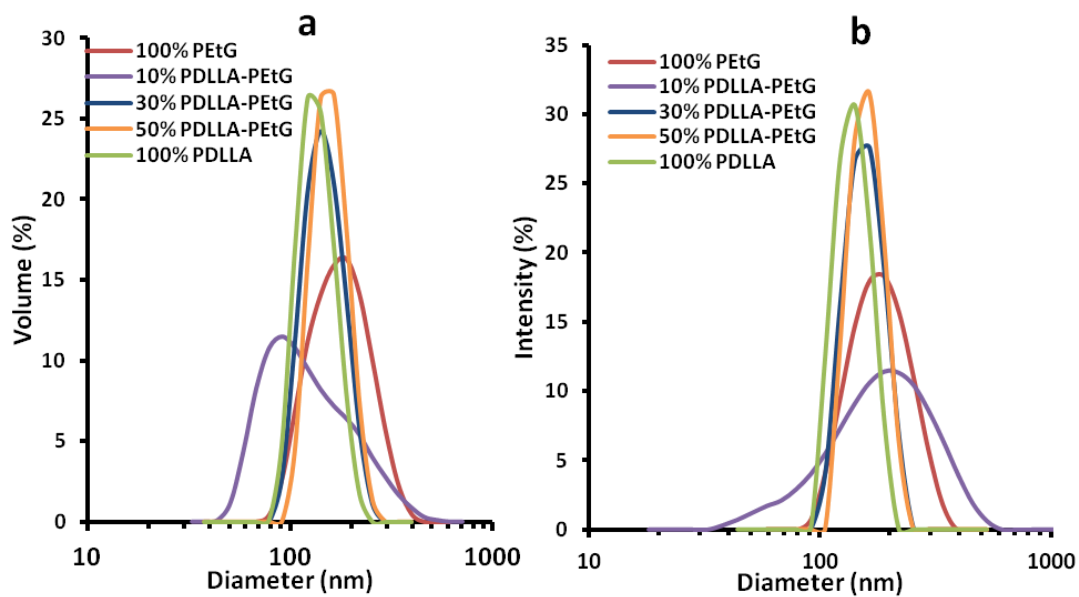
Figure A-5. Determination of particle diameter and dispersity by DLS for PLA-PEtG-disulfide blends. (**a**) intensity distribution and (**b**) volume distribution.

Table A-1. Z-avg. and polydispersity indices for the PLA-PEtG-BnCO & disulfide blends.

Blend	Z-avg. (nm) BnCO	PDI	Z-avg. (nm) disulfide	PDI
0% PLA	128 ± 15	0.11 ± 0.05	129 ± 11	0.17 ± 0.07
10% PLA	144 ± 16	0.17 ± 0.06	130 ± 6	0.11 ± 0.03
30% PLA	127 ± 11	0.11 ± 0.02	122 ± 6	0.09 ± 0.01
50% PLA	131 ± 4	0.14 ± 0.02	124 ± 12	0.12 ± 0.03

Figure A-6. UV-light irradiated letrozole-containing NPs based on **(a)** NVOC-PEtG NPs (containing letrozole precipitates) and **(b)** BnCO-PEtG control, in a dialysis membrane bags.
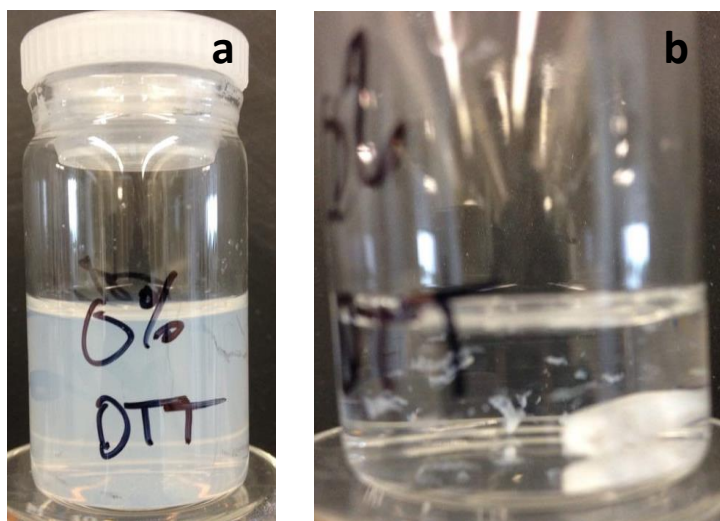
Figure A-7. Celecoxib precipitates formed from celecoxib-containing NPs based on disulfide-PEtG upon the addition of DTT at **(a)** 0 and **(b)** 4 h.
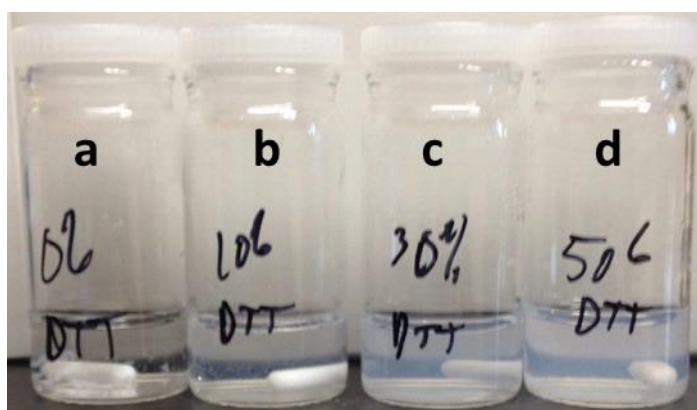
Figure A-8. Celecoxib precipitates formed from celecoxib-containing NPs based on PLA-PEtG-disulfide blends upon the addition of DTT after 4 h. **(a)** 100% PEtG, **(b)** 10% PLA-PEtG, **(c)** 30% PLA-PEtG, and **(d)** 50% PLA-PEtG.
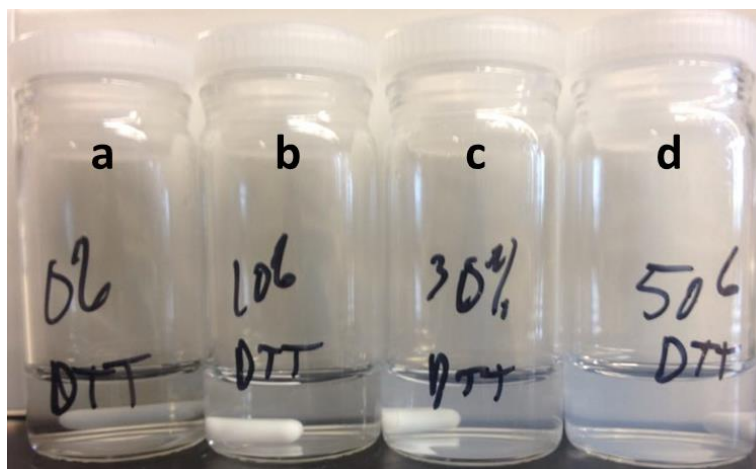
Figure A-9. Celecoxib precipitates formed from celecoxib-containing NPs based on PLA-PEtG-disulfide blends upon the addition of DTT after 24 h. **(a)** 100% PEtG, **(b)** 10% PLA-PEtG, **(c)** 30% PLA-PEtG, and **(d)** 50% PLA-PEtG.

Figure A-10. Celecoxib precipitates formed from celecoxib-containing NPs based on BnCO-PEtG control blends upon the addition of DTT after 4 h. **(a)** 100% PEtG, **(b)** 10% PLA-PEtG, **(c)** 30% PLA-PEtG, and **(d)** 50% PLA-PEtG.
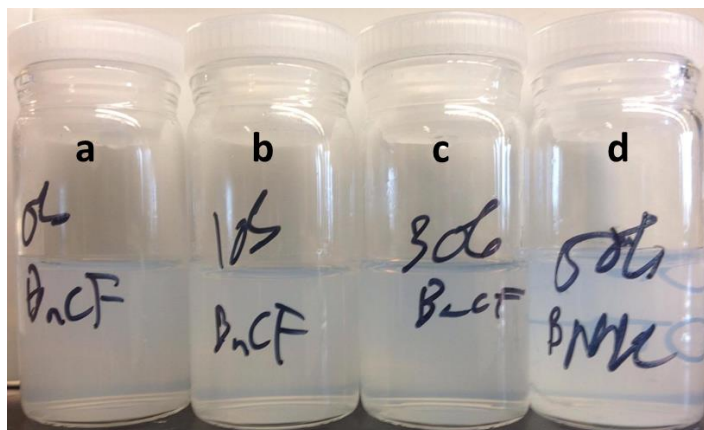
Figure A-11. Celecoxib-containing NPs based on BnCO-PEtG control blends upon the addition of DTT after 24 h. **(a)** 100% PEtG, **(b)** 10% PLA-PEtG, **(c)** 30% PLA-PEtG, and **(d)** 50% PLA-PEtG.

Figure A-12. Celecoxib-containing NPs based on PLA-PEtG-disulfide blends after 4 h. **(a)** 100% PEtG, **(b)** 10% PLA-PEtG, **(c)** 30% PLA-PEtG, and **(d)** 50% PLA-PEtG.
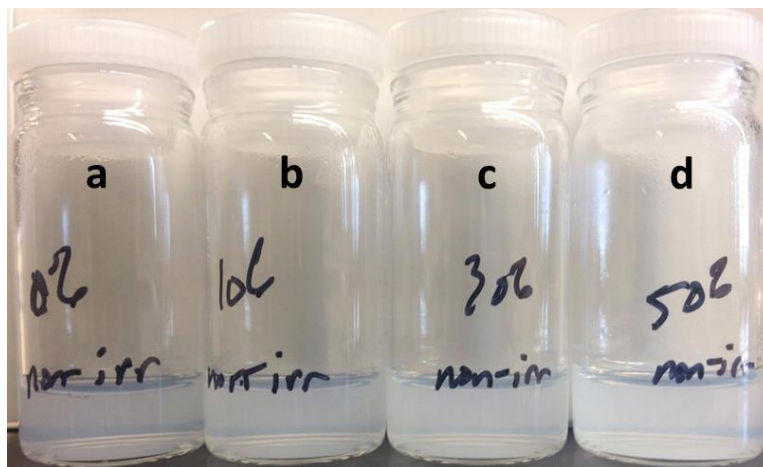
Figure A-13. Celecoxib-containing NPs based on PLA-PEtG-disulfide blends after 24 h. **(a)** 100% PEtG, **(b)** 10% PLA-PEtG, **(c)** 30% PLA-PEtG, and **(d)** 50% PLA-PEtG.
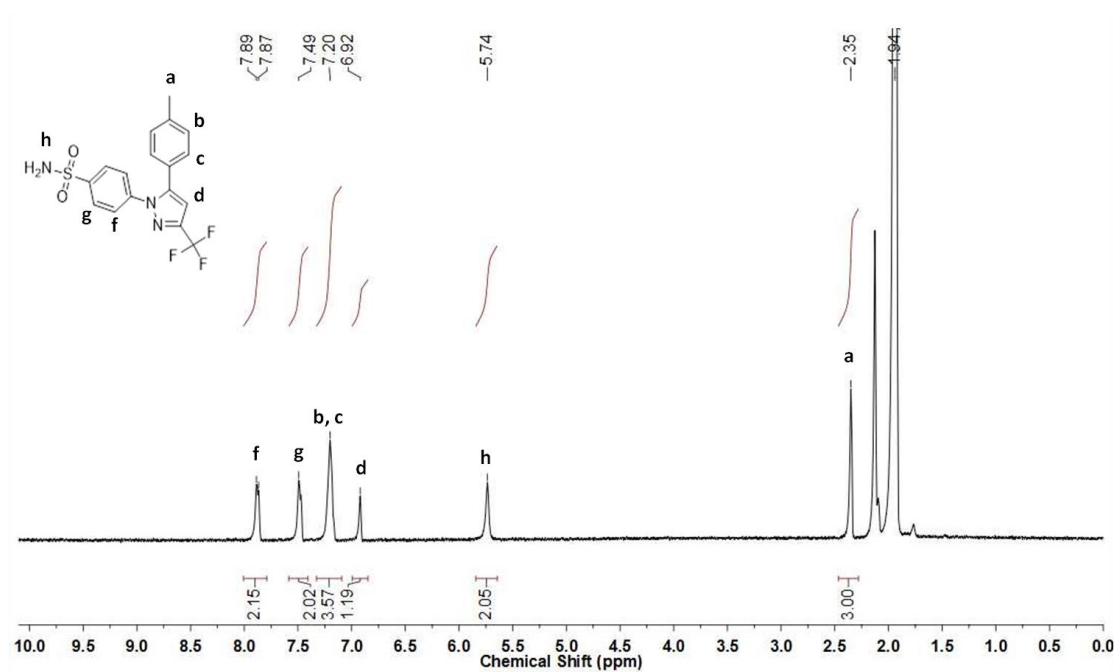
Figure A-14. ^{1}H NMR spectrum of celecoxib (CD$_3$CN, 400 MHz).
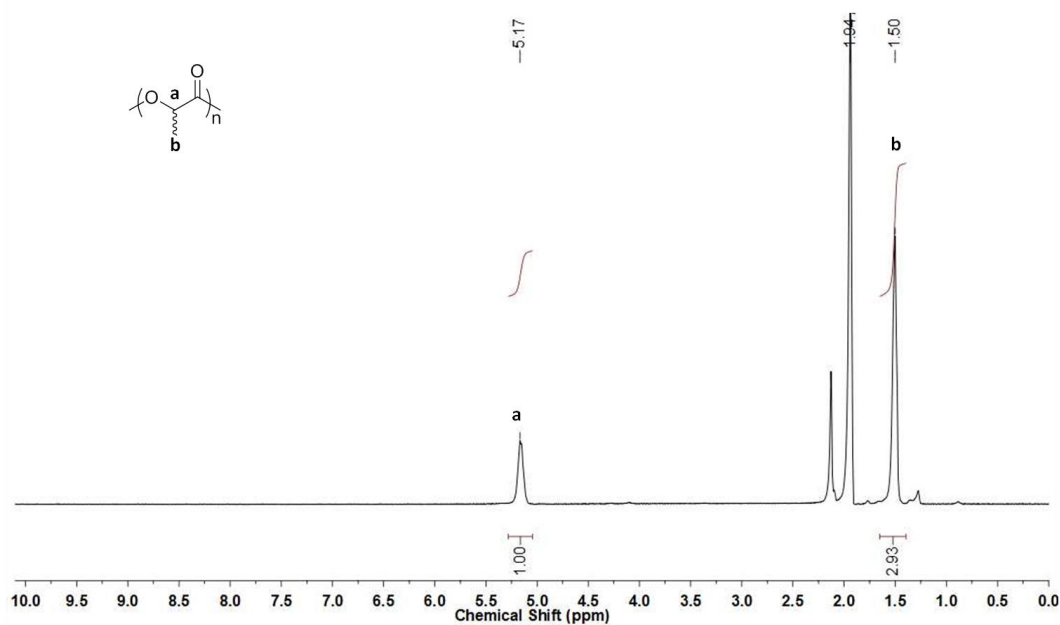
Figure A-15. ^{1}H NMR spectrum of poly(D,L-lactic acid) (CD[3]CN, 400 MHz).
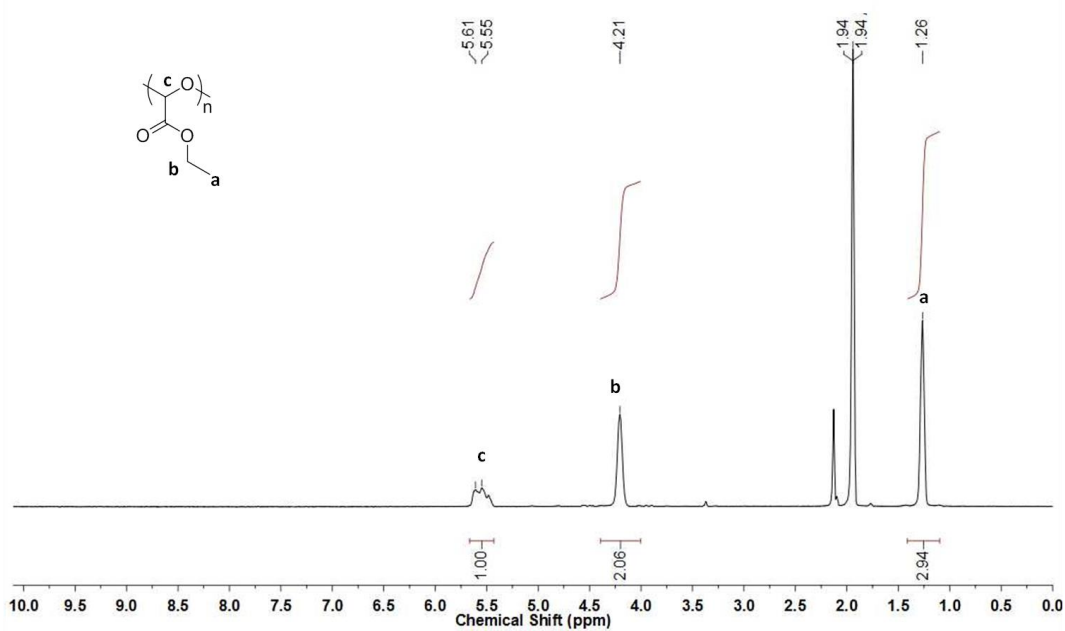
Figure A-16. ^{1}H NMR spectrum of disulfide-PEtG recorded during the celecoxib release studies (CD[3]CN, 400 MHz).
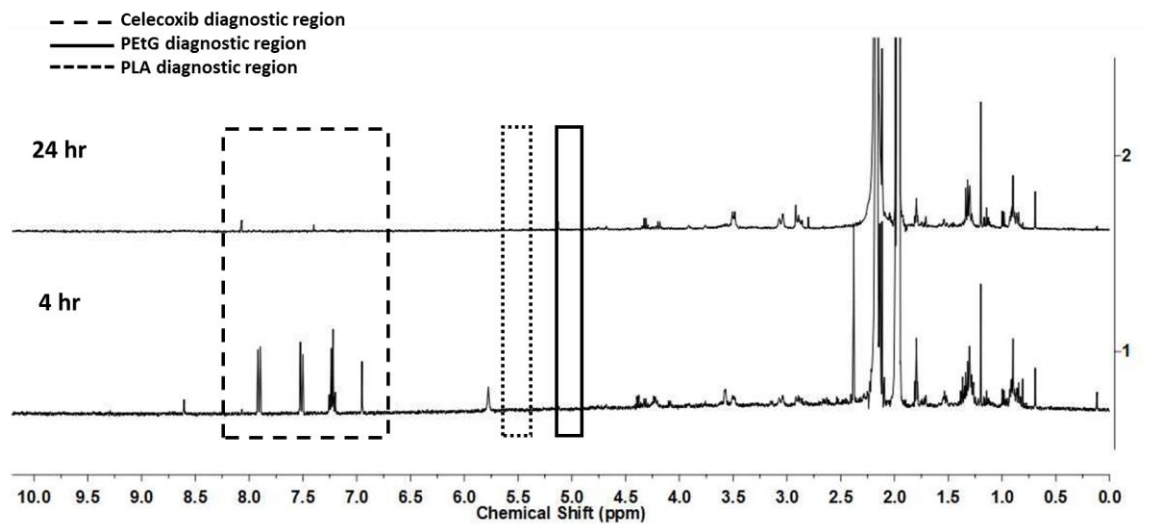
Figure A-17. ^{1}H NMR spectrum of pellet collected from celecoxib release study of 100% disulfide-PEtG sample after 4 and 24 h (CD$_3$CN, 400 MHz).
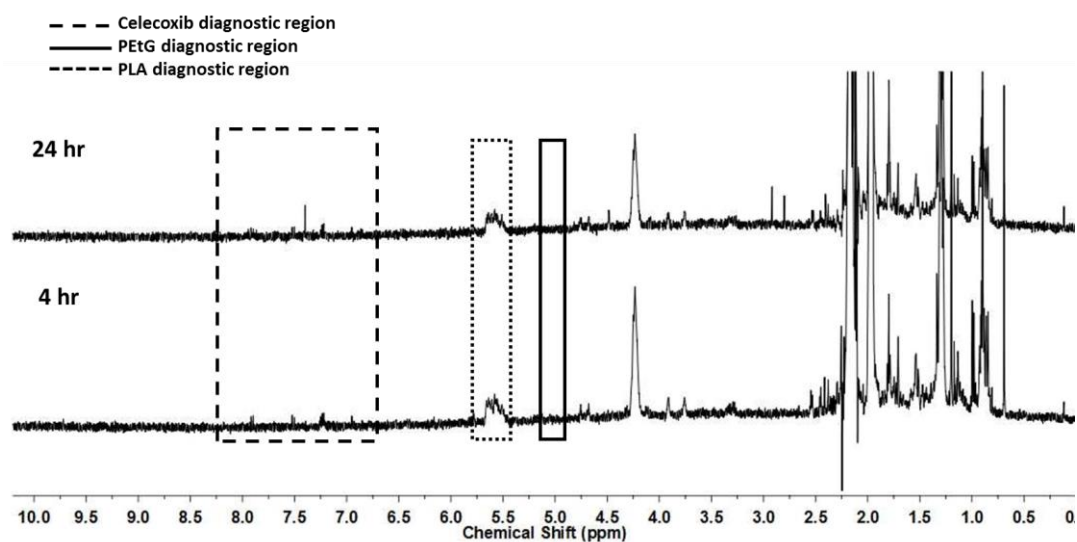
Figure A-18. ^{1}H NMR spectrum of pellet collected from celecoxib release study of 100% disulfide-PEtG no DTT control sample after 4 and 24 h (CD$_3$CN, 400 MHz).
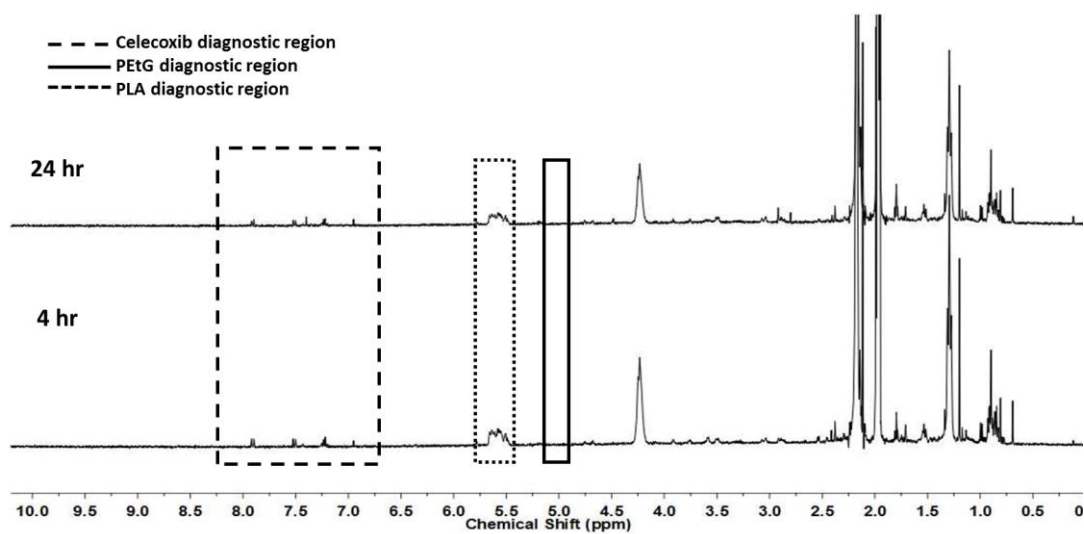
Figure A-19. ^{1}H NMR spectrum of pellet collected from celecoxib release study of 100% BnCO-PEtG control sample after 4 and 24 h (CD$_3$CN, 400 MHz).
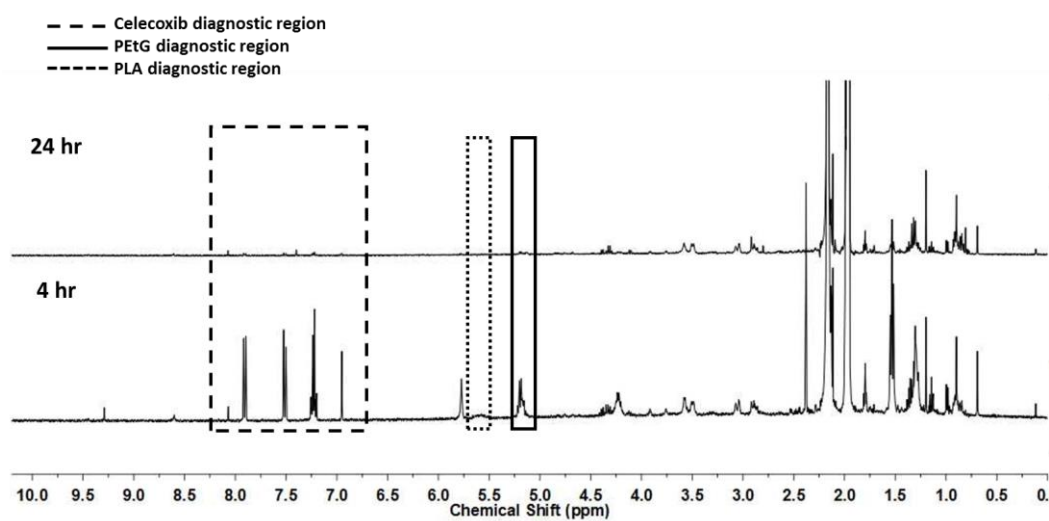
Figure A-20. ^{1}H NMR spectrum of pellet collected from celecoxib release study of 10% PLA-PEtG-disulfide sample after 4 and 24 h (CD$_3$CN, 400 MHz).
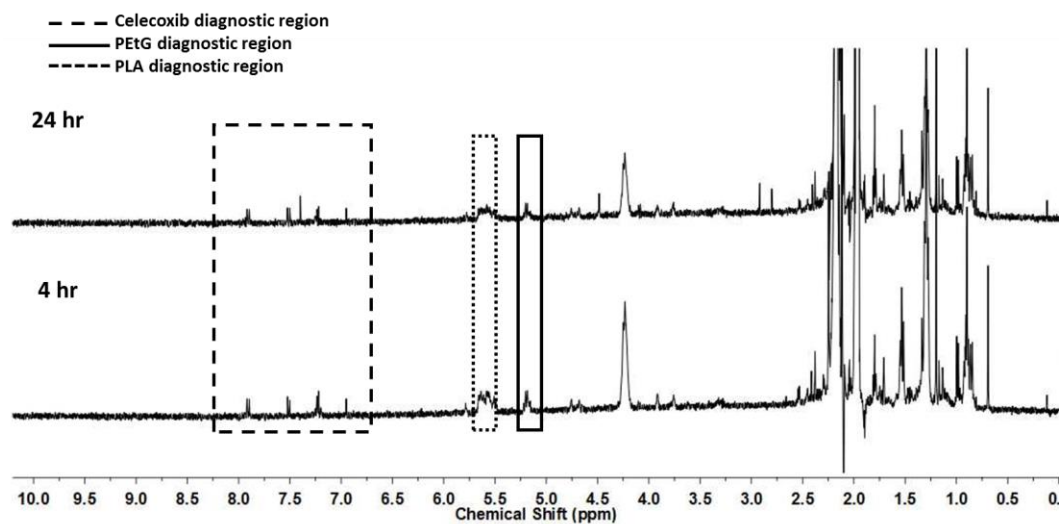
Figure A-21. [^1]H NMR spectrum of pellet collected from celecoxib release study of 10% PLA-PEtG-disulfide no DTT control sample after 4 and 24 h (CD$_3$CN, 400 MHz).
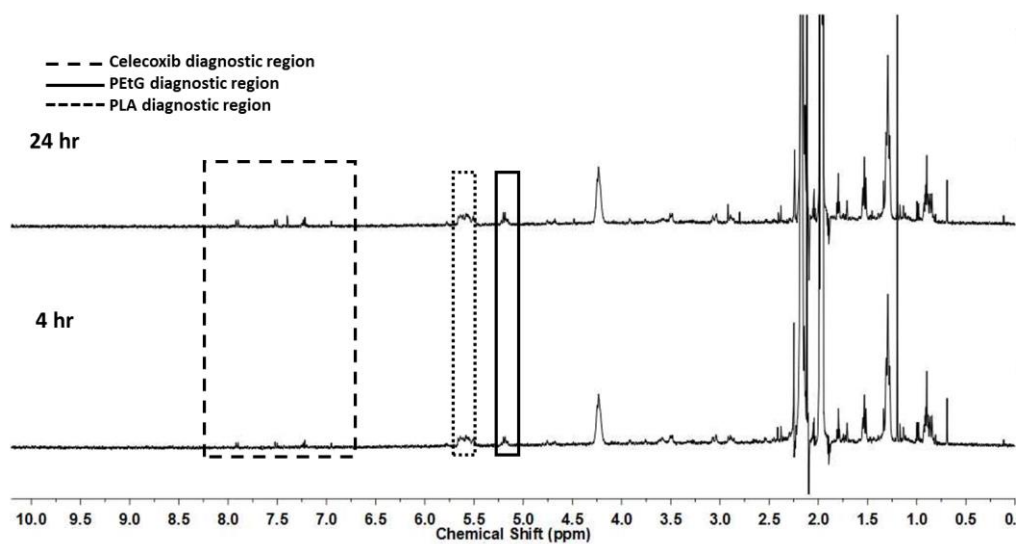
Figure A-22. [^1]H NMR spectrum of pellet collected from celecoxib release study of 10% PLA-PEtG-BnCO control sample after 4 and 24 h (CD$_3$CN, 400 MHz).
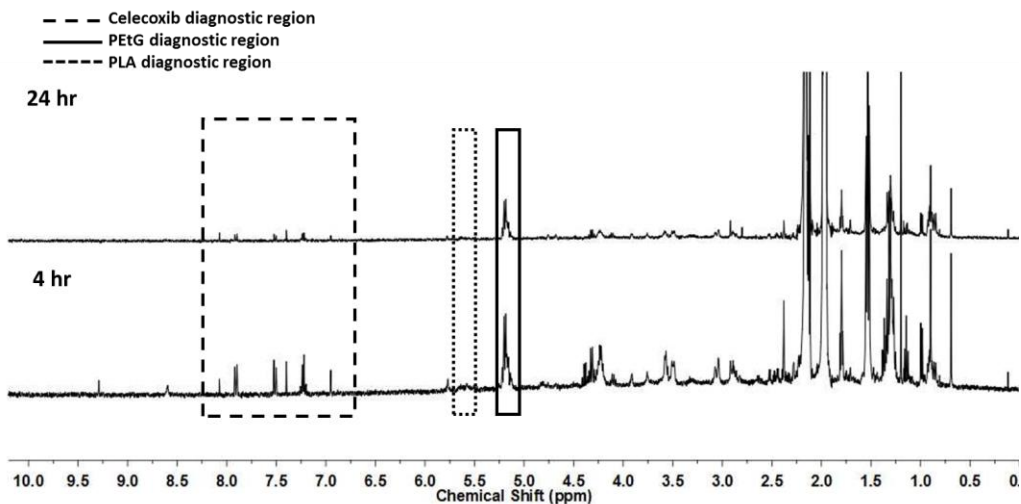
Figure A-23. ^{1}H NMR spectrum of pellet collected from celecoxib release study of 30% PLA-PEtG-disulfide sample after 4 and 24 h (CD₃CN, 400 MHz).
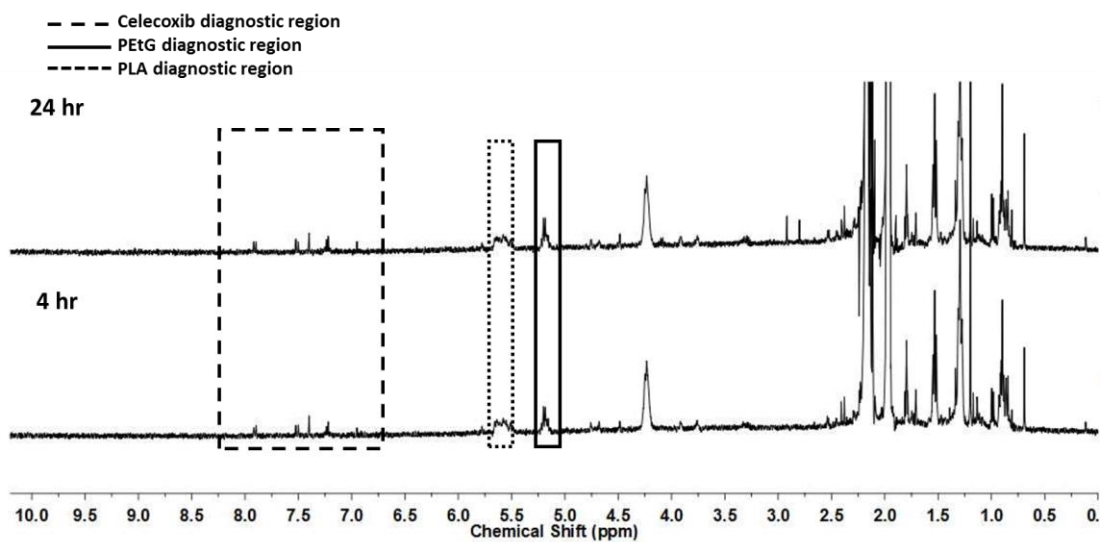
Figure A-24. ^{1}H NMR spectrum of pellet collected from celecoxib release study of 30% PLA-PEtG-disulfide no DTT control sample after 4 and 24 h (CD₃CN, 400 MHz).
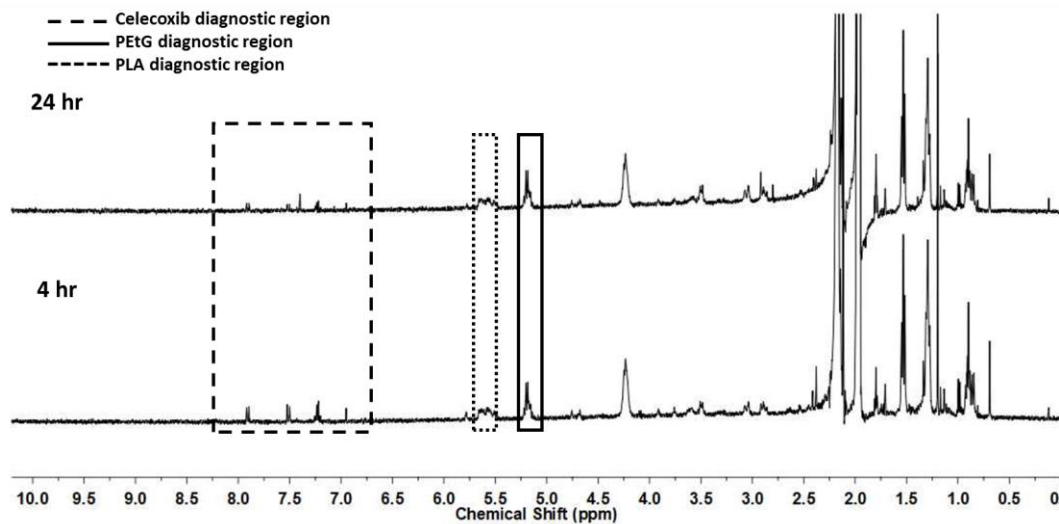
Figure A-25. ^{1}H NMR spectrum of pellet collected from celecoxib release study of 30% PLA-PEtG-BnCO control sample after 4 and 24 h (CD$_3$CN, 400 MHz).
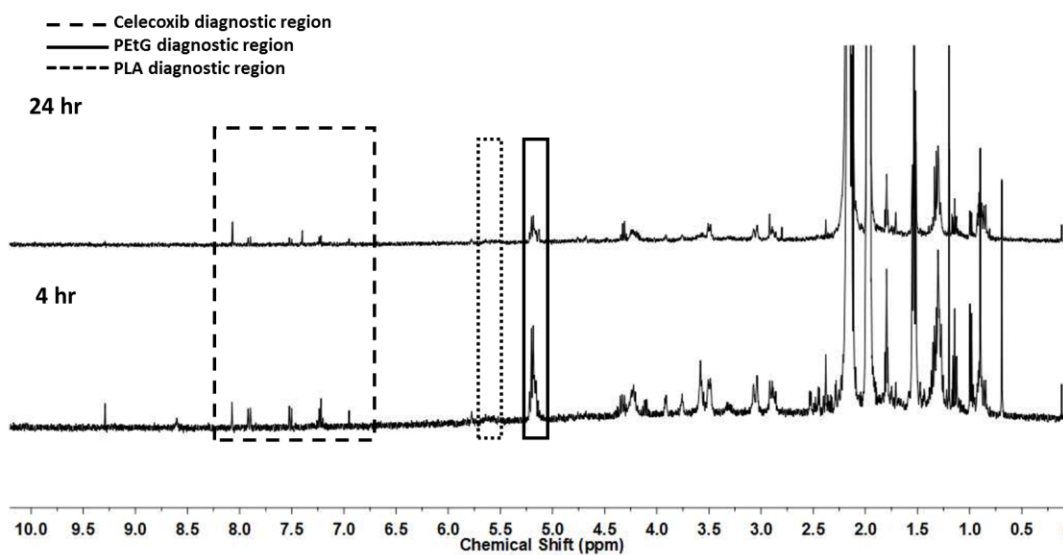
Figure A-26. ^{1}H NMR spectrum of pellet collected from celecoxib release study of 50% PLA-PEtG-disulfide sample after 4 and 24 h (CD$_3$CN, 400 MHz).
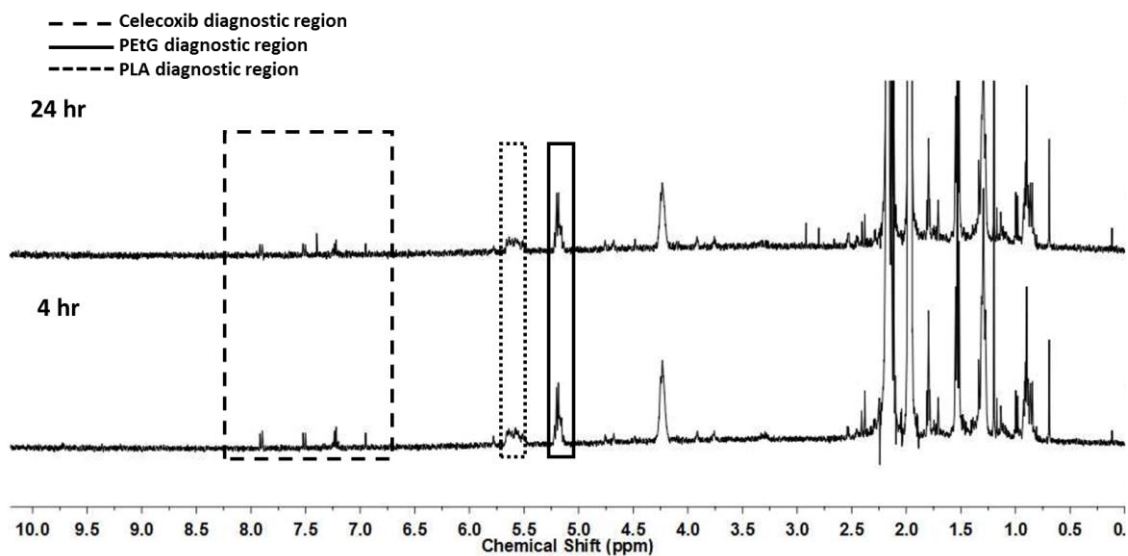
Figure A-27. ^{1}H NMR spectrum of pellet collected from celecoxib release study of 50% PLA-PEtG-disulfide no DTT control sample after 4 and 24 h (CD$_3$CN, 400 MHz).
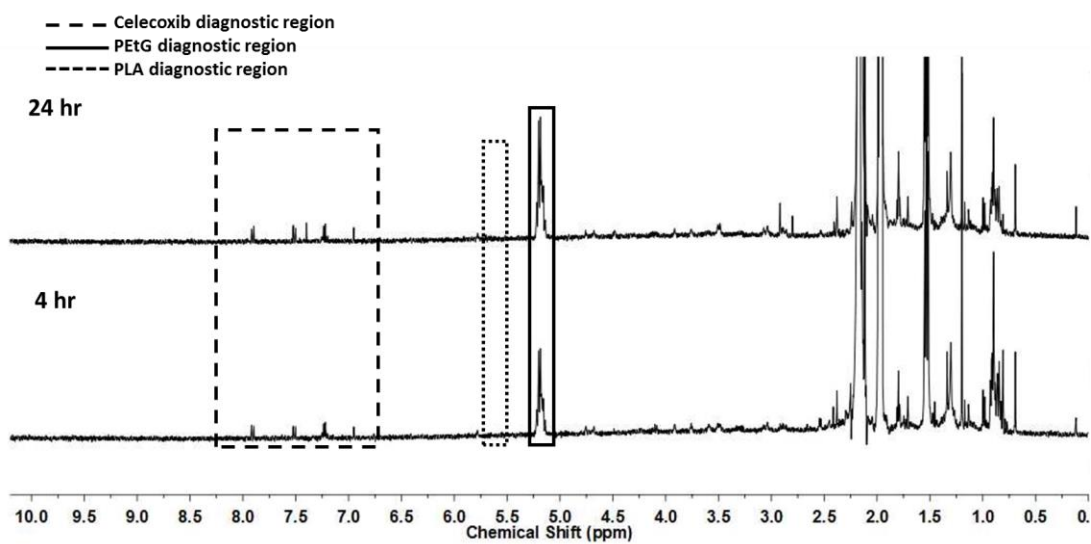
Figure A-28. ^{1}H NMR spectrum of pellet collected from celecoxib release study of 100% PLA sample after 4 and 24 h (CD$_3$CN, 400 MHz).
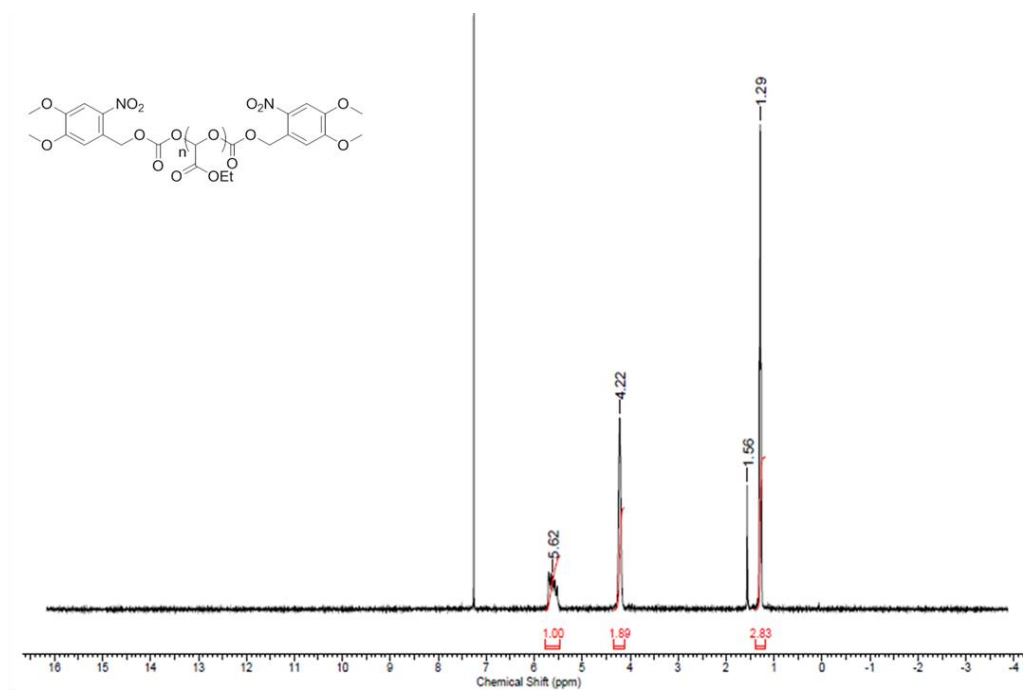
Figure A-29. ^{1}H NMR spectrum of NVOC-PEtG (CDCl$_3$, 400 MHz).
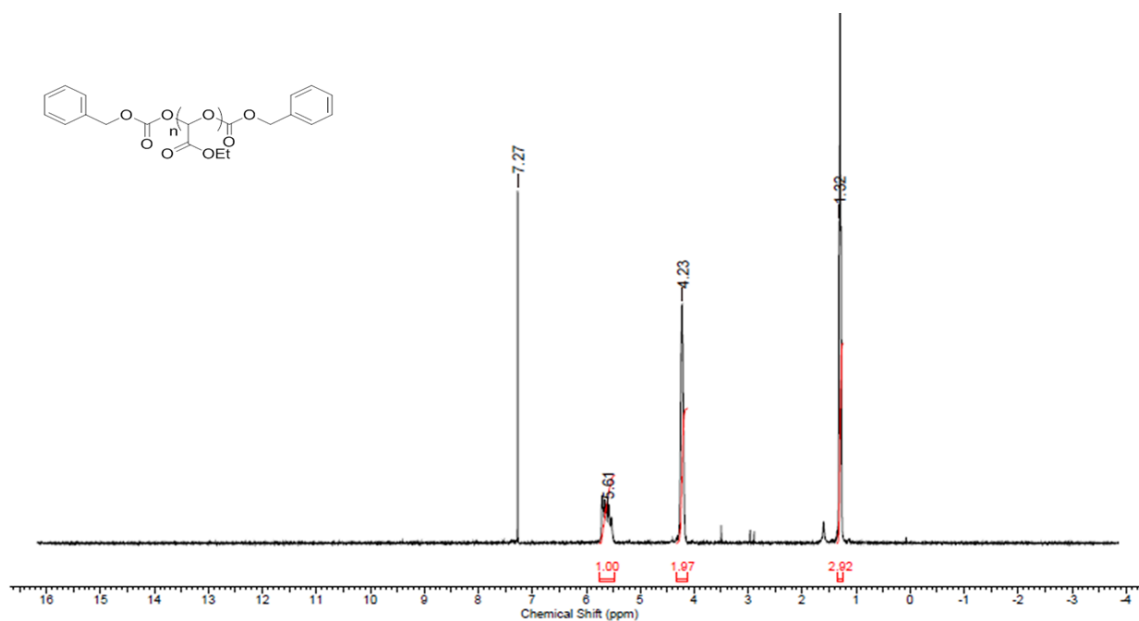
Figure A-30. ^{1}H NMR spectrum of BnCO-PEtG (CDCl$_3$, 400 MHz).
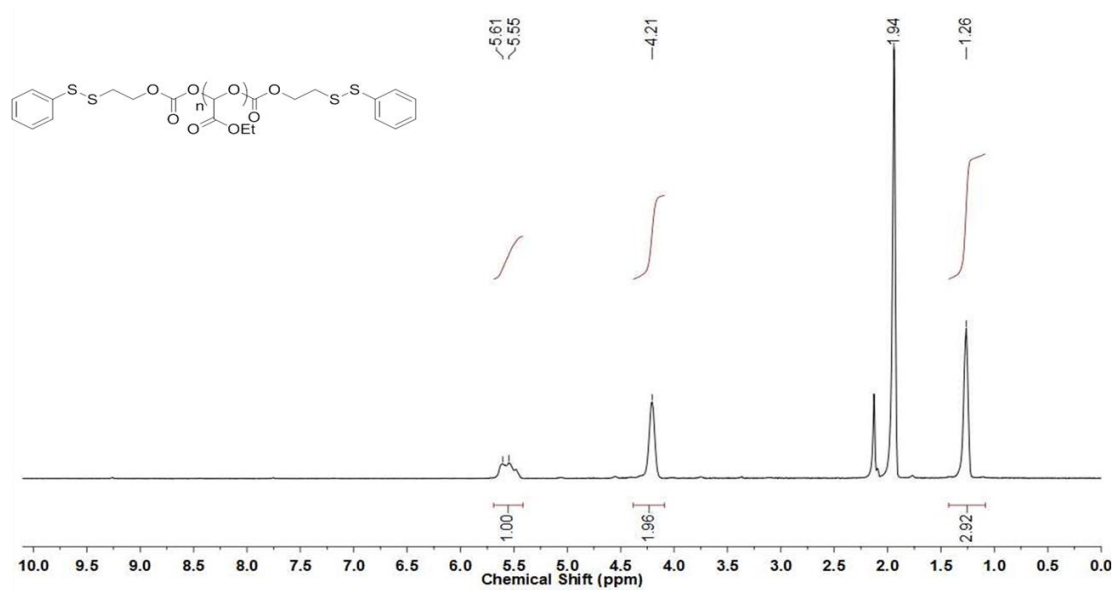
Figure A-31. ^{1}H NMR spectrum of disulfide-PEtG (CD$_3$CN, 400 MHz).

Copyright Clearance Center RightsLink®

ACS Publications
Most Trusted. Most Cited. Most Read.

Title: Self-Immolative Polymersomes for High-Efficiency Triggered Release and Programmed Enzymatic Reactions

Author: Guhuan Liu, Xiaorui Wang, Jinming Hu, et al

Publication: Journal of the American Chemical Society

Publisher: American Chemical Society

Date: May 1, 2014

Copyright © 2014, American Chemical Society

PERMISSION/LICENSE IS GRANTED FOR YOUR ORDER AT NO CHARGE

BACK | CLOSE WINDOW

Curriculum Vitae

Name: M. Thomas Gambles

Post-secondary   University of Utah
Education and   Salt Lake City, UT
Degrees: 2008–2012 B.Sc.

                       The University of Western Ontario
                       London, Ontario, Canada
                       2015–2017 M.Sc.

Honours and Awards: Lipson-Baines Award (Best presentation at "chemistry 9657 seminar course"), June 2017.

Related Work   Teaching Assistant
Experience   The University of Western Ontario
                       2015–2017

Presentations: M. Thomas Gambles, Bo Fan and Elizabeth R. Gillies, Western University, Polyglyoxylate Nano- and Micro-Particles for Triggered Drug Release, 37th Canadian High Polymer Forum, Aug. 2016, Gananoque, ON.